SYNTHESIS AND ELECTROCHEMICAL ANALYSIS OF COMPOSITE ELECTRODES FOR DRY POLYMER LITHIUM ION BATTERY

March 2010

Kazuma Hanai

Index

Introduction

1. Renewable energy and lithium ion batteries

In recent years, the renewable-energy industries such as nuclear-power, solar-collection, wind turbines, and bio-ethanol have been developing rapidly. Besides reduction of greenhouse-gas emissions, the "Strategic Investment" to build a renewable-energy economy is a powerful driving force to develop new industries and create millions of jobs. Renewable-energies are generally converted into electric power which is a widely used energy source. This power can be transported simply by a wire, but it is not easy to store efficiently. Capacitors are well-known as high-speed rechargeable electrical devices which can store electric power directly. Electric double-layer capacitors are able to store more electrons than previous electrolytic condensers, but the capacity is not enough for long term electricity supply. Therefore, electric power needs to be stored in pumped-storage, flywheel-storage, or in a electrochemical reaction as a battery. Pumped or flywheel storage needs large-scale devices. In contrast, batteries, especially Lithium-ion batteries, are well-known as high energy density portable devices which have been used in a large number of applications. The power of redox reaction in batteries can be extracted as Direct Current (DC). Solar cells generate DC power, however electricity is supplied from a power plant to home electrical appliances as high-voltage Alternative Current (AC), which prevents power losses over long distance transmission lines. Some household appliances, such as television, personal computer and LED-lighting, function on DC system. Appliances need to convert AC power into DC power, and there are 5-10% energy loss in the conversion system. Therefore, the electricity generated by solar cells should be used to power DC powered appliances as much as possible. In the case of roof-top solar cells, there is a short line from the roof to a wall socket, making a high voltage current unnecessary. However, the generated DC electricity needs to be converted into AC power for general use due to previous standardized products. In addition to this, appliances with the “Inverter” mark, which means the energy saving control technology, converts the power twice: from supplied AC to DC, then DC to hi-voltage AC again through the inverter. There are many energy losses due to the inefficiency of converters. One of the concerns for building up a low-carbon society is how to store and/or use the generated energy efficiently. Therefore, the combination of Lithium-ion batteries and the AC/DC hybrid system into a “Smart Grid” is considered to be a suitable solution.

2. Lithium-ion battery industries

Lithium ion batteries are indispensable devises for our life. Cellular phones are used as not only for phone call but also as mobile data terminal to obtain some information on internet. The technical development for mass production of Lithium-ion battery improved the energy density to twice or more in 10 years ($280Whl^{-1}$ to $580Wh/^{-1}$, 1995-2005). Figure 1 shows the total sales of rechargeable batteries in Japan (1995-2008). The sales of rechargeable Lithium-ion battery reached 385.8 billion (JPY) in 2008, which is 54% of the totality. In July 2009, i-MiEV, the electric vehicle (EV) with Lithium-ion battery, came out to automobile market by Mitsubishi Motors Corporation. In August 2009, Nissan Motor Co., Ltd. announced that Lithium-ion EV, LEAF, would be put on the market in late 2010.

EV and plug-in hybrid vehicles (PHEV) need high-performance batteries for the power source which have both high-power and safety for long time use. Many automobile companies are cooperating with battery manufacturers to obtain the battery, for example, the battery in i-MiEV is produced by “Lithium Energy Japan” which is a joint-stock company with GS Yuasa, Mitsubishi Corporation and Mitsubishi Motors Corporation. It suggests that Lithium-ion battery industries will increase at least until previous cars are replaced with EV or PHEV completely. On the other hand, Lithium-ion batteries need much amount of rare metals for the electrode. The materials push up a production cost which is considered to be one of barriers for business use. The Ministry of Economy, Trade and Industry (METI) compiled "Strategy for Ensuring Stable Supplies of Rare Metals" in Jury 2009. In this strategy, the development of recycling technology from compact appliances, such as cellular phones and digital cameras, is considered to be one of the most important points for the manufacturing because Japan has poor natural resources.

Producing recyclable Lithium-ion battery and developing a material saving technology are the task of Lithium-ion battery industry.

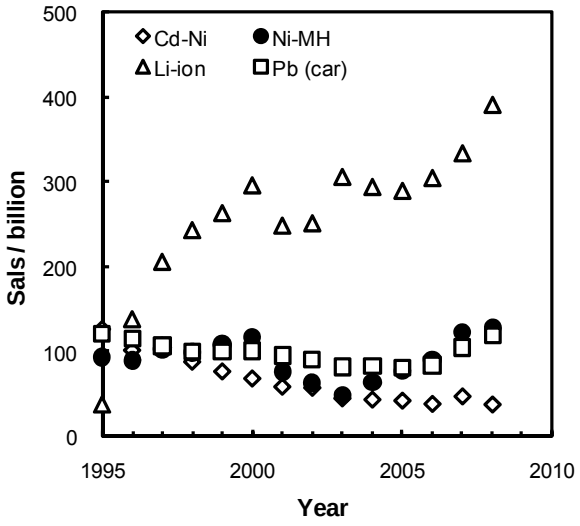

Fig. 1 Sales of Japan (1995-2008)

3. All-solid lithium ion batteries

For any rechargeable Lithium-ion battery, the electrolyte material must permit the repeated and rapid transfer of Li-ions between anode and cathode over the expected range of operating conditions such as voltage, temperature and current. The ideal electrolyte material should be an electronic insulator, ultra-thin, lightweight, hazard-free and inexpensive. However the flammable organic solvent was used as electrolyte in most commercialized Lithium-ion battery due to the operating condition. Room-temperature ionic liquid has been attracting much attention as safe electrolytes for Lithium-ion battery. The low-flammable and low-volatile ionic liquid is able to be an alternative electrolyte, but the viscosity and production cost restrict to practical use. In addition to this, liquid electrolyte needs to be infiltrated into some separators to reach every parts of the electrode, which separator accounts for 10-20% of production cost. For the required rapid transport of lithium ion across the electrolyte, the product of the resistivity and electrolyte thickness should be minimized. An ultra-thin electrolyte provides a considerable savings in terms of volume and mass for the battery. The all-solid lithium ion conductor is considered as the best candidate for the electrolyte, because it can be formed as quite thin film separators on electrode.

4. Solid electrolytes

A large number of solid electrolytes have been investigated for Lithium-ion battery. Typical room temperature conductivities are 10^{-1} Scm^{-1} for liquids, 10^{-2} Scm^{-1} for super-ionic conductors such as β-alumina, 10^{-3} to 10^{-6} Scm^{-1} for dry polymer, and 10^{-4} to 10^{-8} Scm^{-1} for typical grass and ceramic solid electrolytes as shown in table 1.

Inorganic solid electrolyte

One of the principle advantages of inorganic solid electrolytes is that these materials are generally single ion conductors. Only the Li-ions have an appreciable mobility while the anions and other cations from a rigid framework. Many ceramic electrolytes have been reported as follows; Perovskite electrolytes ($La_{2/3-x}Li_{3x}TiO_3$, 10^{-3} Scm^{-1} at 25 ºC), Nasicon-type phosphates ($Li_{1+x}M_2(PO_4)_3$, $<10^{-4}$ at 25 ºC), Lisicon-type materials ($Li_{14}ZnGe_4O_{16}$, 10^{-1} at 200 ºC). However there is some variability in the grain boundary contribution to the total resistance. For some materials the grain boundary contribution to the resistivity is 10 to100 times higher than that of the bulk. Therefore, these materials need to be pressed and sintered of powders produced by solid state reaction.

Glass electrolyte

A number of studies revealed that compositions with a higher concentration of the Li modifier give a higher conductivity and lower activation energy for Li-ion transport. The disadvantage of grain boundary is minimized in ideal glass electrolyte. This profile simplifies the synthesis and handling of the material.

The phosphorous oxynitride glass (LIPON $Li_xPO_yN_z$ 10^{-6}, at 25 ºC) is well-known as glass type solid lithium ion conductors. This material is prepared by RF-sputtering or thermal evaporation. These preparation methods are suitable way to form an ultra-thin electrolyte layer, however the growing speed is about 10 nm min^{-1} which restricts to practical use.

The sulfide and oxysulfide glasses (Li_2S-SiS_2, Li_2S-P_2S_5) also have been reported as glass type electrolytes. The impressive conductivities (10^{-3}-10^{-4} at 25 ºC) and low activation energies compared to the oxide glasses were attributed to the weaker bonding of Li with the non-bridging sulfur anions, due to the higher polarizability and softer basicity of the sulfide ion. This electrolyte is highly reactive with air, therefore great care and a highly efficient glove box are required to synthesize and fabricate.

Dry polymer electrolyte

The polyethylene oxide (PEO) based dry polymer electrolyte was found by Wright et al. as alkali metal ion conductors in 1975. This polymer is widely used as surfactants, cosmetics and food additives, which is commercially available in a relatively pure state at reasonable cost. The PEO electrolyte with $LiN(CF_3SO_2)_2$ (LiTFSI) shows the conductivity of 10^{-3} S cm^{-1} above 60 ºC. This significant conductivity occurs through the amorphous phase where there is segmental motion of the polymer chains. The pure PEO shows semi-crystalline behavior due to the interaction of oxygen atoms in the polymer chain. This phase transition restricts the segmental motion of the polymer chains, which corresponds to the decreasing of lithium ion conduction in the polymer electrolyte. Therefore PEO-LiTFSI electrolyte exhibits the drastic conductivity drop below the melting point of PEO. Generally, polymer electrolytes show no grain boundary disadvantage because of the flexible structure. In addition the polymer can be formed as thin film, which is available to save the volume and mass for the battery.

Table 1 Typical solid electrolytes

Composition	Synthesis	σ at 25 ºC (Scm^{-1})	Ea ($kJmol^{-1}$)
$La_{2/3-x}Li_{3x}TiO_3$ $0.03 \le x \le 0.167$	solid state reaction & pressed	1×10^{-3} x=0.13	28±2
$Li_{1.3}Ti_{1.7}Al_{0.3}(PO_4)_3$	solid state reaction & pressed	3×10^{-4}	-
$Li_{4-x}Ge_{1-x}P_xS_4$	solid state reaction & pressed	2×10^{-3} x=0.65	20
$Li_xPO_yN_z$ $0.24<z<1.2$	Rf sputter in N_2 plasuma	2×10^{-3} (x,y,z)=(2.9,3.3,0.46)	55
Li_2S-SiS_2	Mechanical mill & pressed	1×10^{-4}	30
Li_2S-P_2S_5	Mechanical mill & pressed	2×10^{-4}	37
PEO-LiTFSI		1×10^{-6}	40

5. Solid lithium polymer batteries

Rechargeable solid lithium polymer battery (SLPB) is considered to be the best candidate for next generation Lithium-ion batteries because of their low production cost, high reliability, safety, and flexibility for cell design. In large scale batteries, internal resistances of the cell give cause for anxiety of thermal run away. Therefore it is the key technology to design as large and thin battery which shape is suitable to decrease the electrolyte resistance and heat-generations. The liquid-type Lithium-ion battery is packed in metallic case to prevent a short circuit from outside stresses and leaking out of the electrolyte. This package relates to decreasing the energy density and increasing the production cost. The polymer electrolyte can be formed as quite thin and shock-absorbable separators. In the electrode, the polymer works as binders to retain electrical and ionic passes between active material particles, additives, and current collector, where the electrode shows flexible and tough structure. These advantages lead light-weight and thin cells, such as laminate-packed battery.

In this study, we have investigated the composite electrode for SLPB. The report is divided in to two parts;

Part1 is described the interfacial resistance between $LiFePO_4$/PEO-LiTFSI composite electrode and PEO-LiTFSI electrolyte.

Part2 is mentioned to Graphite/PEO-LiTFSI composite electrode for SLPB, and Si/carbon composite electrode for liquid-type cells.

Reference

[1] N.J. Dudney, Glass and ceramic electrolytes for lithium and lithium-ion batteries, in: G.A. Nazri, G. Pistoia (Eds.), Lithium Batteries: Science and Technology, Kluwer Academic Publishers, USA, 2004, pp. 623-642.

Web reference

[2]https://app3.infoc.nedo.go.jp/informations/koubo/koubo/FA/nedokouboplace.2009-03-18.0619118972/nedokoubo.2009-03-26.6168334273/30ea30c130a630e04e8c6b2196fb6c608ab2984c.pdf, NEDO report, 2007.

[3] http://www.baj.or.jp/, battery association of Japan.

[4] http://www.mitsubishi-motors.co.jp/, Mitsubishi Motors Corporation.

[5] http://www.meti.go.jp/press/20090728004/20090728004.html, Ministry of Economy, Trade and Industry (METI), Announcement of "Strategy for Ensuring Stable Supplies of Rare Metals".

Part 1: Cathode

This part is based on investigations of interfacial resistances between $LiFePO_4$ and PEO-LiTFSI electrolyte. In polymer batteries, the electrolyte can be formed as quite thin film with low-resistance, where the interfacial property will be a key to decrease internal resistances for high-performance safety cells. Liquid electrolytes are able to be infiltrated into the electrode easily, but PEO-LiTFSI electrolyte needs to be mixed with electrode slurry because of its viscosity. The slurry is prepared with active materials, carbon additives, PEO-LiTFSI electrolytes and some solvents, which obtains composite electrodes with complex structures. In this part, we have investigated interfacial resistances between $LiFePO_4$ composite electrode and PEO-LiTFSI electrolyte as follows;

1.1. Enhancement of electrochemical performance of lithium dry polymer battery with $LiFePO_4$/carbon composite cathode

1.2. Study on All Solid Lithium Polymer Batteries with the $LiFePO_4$/C Cathode

1.3. Interfacial properties between $LiFePO_4$ and poly(ethylene oxide)-$Li(CF_3SO_2)_2N$ polymer electrolyte

1.1. Enhancement of electrochemical performance of lithium dry polymer battery with $LiFePO_4$/Carbon composite cathode

1. Introduction

The lithium ion battery can be considered to be a container holding a large amount of energy, and a number of studies have attempted to enhance the energy density of the lithium ion battery. However, at the same time, the remarkable advantages of the lithium ion battery can be a practical problem. If a device can contain higher energy, there is a higher risk of fire explosion. Therefore, safety is a key issue for future applications of the lithium ion battery such as large-scale batteries for electric vehicles and load leveling devices. In order to overcome this problem, the development of all-solid state batteries using a solid electrolyte may be one solution.

Inorganic and organic solid electrolytes have been examined for their potential application in a lithium ion battery. Li_3N [1], $La_{0.5}Li_{0.5}TiO_3$ [2], $Li_{3.6}Si_{0.6}P_{0.4}O_4$ [3], and LIPON [4] are inorganic lithium ionic conductors. Kanno et al. reported a series of sulfide-type lithium conductors called thio-LISICON, among which $Li_{3.25}Ge_{0.25}P_{0.75}S_4$ shows the highest conductivity of 2.2×10^{-3} S cm^{-1} at 25 ◦C [5]. On the other hand, as an organic solid electrolyte, polyethylene oxide (PEO)-based polymer has been widely studied. The fire-resistive characteristics as well as the softness and flexibility of PEO will likely encourage new applications such as wearable devices and flexible displays. The construction of a cell using polymer electrolyte is simpler than that using ceramic electrolyte, because no special attention is necessary to maintain contact between ceramic powders inside the cell. Therefore, we have studied the dry polymer/electrode system for a safer lithium ion battery.

In using a polymer electrolyte, there is a voltage limitation in the positive electrode side. Conventional cathodes such as $LiCoO_2$ and $LiMn_2O_4$, which operate at around 4.0V, are difficult to use stably with PEO electrolyte [6]. Another reversible electrode material, $LiFePO_4$ is known to be safe at elevated temperatures [7,8]. In addition, this material shows a reversible electrode potential of around 3.5V compared to lithium, which is appropriate for use with gel-type polymer electrolyte [9,10]. Note also that $LiFePO_4$ comprises abundant elemental iron, which is environmentally favorable. Among the cathodes, $LiFePO_4$ is considered as a candidate for the positive electrode of the dry polymer lithium ion battery [11–13].

However, polymer electrolyte has a significant drawback in that it has poor ionic conduction near room temperature. The study of the dry polymer battery using PEO as a host polymer has been usually performed above 60 ◦C, which corresponds to the melting point of pure PEO. Not only the bulk of the electrolyte, but also the interface between electrolyte and electrode is the main constituent of the internal resistance. The reduction of this interface resistance is important because the charge transfer resistance becomes relatively larger when preparing a thin-film battery [14–16].

In the present study, the reduction of the operating temperature of $LiFePO_4$ electrode in the dry polymer electrolyte system has been attempted by optimizing the interface structure. In order to characterize the interface, the internal cell resistance was estimated and separated into individual processes by the impedance technique. The details of each process were discussed, and the enhanced electrochemical performances below 60 ◦C were described.

2. Experimental

$LiFePO_4$ as a positive electrode was prepared in the form of a composite with carbon material. Li_2CO_3, $(NH_4)_2HPO_4$, and $FeC_2O_4 \cdot 2H_2O$ were mixed in a 1:2:2 molar ratio, and 6.0 g of the mixture and 0.6 g of polyvinyl chloride (PVC) as a carbon precursor were mixed in tetrahydrofuran (THF). The suspension was dried and pressed into tablet form. The tablet was heated in two steps. The first calcination was performed at 350 ◦C for 6 h under a nitrogen atmosphere. At this temperature, PVC decomposes and becomes a carbonaceous material. The product was then crushed and ground well with new PVC powder at a weight ratio of 8:2. The mixture was annealed again at 700 ◦C for 16 h under a nitrogen atmosphere to obtain the final composite product of $LiFePO_4$/C. The formation of crystalline $LiFePO_4$ was identified by X-ray diffraction (XRD) analysis.

$LiFePO_4$/C and polyvinilidene fluoride (PVDF) at a 9:1 weight ratio were mixed in N-methyl-2-pyrrolidone (NMP) and then spread on aluminum foil. The film was dried in air at 80 ◦C for 1 h, pressed, and dried under a vacuum at 120 ◦C for 1 h. The film thickness after the drying process reached approximately 40–70 μm, and the active electrode area was 2.25 cm^2 (1.5 cm×1.5 cm).

The PEO-based polymer was prepared as a separating electrolyte. PEO (Aldrich, average molecular weight: 3×10^5, 6×10^5, or 9×10^5) and $Li(CF_3SO_2)_2N$ (LITFSI, Fluka) were dissolved in acetonitrile (AN) with Li/O at a molar ratio of 1/18 or 1/10. A polymer electrolyte solution was cast in a PTFE dish under an argon atmosphere.

After the evaporation of AN at room temperature, the film was dried at 100 ◦C for 12 h under a vacuum. The resulting film thickness was approximately 100 μm.

The porous $LiFePO_4$/C film electrode was impregnated with PEO electrolyte by casting an acetnitrile solution of the electrolyte under a depressurized condition. The impregnated electrode was dried under an argon stream at room temperature and then under a vacuum at 100 ◦C overnight. After that, the polymer electrolyte sheet was placed onto the positive electrode mixture, and a lithium metal sheet was placed on the other side as a negative electrode. The entire system, Al/$LiFePO_4$/PEOsheet/Li/Cu, was sealed into a laminate cell for the electrochemical test.

A two-electrode laminate cell was galvanostatically charged and discharged under a current density of 25 μAcm^{-2} (approximately $6mAg^{-1}$ and C/20 rate), a cut-off voltage range of 4.1–2.5V, and at a temperature of 40 or 50 ◦C. The impedance measurement was used to estimate the interface resistance. An ac perturbation of 10mV was applied in the frequency range from 1×10^6 to 0.5 Hz by a Solartron 1260 frequency response analyzer. The temperatures were controlled from 20 to 60 ◦C in order to obtain the Arrhenius plots.

3. Results and discussion

The X-ray diffraction pattern of the prepared $LiFePO_4$/C composite is shown in Fig. 1.

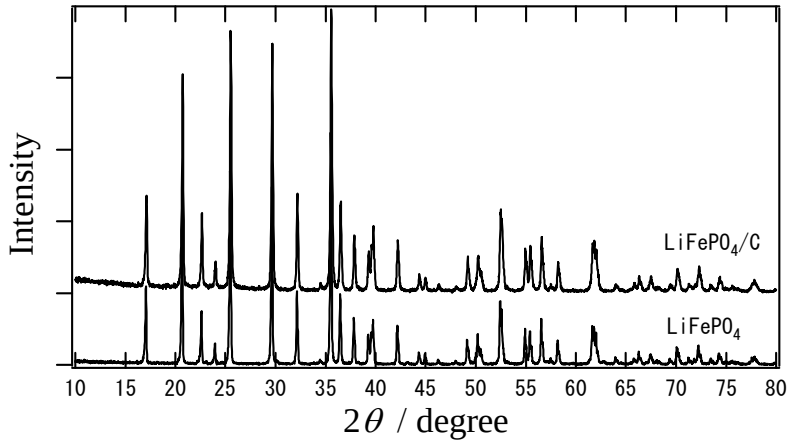

Fig. 1. X-ray diffraction patterns of composite material of $LiFePO_4$/carbon and single-phase $LiFePO_4$. Cu Kα line generated under 40 kV and 150 mA. Continuous scanning was performed at a speed of $1◦ min^{-1}$.

Comparison with the reference pattern reveals that all of the peaks are assigned to genuine $LiFePO_4$ and no peaks of other phases are observed. It is confirmed that the

$LiFePO_4$ and carbon composite was prepared without any residual side reactions. The carbon content in $LiFePO_4$/C composite was estimated to be approximately 10 wt% by elemental analysis using a CHN CORDER MT-5 (Yanaco).

A TEM photograph of the composite product is shown in Fig. 2.

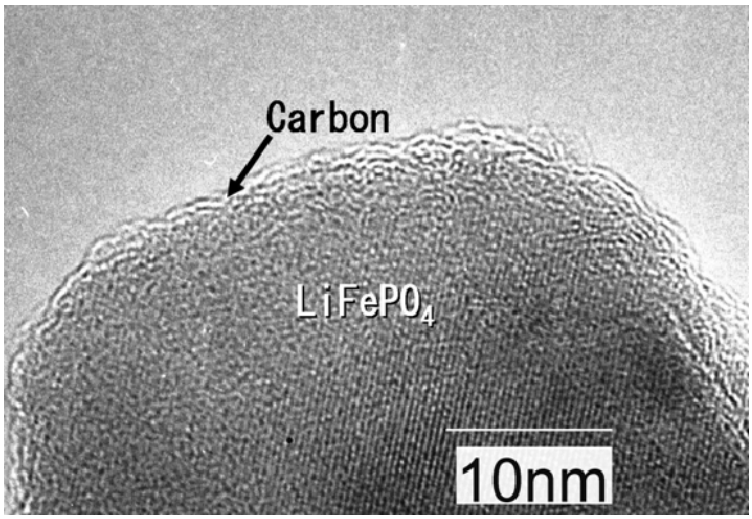

Fig. 2. TEM photograph of the product prepared from Li_2CO_3, $(NH_4)_2HPO_4$, FeC_2O_4, and polyvinyl chloride. The photograph was captured using a Hitachi H-9000 at an accelerating voltage of 300 kV.

A single particle of $LiFePO_4$ shows a clear lattice image. On the surface, there is an amorphous layer showing a degraded image, which is considered to be a carbonaceous material. This photo shows the composite structure of crystal $LiFePO_4$ and amorphous carbon. The electrochemical characterization of the composite was examined using $1MLiClO_4$ dissolved in ethylene carbonate and diethyl carbonate (50:50 vol%) as the liquid electrolyte, which was purchased from Kishida Chemical Co. Ltd.

Fig. 3 shows the charge and discharge curves measured at room temperature and the change in capacity in the first 50 cycles. The capacity was calculated for 1 g of the composite. The $LiFePO_4$/C electrode shows a good capacity retention of over 99.9% per cycle in this liquid electrolyte system. The excellent reversibility of the composite electrode suggests that the carbon around the $LiFePO_4$ particles provides a good electronic network and compensates for the poor electronic conductivity of the active material. The theoretical capacity of the composite is calculated to be 153 mAh g^{-1}, assuming that the carbon content is 10 wt%. The observed capacity is still smaller

than this calculated value. The small capacity of the composite can be accounted for by the occurrence of Fe^{3+} without changing the crystal structure [17].

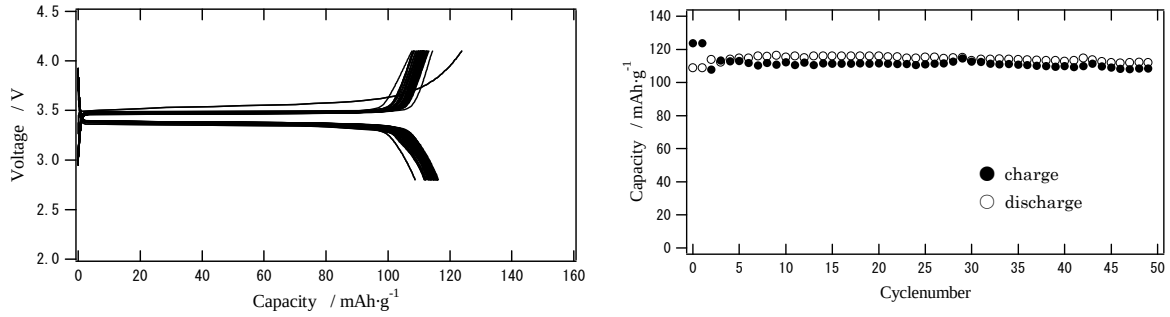

Fig. 3. Charge and discharge curves (above) and cycling behavior (below) of the $LiFePO_4$/C composite electrode in 1M LiClO4 in an EC-DEC liquid electrolyte system. The current density was C/10 (approximately 50 μAcm^{-2}), and a two-electrode laminate cell was used as the test cell.

Fig. 4 shows the charge/discharge behaviours of the $LiFePO_4$/C composite electrode with PEO polymer electrolyte at 50 ◦C.

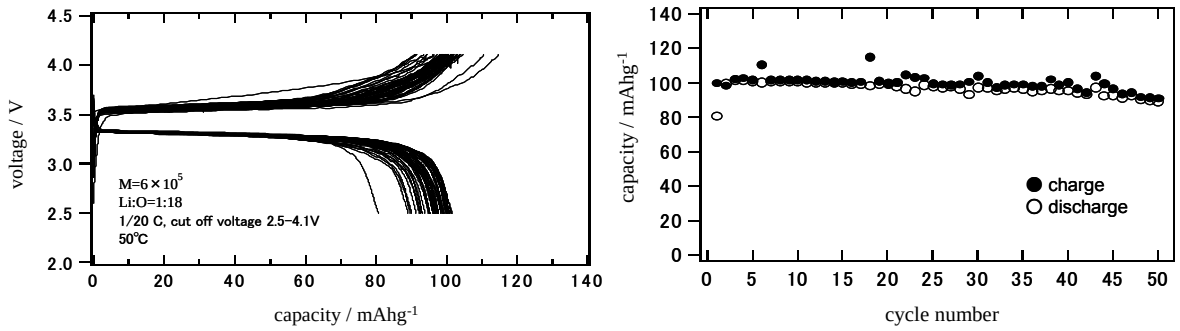

Fig. 4. Charge and discharge curves (above) and cycling behaviour (below) of $LiFePO_4$/C composite electrode in a solid polymer electrolyte system at 50 ◦C. The current density was C/20 (approximately 25 μAcm^{-2}), and a two-electrode laminate cell was used as the test cell.

The capacity of 100 mAh g^{-1} is approximately equivalent to that of the liquid electrolyte system. This performance depends greatly on the dimensions of the electrode with approximately 3 mg of active material per 2.25 cm^2, provides rather thin film morphology. However, our preliminary results [18] indicate that insertion materials such as graphite or silicon show much less capacity at 50 ◦C. The behavior shown in the figure is considered to be specific to $LiFePO_4$. The capacity change with the cycle number indicates that stable charge and discharge behavior can be maintained during the first 50 cycles. After the second cycle, the capacity retention was calculated to be greater

than 99.8% per cycle, and little capacity fading was observed. This performance is attributed to the interfacial contact between $LiFePO_4$ and PEO polymer. The surface of $LiFePO_4$ is considered to have good wettability by PEO polymer or good chemical affinity to the polymer. The fact that $LiFePO_4$ is not charged beyond the electrochemical window of PEO electrolyte also works to maintain stable cycling.

Next, the influence of the different molecular weights of PEO is examined. Fig. 5 shows the first voltage curves with different polymers at 40 ◦C.

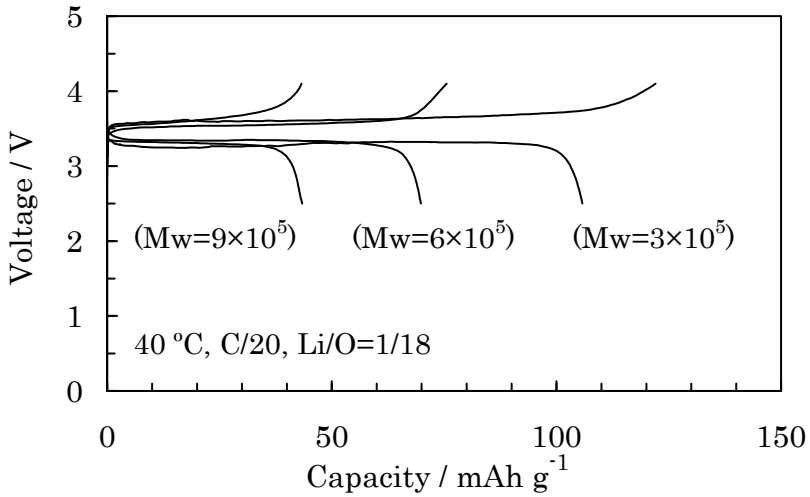

Fig. 5. Charge and discharge curves of $LiFePO_4$/C in the polymer electrolyte system. Comparison among molecular weights of PEO polymer of 3×10^5, 6×10^5, and 9×10^5. The Li/O ratio was fixed at 1/18, and the temperature was adjusted to 40 ◦C.

The capacity strongly depends on the molecular weight of PEO, and the electrolyte with lower molecular weight has better charge–discharge properties. This behavior is interpreted as being caused by a combination of several factors. One is the structure of the solid–solid interface. The interface between the electrode and the hard electrolyte with $Mw=9\times10^5$ consists mainly of a point contact, while the soft electrolyte with$Mw=3\times10^5$ should have a larger contact area. The difference in the actual interfacial areas leads to the different current densities and polarizations. The ionic conductivities of each polymer were measured in order to discuss the influence of ionic conductivity on performance. The conductivities of electrolytes at 40 ◦C with Mw= 9, 6, 3×10^5 were 5.24×10^{-5}, 4.04×10^{-5}, and 4.89×10^{-5} S cm^{-1}, respectively. Since the values are similar, ionic conductivity is assumed not to be the main reason for the different capacities. It is thought that the intercalation is not controlled by the mass transfer process under the

present experimental condition. Uchimoto et al. reported that the charge transfer resistance is dependent on the relaxation of the electrolyte solvent using polyethylene glycol dimethyl ether [19]. Although the polymers used in the present study have molecular weights that are several orders of magnitude higher than those examined by Uchimoto et al., their theory may explain our results.

Fig. 6 shows the influence of salt concentration in the same host polymer (Mw = 9×10^5) at 40◦C.

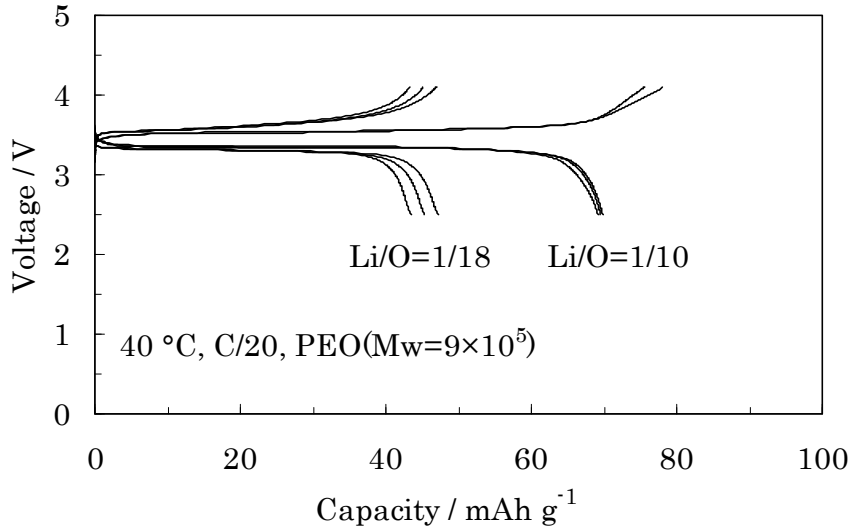

Fig. 5. Charge and discharge curves of $LiFePO_4$/C in the polymer electrolyte system. Comparison among molecular weights of PEO polymer of $3\times10_5$, $6\times10_5$, and $9\times10_5$. The Li/O ratio was fixed at 1/18, and the temperature was adjusted to 40 ◦C.

The electrolyte with a Li/O molar ratio of 1/10 shows a higher performance in that the discharge capacity becomes approximately 1.5 times larger than the standard 1/18 electrolyte. According to our conductivity measurement, PEO with Li/O at 1/10 shows a higher ionic conductivity than 1/18 at 40 ◦C, which suggests that the higher ionic conductivity results in lower interface resistance. It is also possible to apply the same explanation as in the case of the discussion on molecular weight. The electrolyte with Li/O = 1/10 has a soft nature because it contains more plasticizing imide salt. The effects of molecular weight and salt concentration in Figs. 5 and 6 only appear at low temperatures. At temperatures above 60 ◦C, these effects may be cancelled by strong segmental motion of polymer chains.

The interface resistance was analyzed by measuring impedance spectra. Since it is difficult to set a reference electrode in a polymer cell, the symmetrical cell $LiFePO_4$/PEO electrolyte/$LiFePO_4$ was constructed to remove the contribution of lithium electrode. The molecular weight of the PEO used herein is 6×10^5 and the Li/O ratio is fixed at 1/10. In this cell, the detectable components should be an interface between PEO and $LiFePO_4$, a bulk of PEO, and another bulk of $LiFePO_4$.

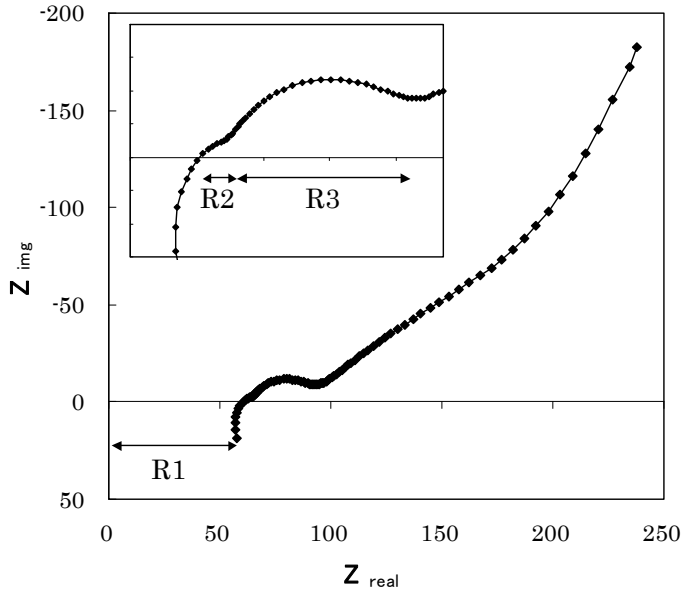

Fig. 7. Complex impedance plot (Cole–Cole plot) of the symmetrical cell, $LiFePO_4$/PEO electrolyte/$LiFePO_4$. The inset shows the enlarged spectrum of the high-frequency region. There are three components, which are designated R1, R2, and R3 (see text). The low-frequency area showing a slope and capacitive behaviour is considered to be caused by ionic diffusion in the polymer inside the electrode.

The typical spectrum is shown in Fig. 7, in which there are four major components. These components are simple ohmic resistance (R1), semicircles of two different sizes (R2, R3), and a straight line with a 45◦ slope indicating diffusion. The component that appears at the highest frequencies corresponds to the sum of the ionic resistance of PEO and the electronic resistance of $LiFePO_4$. On the other hand, the slope appearing in the lowest frequency region can be attributed to the lithium diffusion in the infiltrated PEO electrolyte inside the micro-pores of the electrode. In some cases, the spectrum shows a clear capacitive character following the slope. This is due to the finite diffusion length being limited by the thickness of the cast electrode layer. One of the two semicircles appears in the frequency range from 10^4 to 10^3 Hz. In general, the charge transfer reaction of the electrode has a time constant in this frequency range.

Thus, the resistance of lithium intercalation at the interface between $LiFePO_4$ and PEO is assigned to this larger semicircle (R3). Another small semicircle is located around 10^5 Hz. The frequency range shows a fairly fast charge transfer with a small relaxation time. This component R2 is thought to be part of a series of interfacial ionic transfer processes, such as ionic adsorption and surface diffusion. However, no experimental evidence for identification was obtained in the present study.

The resistance values of R1, R2, and R3 were obtained by fitting the experimental data to the equivalent circuit, which is composed of a serial combination of R1 and two RC pairs consisting of a resistor connected in parallel with a capacitor. Arrhenius plots of these resistances are shown as a function of temperature in Fig. 8.

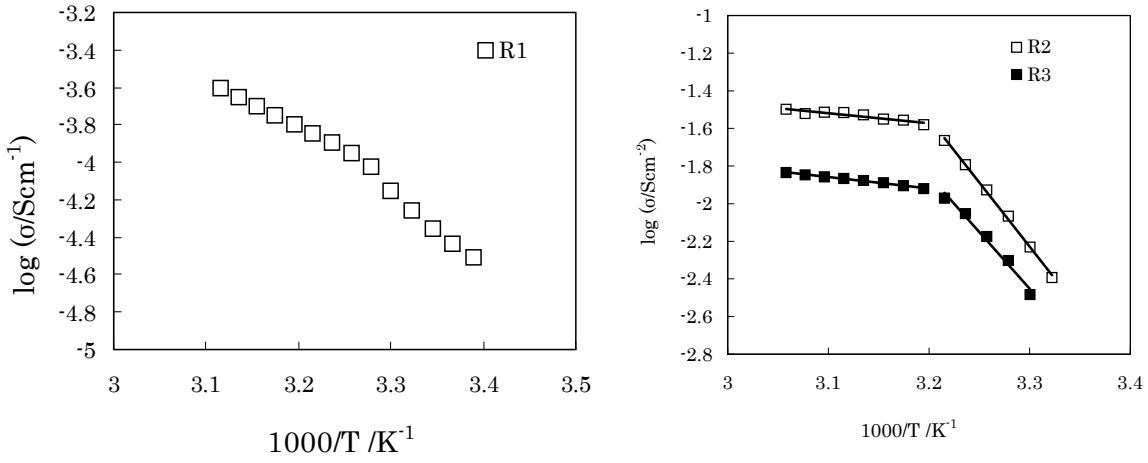

Fig. 8. Arrhenius plots of R1, R2, and R3. Data were recorded every 2 ◦C between 20 and 60 ◦C in the direction of heating. The conductivity values of the R2 and R3 component are expressed in the unit of S cm^{-2}, because they refer to the interface.

The resistance R1, which consists mainly of the polymer electrolyte, shows a slightly bent line, which is characteristic when the salt concentration Li/O is fixed at 1/10. The bending point is located around 35 ◦C, which corresponds to the crystallization (melting) temperature of polymer bulk. R3 is considered to be the charge transfer resistance of LiFePO4, and the small R2 resistance results in the sharp bend in the plot at approximately 40 ◦C. This change is also considered to stem from the crystallization of the polymer. The magnitude of the charge transfer resistance of R3 is controlled by the nature of the polymer, whether in liquid or solid form.

The activation energies are estimated, and they ummarized in Table 1. The energy of charge transfer is only approximately 10 kJ mol^{-1} above 40 ◦C, which is surprisingly small, and this value is comparable to the values measured in the liquid electrolyte system. This data explains the good charge–discharge performance shown in Fig. 4 and indicates that the LiFePO4/PEO system can operate at temperatures down to 40 ◦C. The activation process in the charge transfer in the liquid electrolyte system is considered to be caused by the desolvation of lithium ions at the interface, and the activation energy of the process is calculated to be approximately 50 kJ mol^{-1} [20]. The small activation energies in Table 1 suggest that the lithium ion phase transfer proceeds without complete desolvation. Note also that the Arrhenius plot of R2 has the same profile as R3, which supports the idea that R2 is a process at the electrode/electrolyte interface.

Table 1

Activation energies of the component R2 and R3 are calculated based on the plots shown in Fig. 8

	Activation Energy (40 – 54 ºC) /kJ mol^{-1}	Activation Energy (28 – 38 ºC) /kJ mol^{-1}
R2	10.2	130.5
R3	11.6	115.2

The high-rate performance at 40 ◦C was examined for the composite cell system after optimization such that the molecular weight of PEO was chosen at 3×10^5 and the Li/O ratio was set to be 1/10. For the electrode preparation, another new procedure was adopted whereby $LiFePO_4$/C, vapor-grown carbon fiber (VGCF; Showa Denko), and polymer electrolytes were mixed at 4:1:5 wt%. VGCF as a conducting agent is a graphitized carbon having a diameter of 150 nm and a length of 10–20 μm. The one-dimensional fiber morphology can act as a good current conductor, even in the thicker electrode. No polymeric binders were included because the PEO electrolyte can work to hold the film in a solid shape. The mixture in AN was cast on the aluminum foil and then dried at room temperature in the argon-filled glove box. After being cut into the desired dimensions, the mixture was dried at 120 ◦C under a vacuum

for 12 h in order to remove AN completely. Other components of the laminate cell are subjected to the same conditions.

The charge–discharge performances of the optimized electrode at 40 ◦C are shown in Fig. 9.

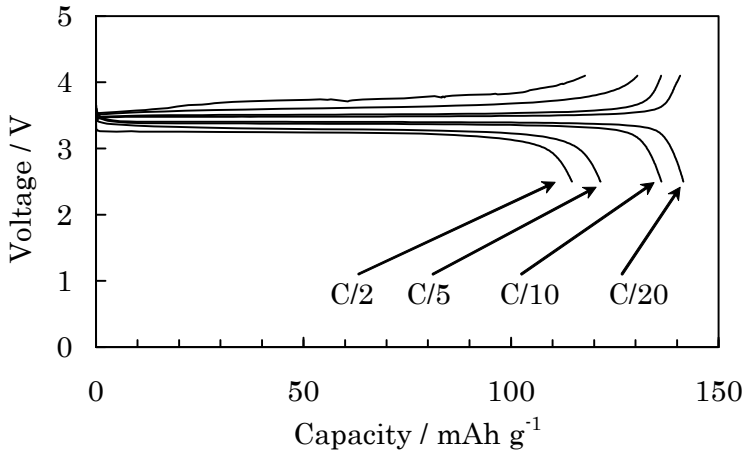

Fig. 9. Rate performance of the optimized positive electrode system measured at 40 ◦C. The $LiFePO_4$/C composite electrode was combined with the polymer electrolyte in which the molecular weight of PEO was 3×10^5 and the Li/O ratio was fixed at 1/10. VGCF was used as a conducting agent.

The capacity at C/20 is 140 mAh g^{-1}, which is comparable to the maximum capacity in the liquid electrolyte system. At C/2, the reversible capacity is greater than 100 mAh g^{-1}. Such high capacity under the high rate with a dry polymer electrolyte at 40 ◦C is remarkable. These performances show the potential possibility of an all-solid lithium ion battery containing the LiFePO4 positive electrode and polymer electrolyte. Furthermore, the optimization of the interface is expected to lead to the enhancement of low-temperature performance.

4. Conclusion

As the positive electrode of a dry polymer lithium ion battery, $LiFePO_4$ and carbon composite materialwas revealed to provide promising performance. This is attributed to the particularly low activation energy between $LiFePO_4$ and PEO electrolyte in the liquid phase. This unique interface allows considerable opportunity for modification, and a consequent improvement in the charge transfer rate. If the crystallization temperature of the component R3 is further reduced, an all-solid state polymer battery,

which operates practically at room temperature, can be realized. However, softening of the polymer electrolyte results in a safety problem. It is important to develop a total cell system to reconcile the good compatibility of electrode/electrolyte and adequate safety at the same time.

References

[1] T. Lapp, S. Skaarup, A. Hooper, Solid State Ionics 11 (1983) 97.

[2] Y. Inaguma, L. Chen, M. Itoh, T. Nakamura, T. Uchida, M. Ikuta, M. Wakihara, Solid State Commun. 86 (1993) 689.

[3] P.G. Bruce, A.R. West, J. Solid State Chem. 53 (1984) 430.

[4] J.B. Bates, N.J. Dudney, G.R. Gruzalski, R.A. Zuhr, A. Choudhury, C.F. Luck, J. Power Sources 43 (1993) 103.

[5] R. Kanno, M. Murayama, J. Electrochem. Soc. 148 (2001) A742.

[6] S. Seki, Y. Kobayashi, H. Miyashiro, A. Yamanaka, Y. Mita, T. Iwahori, J. Power Sources 146 (2005) 741.

[7] K. Amine, J. Liu, I. Belharouak, Electrochem. Commun. 7 (2005) 669.

[8] M. Koltypin, D. Aurbach, L. Nazar, B. Ellis, Electrochem, Solid State Lett. 10 (2007) A40.

[9] K. Zaghib, P. Charest, A. Guerfi, J. Shim, M. Perrier, K. Striebel, J. Power Sources 134 (2004) 124.

[10] P. Reale, S. Panero, B. Scrosati, J. Garche, M. Wohlfahrt-Mehrens, M. Wachtlerb, J. Electrochem. Soc. 151 (2004) A2138.

[11] G.B. Appetecchi, J. Hassoun, B. Scrosati, F. Croce, F. Cassel, M. Salomon, J. Power Sources 124 (2003) 246.

[12] A. D'Epifanio, F. Serraino Fiory, S. Licoccia, E. Traversa, B. Scrosati, F. Croce, J. Appl. Electrochem. 34 (2004) 403.

[13] H. Miyashiro, Y. Kobayashi, T. Nakamura, S. Seki, Y. Mita, A. Usami, Electrochemistry 74 (2006) 321.

[14] Y. Kato, T. Ishihara, Y. Uchimoto, M. Wakihara, J. Phys. Chem. B 108 (2004) 4794.

[15] F. Serraino Fiory, F. Croce, A. D'Epifanio, S. Licoccia, B. Scrosati, E. Traversa, J. Eur. Ceram. Soc. 24 (2004) 1385.

[16] J.B. Kerr, Y.B. Han, G. Liu, C. Reeder, J. Xie, X. Sun, Electrochim. Acta 50 (2004) 235.

[17] A. Yamada, S.C. Chung, K. Hinokuma, J. Electrochem. Soc. 148 (2001) A224.

[18] Y. Liu, J. Yang, N. Imanishi, A. Hirano, Y. Takeda, O. Yamamoto, J. Power Sources 146 (2005) 376.
[19] Y. Uchimoto, K. Amezawa, T. Furushita, M.Wakihara, I. Taniguchi, Solid State Ionics 176 (2005) 2377.
[20] T. Abe, F. Sagane, M. Ohtsuka, Y. Iriyama, Z. Ogumi, J. Electrochem. Soc. 152 (2005) A2151.

1.2. Study on All Solid Lithium Polymer Batteries with the $LiFePO_4$/C Cathode

1. Introduction

Recently, many scientists and engineers are interested in new lithium ion batteries. It is considered that the liquid electrolyte should be replaced by ionic liquid or solid electrolyte, because these electrolyte cause safety problem for large scale battery. The polymer battery, with all-solid polymer electrolyte, is considered as the most suitable device for electric vehicle (EV) and plug-in hybrid vehicle (PHEV) due to their production cost, light-weight and flexibility for cell design [1, 2]. Polyethylene oxide (PEO) is widely used as surfactants, cosmetics and food additives, which are commercially available in a relatively pure state at reasonable cost. This polymer also is well known as alkali metal ion conductor and PEO electrolyte with $LiN(CF_3SO_2)_2$ (LiTFSI) shows the conductivity of 10^{-3} above 60 ºC. The significant conductivity occurs through the amorphous phase where there is segmental motion of the polymer chains. However, PEO based electrolyte shows the semi-crystalline behavior. The phase transition restricts the segmental motion, which corresponds to the decreasing of lithium ion conduction in the polymer electrolyte [3, 4]. G.B. Appetecchi et al. reported that the PEO based polymer battery, $LiFePO_4$/SPE/Li, showed excellent performance at high temperature around 100 ^oC [5]. $LiCoO_2$ and $LiMn_2O_4$ are widely used for lithium ion battery researches. However, the choice of these materials as cathodes is restricted in this report because the stability window of PEO based electrolytes does not exceed 4 V vs. Li/Li^+ and PEO-LiTFSI electrolyte lead to dissolve the aluminum foil as current collector[6, 7]. It was reported that $LiFePO_4$ was the best candidate for the cathode material in solid lithium ion batteries with PEO based electrolyte, due to the low volume change by lithium insertion and extraction, a low working potential of 3.5 V vs. Li/Li^+, low cost, and a high thermal decomposition temperature. In our previous work, we reported the low temperature performance of a Li/PEO-LiTFSI/$LiFePO_4$ cell [8]. Polymer electrolytes can be formed as quite thin film, therefore decreasing the interfacial resistances between electrode and electrolyte is indispensable to low-temperature working of the cell. In this study, the interface resistance between Li_xFePO_4 and PEO-LiTFSI was examined using a symmetrical cell Li_xFePO_4/PEO-LiTFSI/Li_xFePO_4 as a function of the molecular weight of PEO and the content of LiTFSI in PEO.

2. Experimental

Electrolytes

The PEO based electrolyte was prepared according to the previously reported solvent casting technique with acetonitrile (AN) as a solvent. PEO (Aldrich Chemical, average molecular weight 3×10^5, 6×10^5 and 9×10^5) and $Li(CF_3SO_2)_2N$ (LiTFSI, Wako) were dissolved in AN with a molar ratio of Li/O = 1/10, 1/15 and 1/18. The polymer electrolyte solution was cast in a polytetrafluoroethylene (PTFE) dish under a dry argon atmosphere. After evaporation of AN at room temperature, the film was dried at 110 °C for 12 h under vacuum. The thicknesses of the polymer electrolytes used for AC impedance measurements and charge-discharge tests were ca. 500 μm, and ca. 1 mm for conductivity measurements.

Composite electrodes

The cathode electrodes consisted of carbon-coated $LiFePO_4$ (Hohsen Co., carbon content 2.0 wt%, average particle size 3.3 μm), vapor grown carbon fiber (VGCF; Showa Denko, Japan, average diameter 150 nm, length ca. 20 μm) and the polymer electrolyte mixed in AN (4:1:5 weight ratio). The solution was painted on aluminum foil and the AN solvent was allowed to slowly evaporate at room temperature under a dry argon atmosphere, and was then dried at 110 °C for 12 h under vacuum. The electrode film thickness was in a range of 20-70 μm and the active electrode area was 2.25 cm^2 (1.5×1.5 cm^2). The reversible capacity of the composite $LiFePO_4$ electrode at 50 °C was 140 mAh g^{-1} at 1/10 C and 100 mAh g^{-1} at 3 C.

Cell assembling

The conductivities of the polymer electrolytes were measured using a symmetrical blocking cell, Cu/PEO-LiTFSI/Cu. A symmetrical non-blocking cell was used to measure the interfacial resistance between the electrolyte and the electrode. The lithium content in Li_xFePO_4 was changed using a Al/Li_xFePO_4/PEO-LiTFSI/SS-mesh/PEO-LiTFSI/Li_xFePO_4/Al cell (SS: stainless steel). The cell was assembled with two working electrodes arranged face to face. A constant current was passed between the SS-mesh and the Al foil as a current corrector to deposit Li metal on the SS-mesh. AC impedance measurements of the electrolyte were performed in the temperature range of 40 to 60 °C. An AC perturbation of 10 mV was applied in the frequency range from 1×10^6 to 0.1 Hz using a Solartron1260

frequency response analyzer. In order to ensure good contact between the electrolyte and electrode, the cells were initially heated to 80 °C and then cooled down to the measurement temperature.

3. Results and discussion

PEO-LiTFSI electrolyte

Conductivities of PEO-LiTFSI electrolytes with different compositions are plotted in figure 1. Fig.1-A shows the temperature dependence of the electrical conductivity (σ) for PEO_{18} LiTFSI with different molecular weight (M_w) of PEO. PEO-LiTFSIs have conductivity knees around 50 °C which corresponds to the phase transition temperature of the electrolyte. The transition temperature decreases with decreasing molecular weight of PEO. Fig.1-B shows the temperature dependence of the electrical conductivity for PEO (M_w=6x10^5)-LiTFSI with different content of LiTFSI. According to the phase diagram of PEO-LiTFSI, in some compositions, the electrolyte shows crystalline behavior around 50 °C and PEO_{12}LiTFSI shows eutectic point [3, 4]. The PEO_{10}LiTFSI electrolyte shows no clear phase transition until 30 ºC.

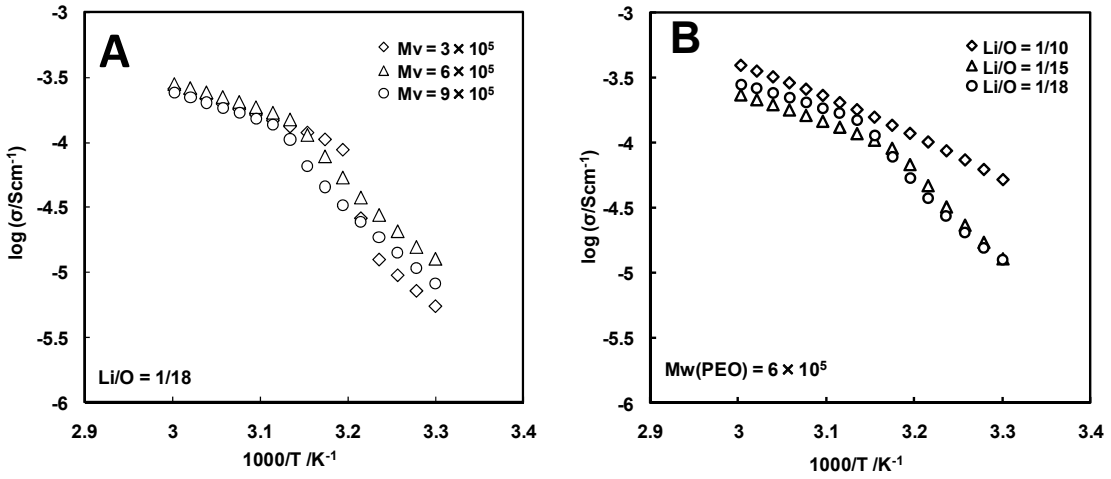

Fig. 1 Temperature dependence of the electrical conductivity (σ) for PEO-LiTFSI

A: PEO18LiTFSI with different molecular weight of PEO, B; PEO-LiTFSI with different content of LiTFSI.

Composite electrodes

Optical microscope images of the $LiFePO_4$-VGCF-PEO-LITFSI composite electrodes on Al foil are shown in Figure 2. These photos indicate that carbon fibers, VGCF, are uniformly dispersed over the PEO-$LiFePO_4$ matrix. It leads good electronic conduction points in the electrode. Acetylene black (AB) is well-known as electron conducting additives for lithium ion batteries. However, in polymer composite electrode, fine particles are unsuitable element because the dispersed polymer electrolyte intercepts the conduction path between active materials and current collectors. Therefore, VGCF is used as conducting additive in this report.

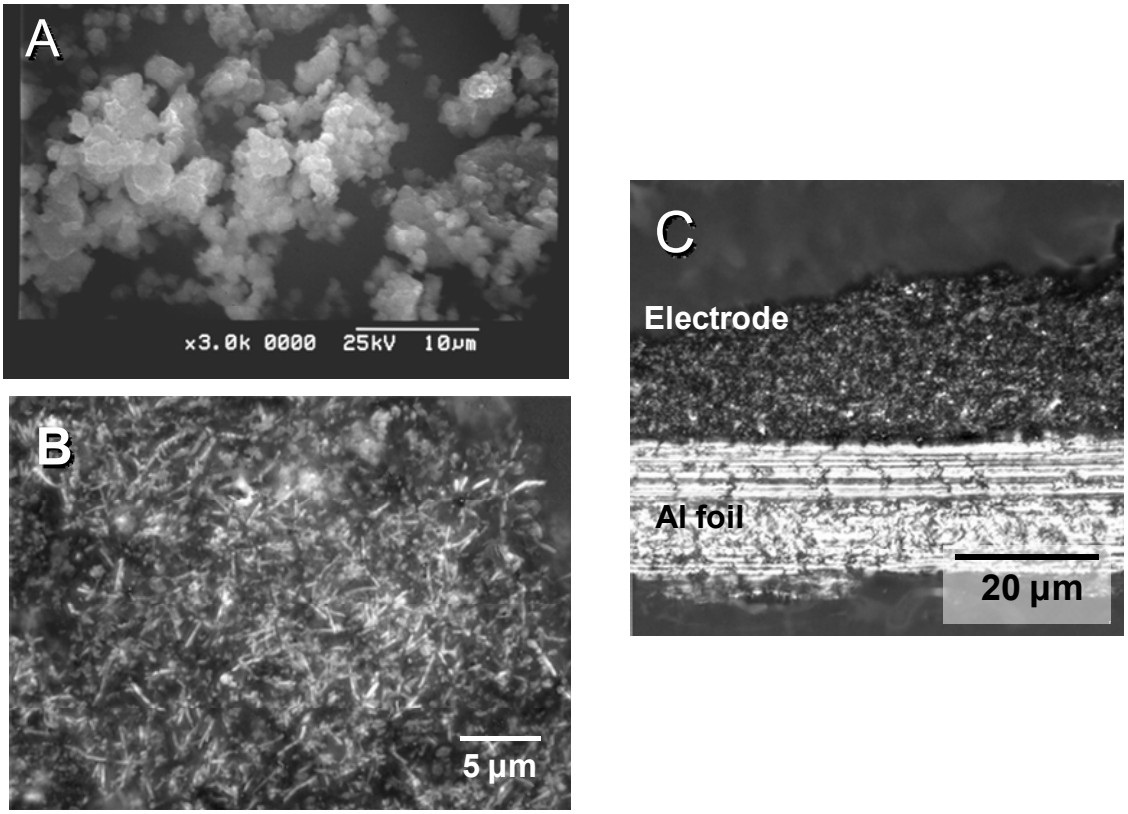

Fig. 2 SEM and photomicroscope images of $LiFePO_4$-C.

A; SEM image of $LiFePO_4$-C, B: Surface photomicroscope image of the composite electrode

C; Cross section image of the composite electrode

Electrochemical properties

Figure 3 shows the impedance spectrum of a symmetrical cell ($Al/Li_{0.98}FePO_4$-C/PEO_{10}LiTFSI/$Li_{0.98}FePO_4$-C/Al) at 50 °C, in which there are four major resistance components. These resistance components are a simple ohmic resistance (R0), a resistance in the high frequency range (small semicircle, R1), a resistance in the middle frequency range (semicircle, R2), and a resistance in the low frequency range (large semicircle, R3). The R0 and R1 resistances have the same profiles as that observed for Cu/PEO_{10}LiTFSI/Cu. Polyethylene oxide shows both crystalline (or semicrystalline) structure at room temperature, and amorphous one at the temperature above the melting point of the polymer. Therefore, both R0 and R1 are assigned to the resistances of the PEO electrolyte which are caused by the ionic transport through mixed phases of crystalline and amorphous domains occurred at room temperature. To attribute the resistance R2 and R3, the impedance profile was investigated as a function of x in Li_xFePO_4, in next paragraph.

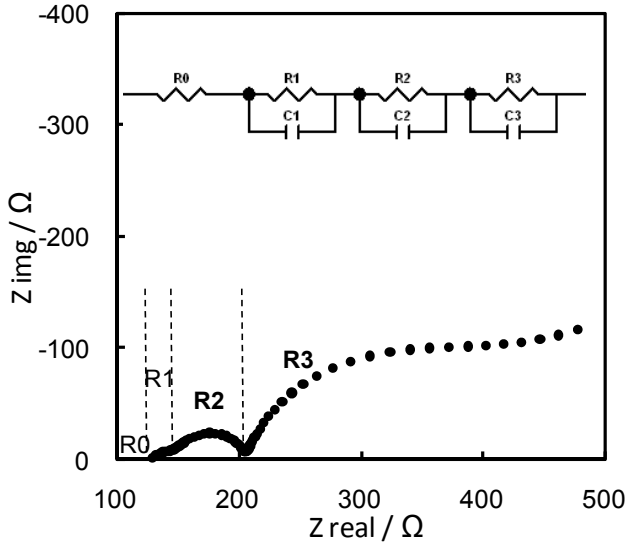

Fig. 3 Impedance profile of the symmetrical cell, $Al/Li_{0.98}FePO_4/PEO_{10}$.LiTFSI/$Li_{0.98}FePO_4$/Al at 50 ºC
PEO: $M_W=6x10^5$

The function of the Li content in Li_xFePO_4 is shown in figure 4 which value was changed with the help of following cell; Al/Li_xFePO_4 /PEO_{10}LiTFSI/SS-mesh/ PEO_{10}LiTFSI /Li_xFePO_4/Al. The Li content in Li_xFePO_4 was changed *in situ* using a third SS-mesh electrode inserted into the polymer electrolyte, as described in the experimental section. The electrode containing $LiFePO_4$ exhibits blocking behavior as

a vertical spike, and only two semicircles are observed (R1 and R3). Saturation of the $LiFePO_4$ structure with lithium ions is indicated by the blocking characteristics, whereas lithium deficient $Li_{0.98}FePO_4$ exhibits non-blocking behavior. The R2 and R3 resistance values were obtained by fitting the experimental data using the equivalent circuit shown in Figure 3.

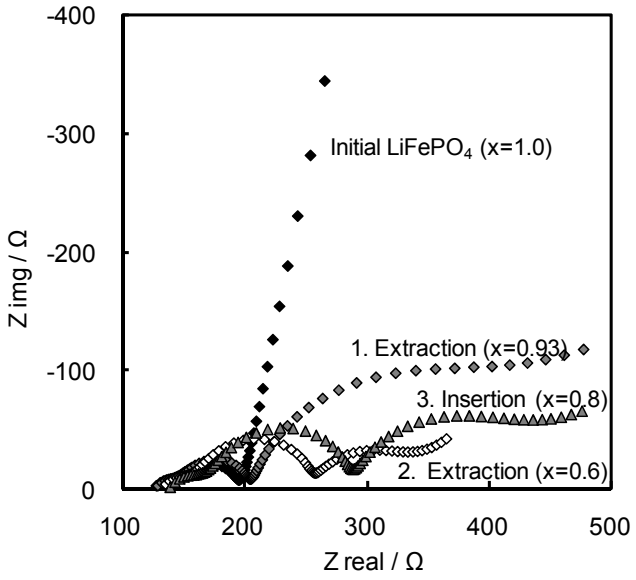

Fig. 4 Impedance profile of the symmetrical cell, Al/Li_xFePO_4/PEO_{10}-LiTFSI/Li_xFePO_4/Al at 50 ºC as a function of the Li content of Li_xPO_4 (PEO: M_W=6x10^5)

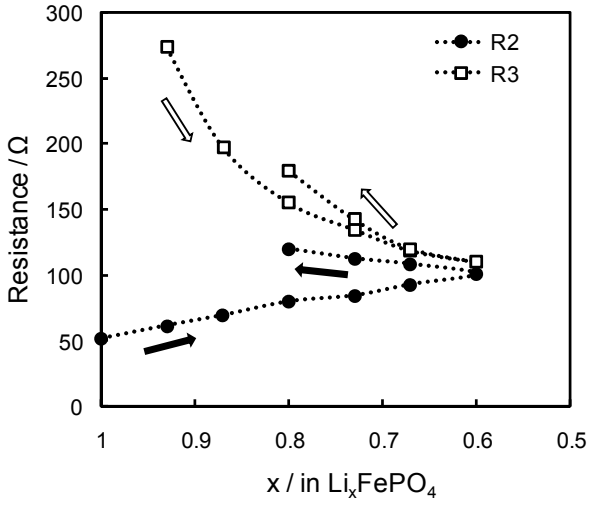

Fig. 5 R2 and R3 vs. x in Li_xFePO_4 curves at 50 ºC (PEO;Mw=6x105, Li/O=1/10)

The compositional dependence of R2 and R3 is shown in Figure 5. R2 (10^4 to 10^3 Hz) increases and R3 (10 to 1 Hz) decreases with decreasing x in Li_xFePO_4. There are reversible change (R3) and irreversible one (R2) with the change in x, which suggests that R3 corresponds to the charge transfer resistance between the polymer electrolyte and Li_xFePO_4. R2 can be reasonably assigned from its arising frequencies to the ionic transport in the polymer electrolyte inside the composite electrode. The linear increase in the resistance may be attributed to the SEI formation near the boundary between polymer and $LiFePO_4$ particles.

To clarify the origin of R2 and R3, the cell impedance of Al/$Li_{0.98}FePO_4$-C/PEO_xLiTFSI (x=10 and 18)/$Li_{0.98}FePO_4$-C/Al was measured and the temperature dependence of R2 and R3 as Arrhenius plots are shown in Figure 6. In Fig.6-A, R2 observed in the cell with PEO_{18}LiTFSI has a jump in conductivity near 50 °C and R3 is a straight line. In contrast, R2 and R3 for the cell with PEO_{10}LiTFSI exhibits no clear knee in the temperature range measured. The Activation energies of R3 for PEO_{10}LiTFSI and PEO_{18}LiTFSI were calculated as 75 kJ mol^{-1} and 87 kJ mol^{-1}, respectively. The activation process for R3 is not affected by the electrolyte phase transition, which suggests that R3 could be considered as the charge transfer resistance. On the other hand, the R2 resistance is affected by the phase transition of the polymer electrolyte; R2 with PEO_{18}LiTFSI jumps at around 50 °C, the temperature that corresponds to the phase transition of the polymer electrolyte. Therefore, R2 could be attributed to an ion transfer to the active site for charge transfer in the composite electrode.

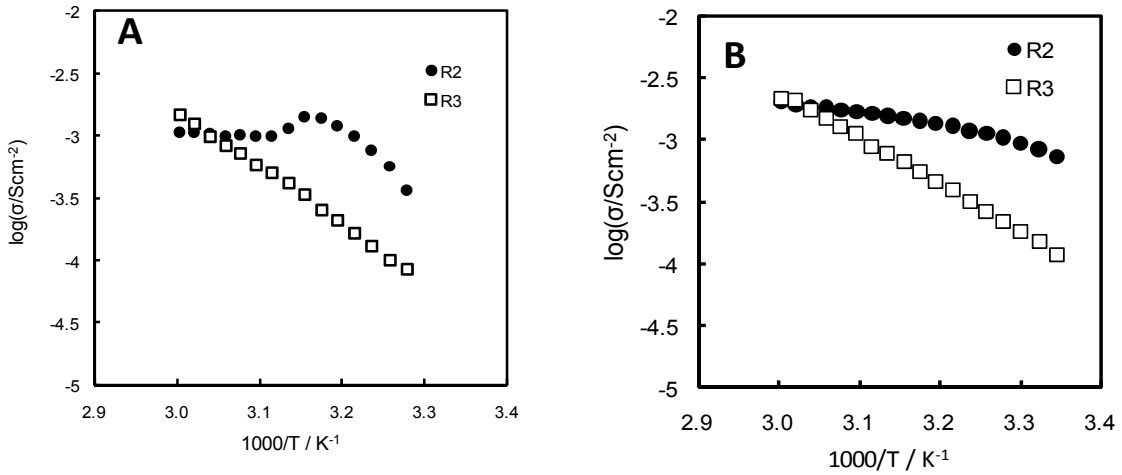

Fig. 6 Temperature dependence of R2 and R3 for the cell, Al/$Li_{0.98}FePO_4$/PEO_xLiTFSI/$Li_{0.98}FePO_4$/Al (PEO: M_W =6×10^5) A: Li/O=1/18, B: Li/O=1/10

The activation energies of R2 and R3 were estimated and summarized in Table 1. The activation energy of R2 increases with increasing of LiTFSI content in the electrolyte which is considered as a reasonable profile because PEO-LiTFSI electrolytes have a maximum conductivity at the content of LITFSI around Li/O=1/20. The activation energy of R3 decreases slightly with increasing of the LiTFSI content. In contrast, the molecular weight of PEO leads no significant change for both R2 and R3. These results suggest that the charge transfer resistance (R3) is dominated by the SEI near the boundary between polymer and $LiFePO_4$ particles.

Table 1 Activation energies for the charge transfer resistance and for the interfacial layer resistance as a function of the Li/O ration and the molecular weight of PEO.

Mv(PEO)	Li salt content (Li/O)	Li salt	Activation energy R2 ($kJmol^{-1}$)	Activation energy R3 ($kJmol^{-1}$)
$6x10^5$	1/18	LiTFSI	7	87
$6x10^5$	1/15	LiTFSI	10	85
$6x10^5$	1/10	LiTFSI	16	74
$3x10^5$	1/10	LiTFSI	13	73
$9x10^5$	1/10	LiTFSI	12	74

4. Conclusions

The interface resistance between Li_xFePO_4 and PEO-LiTFSI was examined using AC impedance measurements with a symmetrical cell as a function of the PEO molecular weight and the content of LiTFSI in PEO in the temperature range of 30-60 °C. Four resistances, R0, R1, R2 and R3 were distinguished. The resistances in the high frequency region (R0 and R1) were considered to be resistance of the PEO electrolyte. R2 and R3 are dependent on x in Li_xFePO_4 and this dependence suggests that R3 in the low frequency region is related to the charge transfer resistance. R2 was considered to be related to the internal resistance of the composite electrode. The activation energies were affected by the conductivity of polymer electrolyte. On the other hand, the molecular weight of PEO leads no significant change for both R2 and R3. These results suggest that the charge transfer resistance (R3) is dominated by the SEI near the boundary between polymer and $LiFePO_4$ particles.

References

1) B. Scrosati, F. Croce, S. Panero: “Progress in lithium battery R&D” J. Power Sources, **100** (2001) 93-100.

2) M. Gauthier, D. Fauteux, G. Vassort, A. Bélanger, M. Duval. P. Ricoux, J. -M. Chabagno, D. Muller, P. Rigaud, M. B .Armand, D. Deroo: “Assessment of Polymer-Electrolyte Batteries for EV and Ambient Temperature Applications” J. Electrochem. Soc., **132** (1985) 1333-1340.

3) S. Lascaud, M. Perrier, A. Vallée, S. Besner, J. Prud’homme, M. Armand: “Phase Diagrams and Conductivity Behavior of Poly(ethylene oxide)-Molten Salt Rubbery Electrolytes” Macromolecules, **27** (1994) 7469-7477.

4) C. Labrèche, I. Lévesque, J. Prud’homme Macromolecues: “An Appraisal of Tetraethilsulfamide as Plasticizer for Poly(ethylene oxide)-LiN(CF3SO2)2 Rubbery Electrolytes” Macromolecules, **29** (1996) 7795-7801.

5) G.B. Appetecchi, J. Hassoun, B. Scrosati, F. Croce, F. Cassel, M. Salomon: “Hot-pressed, solvent-free, nanocomposite, PEO-based electrolyte membranes Ⅱ. All solid-state Li/$LiFePO_4$ polymer batteries” J. Power Sources, **124** (2003) 246-253.

6) Y. Xia, K. Tatsumi, T. Fujieda, P.P. Prosini, T. Sakai: “Solid-State Lithium-Polymer Batteries Using Lithiated MnO_2 Cathodes”J. Electrochem. Soc., **147** (2000) 2050-2056.

7) Q. Li, N. Imanishi, A. Hirano, Y. Takeda, O. Yamamoto: “Four volts class solid lithium polymer batteries with a composite polymer electrolyte” J. Power Sources, **110** (2002) 38-45.

8) K. Hanai, T. Maruyama, N. Imanishi, A. Hirano, Y. Takeda. O. Yamamoto: “Enhancement of electrochemical performance of lithium dry polymer battery with $LiFePO_4$/C composite cathode” J. Power Sources, **178** (2008) 789-794.

1.3. Interfacial properties between $LiFePO_4$ and poly(ethylene oxide)-$Li(CF_3SO_2)_2N$ polymer electrolyte

1. Introduction

Rechargeable solid lithium polymer batteries (SLPB) are considered to be a promising candidate for large-scale batteries in electric vehicles (EV), plug-in hybrid vehicles (PHEV), and as back-up storage for solar cells, because of their low production cost, high reliability, safety, and flexibility for cell design [1,2]. Conventional SLPBs have used lithium metal anodes and oxide cathodes such as V_2O_5 to ensure high-energy density [3]. However, this type of SLPB, with a lithium metal anode, has been reported to have serious safety problems. Recently, Imanishi et al. reported the possibility of using a carbon anode with a solid lithium polymer electrolyte [4]. A carbon anode could be coupled with cathode materials containing lithium, such as $LiCoO_2$, $LiMn_2O_4$, and $LiFePO_4$. However, the choice of cathode materials is somewhat restricted by the thermodynamic stability of the polymer electrolyte. The stability window of typical solid polymer electrolytes, such as poly(ethylene oxide) (PEO) based electrolytes, does not exceed 4 V vs. Li/Li^+ [5]. The typical cathode materials for lithium ion batteries, such as $LiCoO_2$ and $LiMn_2O_4$, can not be used for the cathode in PEO electrolyte cells, because their working potentials are around 4 V vs. Li/Li^+. Croce et al. reported that $LiFePO_4$ was the best candidate for the cathode material in SLPBs with PEO based electrolyte, due to the low volume change by lithium insertion and extraction, a low working potential of 3.5 V vs. Li/Li^+, low cost, and a high thermal decomposition temperature [6]. A reversible capacity of 140 mAh g^{-1} at 100 °C was observed for a Li/PEO-$LiCF_3SO_3$/$LiFePO_4$ cell, which is comparable with 165 mAh g^{-1} obtained for Li/PC-DMC-$LiPF_6$/$LiFePO_4$ at room temperature [7]. In previously reported solid lithium polymer cells with $LiFePO_4$ cathodes, high capacity was observed only at higher temperatures and low current density, such as 0.05 mA cm^{-2} [8]. The charge-discharge performance of SLPBs is strongly dependent on the interface resistance between the electrode and the electrolyte, especially at low temperature [9,10].

In our previous work, we reported the low temperature performance of a Li/PEO-LiTFSI/$LiFePO_4$ cell; the interfacial resistance between PEO-LiTFSI and $LiFePO_4$ was not significantly dependent on the molecular weight of PEO and the

content of LiTFSI in PEO [11,12]. In this study, the interface resistance between Li_xFePO_4 and PEO-LiTFSI was examined using a symmetrical Li_xFePO_4/PEO-LiTFSI/Li_xFePO_4 cell and the interface resistances were analyzed as a function of the operation temperature and the electrode composition (x in Li_xFePO_4).

2. Experimental

The PEO based electrolyte was prepared according to the previously reported solvent casting technique with acetonitrile (AN) as a solvent [13]. PEO (Aldrich Chemical, average molecular weight 6×10^5) and $Li(CF_3SO_2)_2N$ (LiTFSI, Wako) were dissolved in AN with a molar ratio of Li/O = 1/10. The polymer electrolyte solution was cast in a polytetrafluoroethylene (PTFE) dish under a dry argon atmosphere. After evaporation of AN at room temperature, the film was dried at 110 °C for 12 h under vacuum. The thicknesses of the polymer electrolytes used for AC impedance measurements and charge-discharge tests were ca. 500 μm, and ca. 1 mm for conductivity measurements.

The cathode electrodes consisted of carbon-coated $LiFePO_4$ (Hohsen Co., carbon content 2.0 wt%, average particle size 3.3 μm), vapor grown carbon fiber (VGCF; Showa Denko, Japan, average diameter 150 nm, length ca. 20 μm) and the polymer electrolyte mixed in AN (4:1:5 weight ratio). The solution was painted on aluminum foil and the AN solvent was allowed to slowly evaporate at room temperature under a dry argon atmosphere, and was then dried at 110 °C for 12 h under vacuum. The electrode film thickness was in a range of 20-70 μm and the active electrode area was 2.25 cm^2 (1.5×1.5 cm^2). The reversible capacity of the composite $LiFePO_4$ electrode at 50 °C was 140 mAh g^{-1} at 1/10 C and 100 mAh g^{-1} at 3 C.

A target for sputtering $LiFePO_4$ was prepared by a solid state reaction method [14]. Li_2CO_3, $FeC_2O_4\cdot H_2O$ and $(NH_4)H_2PO_4$ powders (Nacalai Tesque) were mixed in a 1:2:2 molar ratio. The mixture was ground and pressed into a tablet, which was then sintered at 700 °C for 6 h under 2% H_2-Ar. The product was crushed and the procedure repeated. The final powder was pressed into a tablet of 5.5 cm in diameter as the sputtering target. The $LiFePO_4$ film was deposited on Au foil by RF magnetron sputtering (Ulvac, SCOTT-C3). Sputtering of $LiFePO_4$ was carried out for 15 min in pure Ar at a working pressure of 2×10^{-2} Torr. The as-sputtered $LiFePO_4$ film was then annealed at 700 °C under 2% H_2-Ar. The thickness of the electrode was approximately 500 nm, as measured by cross sectional observation of scanning electron microscope image (SEM; Hitachi, S-2300S).

The conductivities of the polymer electrolytes were measured using a symmetrical blocking cell, Cu/PEO-LiTFSI/Cu. A symmetrical non-blocking cell was used to measure the interfacial resistance between the electrolyte and the electrode. The lithium content in Li_xFePO_4 was changed using a Al/Li_xFePO_4/PEO-LiTFSI/SS-mesh/PEO-LiTFSI/Li_xFePO_4/Al cell (SS: stainless steel). The cell was assembled with two working electrodes arranged face to face. A constant current was passed between the SS-mesh and the Al foil as a current corrector to deposit Li metal on the SS-mesh. AC impedance measurements of the electrolyte were performed in the temperature range of 30 to 60 °C. An AC perturbation of 10 mV was applied in the frequency range from 1×10^6 to 0.1 Hz using a Solartron1260 frequency response analyzer. In order to ensure good contact between the electrolyte and electrode, the cells were initially heated to 80 °C and then cooled down to the measurement temperature.

3. Results and discussion

Figure 1 shows the impedance spectrum of a symmetrical cell (Al/$Li_{0.98}FePO_4$-C/PEO_{10}LiTFSI/$Li_{0.98}FePO_4$-C/Al) at 50 °C, in which there are four major resistance components.

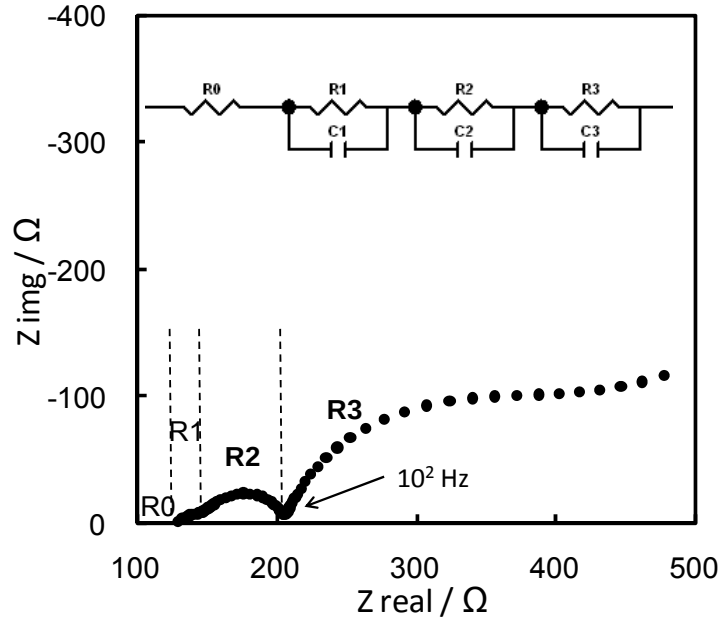

Fig.1. Impedance spectrum for Al/$Li_{0.98}FePO_4$/PEO_{10}LiTFSI/$Li_{0.98}FePO_4$/Al at 50 °C.

These resistance components are a simple ohmic resistance (R0), a resistance in the high frequency range (small semicircle, R1), a resistance in the middle frequency range (semicircle, R2), and a resistance in the low frequency range (large semicircle, R3). The R0 and R1 resistances have the same profiles as that observed for Cu/PEO_{10}LiTFSI/Cu. Therefore, both R0 and R1 are assigned to the resistances of the PEO electrolyte which are caused by the ionic transport through mixed phases of crystalline and amorphous domains occurred at room temperature.

Figure 2 shows the impedance profiles of a symmetrical cell (Al/Li_xFePO_4-C/PEO_{10}LiTFSI/Li_xFePO_4-C/Al) at 50 °C as a function of x in Li_xFePO_4. The Li content in Li_xFePO_4 was changed *in situ* using a third SS-mesh electrode inserted into the polymer electrolyte, as described in the experimental section. The electrode containing $LiFePO_4$ exhibits blocking behavior with a vertical spike, and only two semicircles are observed. Saturation of the $LiFePO_4$ structure with lithium ions is indicated by the blocking characteristics, whereas lithium deficient $Li_{0.98}FePO_4$ exhibits non-blocking behavior.

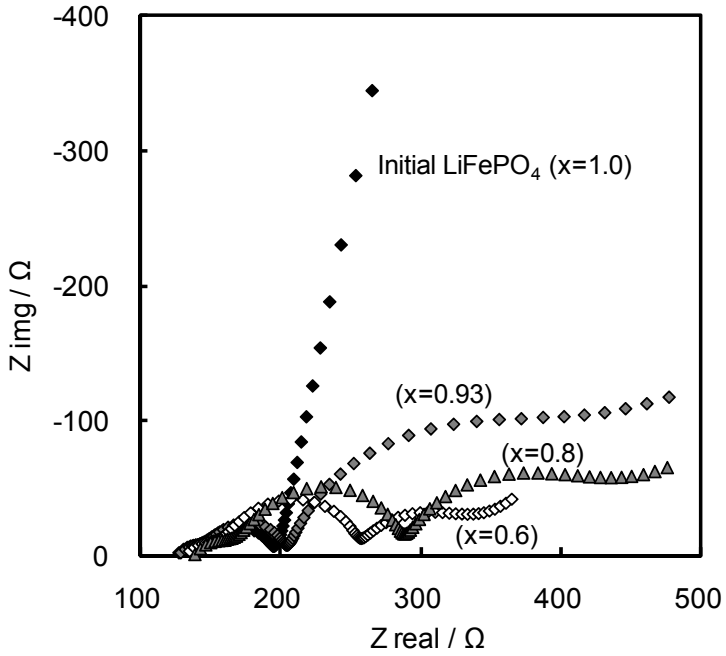

Fig. 2. Impedance spectra for Al/Li_xFePO_4/PEO_{10}LiTFSI/Li_xFePO_4/Al at 50 °C for various x in Li_xFePO_4.

The R2 and R3 resistance values were obtained by fitting the experimental data using the equivalent circuit shown in Figure 1. The compositional dependence of R2 and R3 is shown in Figure 3.

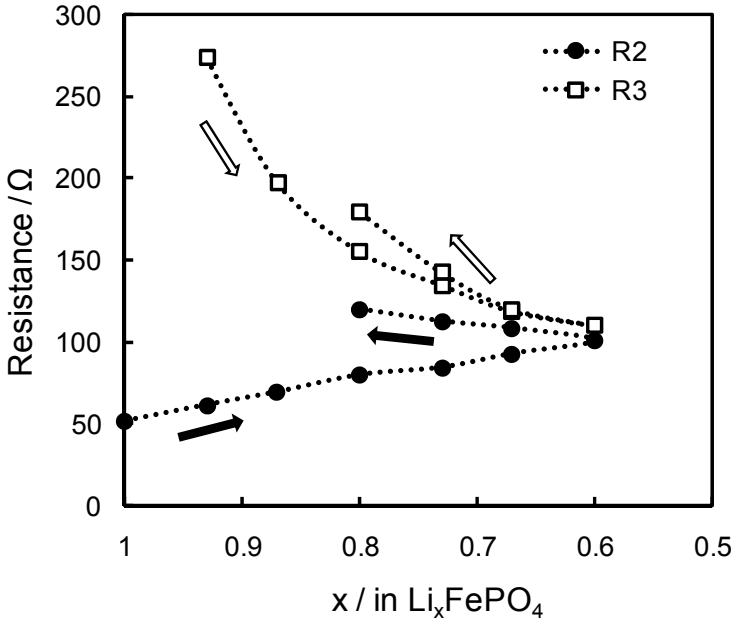

Fig. 3. Interface resistances of R2 and R3 as a function of x in Li_xFePO_4 at 50 °C.

R2 (10^4 to 10^3 Hz) increases and R3 (10 to 1 Hz) decreases with decreasing x in Li_xFePO_4. R3 changed reversibly and R2 irreversibly with the change in x, which suggests that R3 corresponds to the charge transfer resistance between the polymer electrolyte and Li_xFePO_4. Srinivasan et al. [15] reported that Li_xFePO_4 was a two phase mixture of $LiFePO_4$ and $FePO_4$ in the range x=0.9525 to 0.002. Therefore, the active area for the charge transfer reaction increases with decreasing x, which results in a decrease of the charge transfer resistance. Bruce [16] and Franger et al. [17] reported similar impedance profiles for cells with a polymer electrolyte and liquid electrolyte, respectively. They suggested that the two semicircles are consistent with a complex electrochemical reaction that involves more than a simple electron transfer between the redox couple and the electrode. The reaction may involve adsorption or a chemical step in addition to the charge transfer process. The impedance spectra of $LiFePO_4$ with a liquid electrolyte, as reported by Shin et al. [18], showed two depressed semicircles, and those by Takahashi et al. [19] only one depressed semicircle; however, these reports did not report the content of Li in Li_xFePO_4.

To clarify the origin of R2 and R3, the cell impedance of Al/$Li_{0.98}FePO_4$-C/PEO_xLiTFSI (x=10 and 18)/$Li_{0.98}FePO_4$-C/Al was measured and the temperature dependence of R2 and R3 are shown in Figure 4. PEO-LiTFSI has a knee in the conductivity curve at

around 60 °C, which corresponds to the phase transition temperature of the electrolyte. PEO_{18}LiTFSI has a conductivity knee at near 50 °C, and PEO_{10}LiTFSI shows no clear phase transition behavior until 30 °C [20,21]. R2 and R3 for the cell with PEO_{10}LiTFSI exhibits no clear knee in the temperature range measured. In contrast, R2 observed in the cell with PEO_{18}LiTFSI has a jump in conductivity near 50 °C and R3 is a straight line. The activation energies of R3 for PEO_{10}LiTFSI and PEO_{18}LiTFSI were calculated as 75 kJ mol^{-1} and 87 kJ mol^{-1}, respectively. The activation process for R3 is not affected by the electrolyte phase transition, which suggests that R3 could be considered as the charge transfer resistance. On the other hand, the R2 resistance is affected by the phase transition of the polymer electrolyte; R2 with PEO_{18}LiTFSI jumps at around 50 °C, the temperature that corresponds to the phase transition of the polymer electrolyte. Therefore, R2 could be attributed to an ion transfer to the active site for charge transfer in the composite electrode.

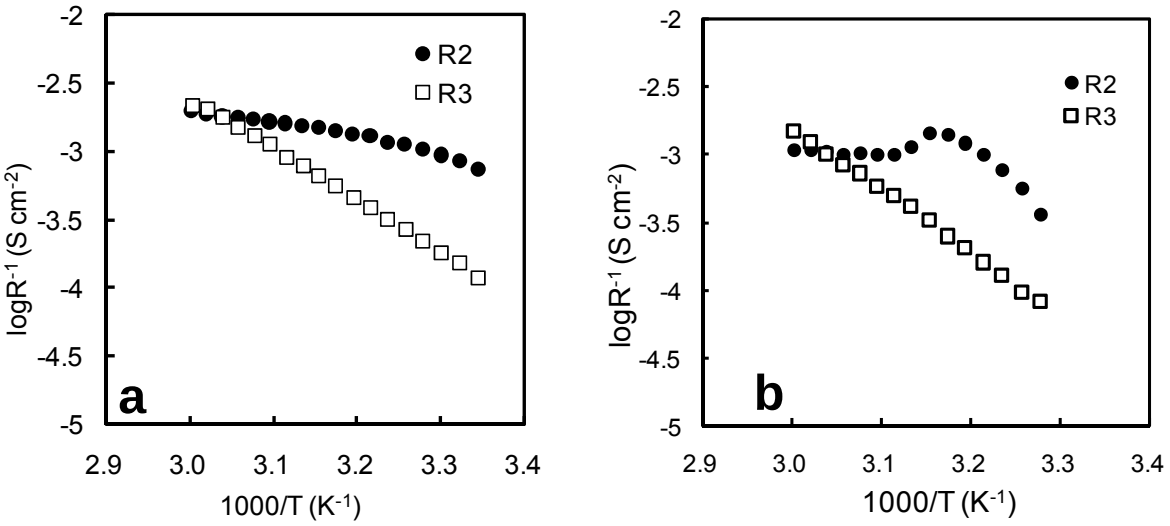

Fig. 4. Temperature dependence of the interface resistance of R2 and R3 measured for cells with different polymer electrolytes. a: Al/$Li_{0.98}FePO_4$/PEO_{10}LiTFSI/$Li_{0.98}FePO_4$/Al, b: Al/$Li_{0.98}FePO_4$/PEO_{18}LiTFSI/$Li_{0.98}FePO_4$/Al.

To confirm the effect of the additive in the electrode, a $LiFePO_4$ thin film electrode was prepared by RF sputtering on an Au substrate to eliminate the effect of the polymer electrolyte and the conductive VGCF additive in the composite electrode. The obtained sputtered film had the same XRD pattern as that for powdered $LiFePO_4$. The thickness of the film estimated from SEM images was approximately 500 nm. Figure 5

shows impedance spectra of a symmetrical cell with the sputtered $LiFePO_4$ thin film electrode and $PEO_{18}LiTFSI$ electrolyte at 50 °C. The as-sputtered electrode exhibits blocking behavior and only the sum of $PEO_{18}LiTFSI$ resistance, R0-R1, is obtained, that is, the composition of the film is considered to be $LiFePO_4$. Lithium was extracted from $LiFePO_4$ using the SS-mesh in the polymer electrolyte. The impedance profile of $Li_{0.1}FePO_4$ is also shown in Figure 5. A small semicircle in the high frequency range and a large depressed semicircle are observed. The first semicircle corresponds to the resistance of the polymer electrolyte. The frequency range of the second semicircle is similar that of R3 for the composite electrode shown in Figure 2. It should be emphasized that the thin film electrode without the polymer electrolyte and the conductive VGCF additive has no semicircle in the intermediate frequency range, which corresponds to R2. Therefore, R2 can be reasonably assigned from its arising frequencies to the ionic transport in the polymer electrolyte inside the composite electrode. The linear increase in the resistance may be attributed to the SEI formation near the boundary between polymer and $LiFePO_4$ particles.

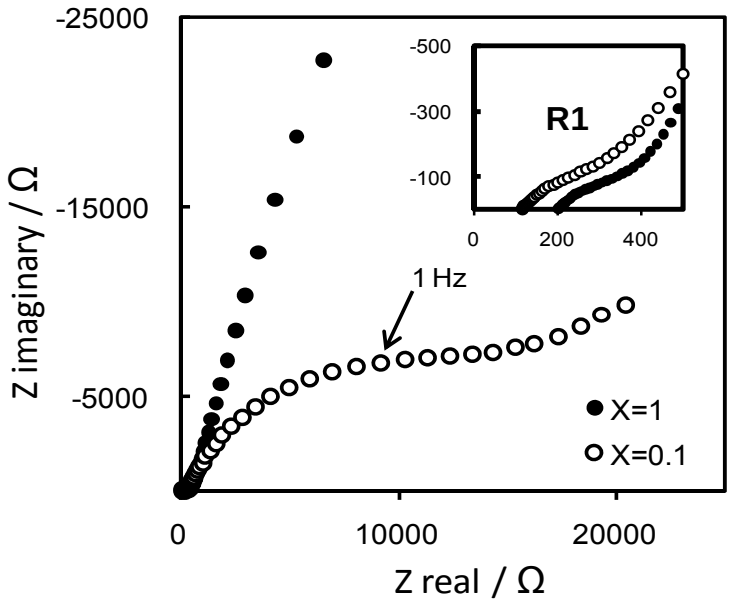

Fig. 5. Impedance spectra for Au/sputtered Li_xFePO_4/$PEO_{10}LiTFSI$/sputtered Li_xFePO_4/Au at 50 °C.

An Arrhenius plot of the R3 resistance for the sputtered electrode with $PEO_{18}LiTFSI$ is shown in Figure 6. The activation energy calculated from the temperature dependence is 77 kJ mol^{-1}, the value of which is comparable to that of the composite electrode with $PEO_{18}LiTFSI$, as shown in Figure 4. It is concluded that R2 is dominated by the

polymer electrolyte in the composite electrode, and R3 is due to the charge transfer resistance between the polymer electrolyte and Li_xFePO_4.

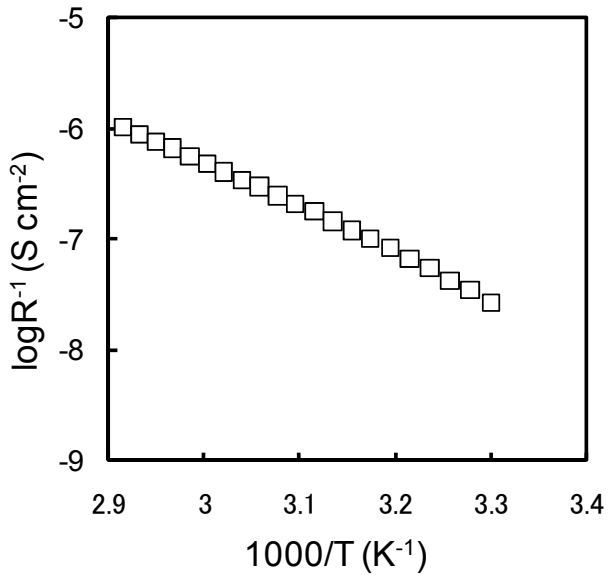

Fig. 6. Arrhenius plot of the R3 interface resistance obtained for Au/sputtered Li_xFePO_4/PEO_{10}LiTFSI/sputtered Li_xFePO_4/Au.

The influence of electrode thickness on the interface resistance of the composite electrode with $LiFePO_4$-C:VGCF:PEO_{10}LiTFSI (4:1:5 weight ratio) was examined in the temperature range of 60-40 °C and the results are summarized in Table 1.

Table 1. Dependence of the interface resistance and activation energy on electrode thickness of the $LiFePO_4$:VGCF:$(PEO)_{10}$LiTFSI (4:1:5 weight ratio) composite electrode in the temperature range of 60-40 °C.

Electrode properties			Resistance at 50 °C (x=0.7)		Activation energy	
Thickness	Weight	Active material weight	R2	R3	R2	R3
μm	mg cm^{-2}	mg cm^{-2}	Ω cm^{-2}	Ω cm^{-2}	kJ mol^{-1}	kJ mol^{-1}
21	1.1	0.4	616	1796	6	63
36	3.6	1.4	167	580	26	73
56	6.0	2.4	149	225	40	70

R2 and R3 decrease with increasing electrode thickness. These resistances depend on the surface area of $LixFePO_4$-C/polymer electrolyte, which are enlarged by increasing the thickness of the electrode. This clearly indicates that R2 is assigned to the ionic transport across the polymer layer formed on the $LiFePO_4$ particles. Activation energies for R3 revealed no significant change with the thickness. On the other hand, the activation energies for R2 show a clear dependence on the thickness, and that of a thick 56 μm electrode was 40 kJ mol^{-1}. The value of the activation energy is comparable to that for the electrical conductivity of PEO_{10}LiTFSI, which suggests that the diffusion of lithium ions in the polymer electrolyte with a thick composite electrode is the rate determining step for R2.

Table 2 shows the dependence of the ratio of electrode materials ($LiFePO_4$-C,VGCF) and PEO_{10}LiTFSI on R2 and R3. R2 and R3 decrease with decreasing polymer electrolyte content in the electrode. Activation energies for R3 have no dependence on the polymer electrolyte content of the electrode. In contrast, the activation energy for R2 increases with decreasing polymer electrolyte content in the electrode. The frequency range of R2 is slightly lower than that of the bulk polymer electrolyte. It is considered that the R2 resistance is dominated by the PEO electrolyte within the electrode; the segmental conduction polymer is restricted to of lithium ions due to the complicated structure of the electrode.

Table 2. Dependence of the interface resistance and activation energy on the electrode composition of the $LiFePO_4$-VGCF-PEO_{10}LiTFSI composite electrode.

Electrode composition ($4LiFePO_4$-VGCF) : (PEO_{10}LiTFSI)	Electrode properties			Resistance at 50 °C (x=0.7)		Activation energy	
	Thickness	Weight	Active material weight	R2	R3	R2	R3
	μm	mg cm^{-2}	mg cm^{-2}	Ω cm^{-2}	Ω cm^{-2}	kJ mol^{-1}	kJ mol^{-1}
40 : 60	42	3.1	0.97	653	527	10	67
70 : 30	44	4.4	1.0	180	324	44	76

4. Conclusions

The interface resistance between Li_xFePO_4 and PEO-LiTFSI was examined using AC impedance measurements with a symmetrical cell in the temperature range of 30-60 °C. Four resistances, R0, R1, R2 and R3 were distinguished. The resistances in the high frequency region (R0 and R1) were considered to be resistance of the PEO electrolyte. R2 and R3 are dependent on x in Li_xFePO_4 and this dependence suggests that R3 in the low frequency region is related to the charge transfer resistance. R2 was considered to be related to the internal resistance of the composite electrode, because the sputtered $LiFePO_4$ electrode had no semicircle corresponding to R2 in the same frequency range. The activation energy for R2 was affected by the thickness and composition of the electrode. The activation energy for a thick composite electrode with a low content of polymer electrolyte was comparable to that of the polymer electrolyte. On the other hand, the activation energy for R3 was not affected by the thickness and composition of the electrode.

References

[1] B. Scrosati, F. Croce, S. Panero, *J. Power Sources* 100 (2001) 93-100.

[2] M. Gauthier, D. Fauteux, G. Vassort, A. Bélanger, M. Duval. P. Ricoux, J.-M. Chabagno, D. Muller, P. Rigaud, M. B .Armand, D. Deroo, *J. Electrochem. Soc*. 132 (1985) 1333-1340.

[3] G. B. Appetecchi, J. H. Shin, F. Alessandrini, S. Passerini, *J. Power Sources* 143 (2005) 236-242.

[4] N. Imanishi, Y. Ono, K. Hanai, R. Uchiyama, Y. Liu, A. Hirano, Y. Takeda, O. Yamamoto, *J. Power Sources* 178 (2008) 744-750.

[5] Y. Xia, K. Tatsumi, T. Fujieda, P. P. Prosini, T. Sakai, *J. Electrochem. Soc*. 147 (2000) 2050-2056.

[6] F. Croce, F. S. Fiory, L. Persi, B. Scrosati, *Electrochem. and Solid-State Letters* 4 (2001) A121-A123.

[7] A. Yamada, S. C. Chung, K. Hinokuma, *J. Electrochem. Soc*. 148 (2001) A224-A229.

[8] G. B. Appete*cchi, J. Hassoun, B. Scrosati, F. Croce, F. Cassel, M. Salomon,* J. Power Sources 124 (2003) 246-253.

[9] Q. Li, T. Itoh, N. Imanishi, A. Hirano, Y. Takeda, O. Yamamoto, *Solid State Ionics* 159

(2003) 97-109.
[10] Q. Li, N. Imanishi, Y. Takeda, A. Hirano, O. Yamamoto, *Electrochem. and Solid-State Letters* 7 (2004) A470-A473.
[11] K. Hanai, T. Matsumura, N. Imanishi, A. Hirano, Y. Takeda, O. Yamamoto, *J. Power Sources* 178 (2008) 789-794.
[12] K. Hanai, R. Uchiyama, N. Imanishi, A. Hirano, Y. Takeda, O. Yamamoto, *J. Jpn. Soc. Power Powder Metallurgy* 56 (2009) 71-75.
[13] C. Capiglia, J. Yang, N. Imanishi, A. Hirano, Y. Takeda, O. Yamamoto, *J. Power Sources* 119-121 (2003) 826-832.
[14] K. F. Chiu, H. Y. Tang, B. S. Lin, *J. Electrochem. Soc.* 154 (2007) A364-A368.
[15] V. Srinivasan and J. Newman, *J. Electrochem. Soc.* 151 (2004) A1517-A1529.
[16] P. G. Bruce, *Electrochimica Acta* 40 (1995) 2077-2085.
[17] S. Franger, S. Bach, J. Farcy, J.-P. Pereira-Ramos, N. Baffier, *Electrochimica Acta* 48 (2003) 891-900.
[18] H. C. Shin, W. H. Cho, H. Jang, *Electrochimica Acta* 52 (2006) 1472-
[19] M. Takahashi, S. Tobishima, K. Takei, Y. Sakurai, *Solid State Ionics* 148 (2002) 283-289.
[20] S. Lascaud, M. Perrier, A. Vallée, S. Besner, J. Prud'homme, M. Armand, *Macromolecules* 27 (1994) 7469-7477.
[21] C. Labrèche, I. Lévesque, J. Prud'homme, *Macromolecues* 29 (1996) 7795-7801.

Part 2: Anode

The first half of Part2 is based on the investigation of the combination of Graphite and PEO-LiTFSI. Most commercialized liquid-type Lithium-ion batteries are based on the graphite anode. To prepare graphite anode slurry, we need to add some surfactants because of the hydrophobic behaviors of carbons. PEO-based electrolyte shows the hydrophilic behavior. This mismatching restricts the practical use of carbon anode for SLPB. Surface-modification on graphite is considered to be one of solutions to combine graphite and PEO-based electrolyte. In this section, the electrochemical behaviors of Surface-modified meso-carbon micro-beads (MCMB) were investigated as composite anode materials for SLPB.

In the latter half of part2, Si-based anode materials have investigated for liquid-type Lithium-ion battery. Silicon is well-known as high-capacity anode materials. However, silicon shows poor capacity retention due to the low-conductivity and large volume change during the charge-discharge process. Silicon-carbon composite anode is considered to be a suitable solution to overcome the capacity-fading. In this study, high energy mechanical milling (HEMM) and thermal pyrolysis reactions with polyvinilchloride (PVC) were combined to prepare the silicon/disordered carbon composite.

2.1. Surface-modified meso-carbon micro-beads anode for dry polymer lithium-ion batteries

2.2. Morphology-stable silicon-based composite for Li-intercalation

2.3. Electrochemical studies of the Si-based composites with large capacity and good cycling stability as anode materials for rechargeable lithium ion batteries

2.1. Surface-modified meso-carbon microbeads anode for dry polymer batteries

1. Introduction

Lithium polymer batteries have been considered as a promising technology, for it is able to satisfy the requirements of future applications such as stand-by power and electric vehicles (EV) [1]. Polymer batteries reported previously have used a lithium metal anode and an oxide cathode to attain a high-energy density [2,3]. Generally, formation of lithium dendrites during charging the lithium metal anode remains one of the major issues of battery with liquid electrolyte [4]. Even in the case of polymer electrolyte, this phenomenon exists, although it was shown to be less important than in liquid electrolyte. Dolle et al. reported the visual dendrite growth on lithium and copper sheet at 80 ◦C in lithium/polymer batteries with help of in situ scanning electron microscope [5,6].

A significant improvement in lithium/polymer electrolyte interface has been achieved by use of polymer electrolytes with an inorganic filler [7]. However, the polymer battery with large amount of metallic lithium is not a practical choice, if considering the abuse of large scale batteries for EV or hybrid electric vehicles (HEV). It seems necessary to explore alternative anodes other than lithium metal for polymer batteries.Yang et al. have proposed alloy anodes, which consist of Sn (or SnSb) and $Li_{2.6}Co_{0.4}N$. This new concept anode for polymer electrolyte showed the initial reversible capacity as high as 800 mAh g^{-1}, but the capacity gradually decreased to 400 mAh g^{-1} after 10 cycles [8]. More recently, Liu et al. reported the composite anode of $Li_{2.6}Co_{0.4}N/Co_3O_4$ for polymer batteries with less capacity fading by cycling. The initial capacity recorded 600 mAh g^{-1}, but the capacity fadingwas not suppressed adequately [9]. Effort for searching a higher reversible anode for polymer electrolyte is still necessary.

The chemical reactivity of anode and polymer electrolyte is another factor for choosing a safe anode material. Reaction tendency between the anode candidates and polymer electrolyte were examined by a differential scanning calorimetry. The reaction heat of the $Li_{2.6}Co_{0.4}N/Co_3O_4$ composite anode is 1.2 $J(mAh)^{-1}$, which is much lower compared to that of lithium metal anode of 5 $J(mAh)^{-1}$. Whereas, the reaction heat of the graphite anode and polymer was estimated as low as 0.9 $J(mAh)^{-1}$ by our preliminary experiment. Thus, the carbon anode is found most attractive with respect of the safety issue. However, only few papers have been reported on the polymer batteries

with carbon materials anode. Tsumura et al. reported brief results for natural graphite and surface-modified graphite anode in polymer electrolyte [10]. It is commonly recognized that the interface resistances between the graphite and the polymer electrolyte are quite large and it is difficult to pass a large current. This is due to poor compatibility between the carbon and polymer electrolyte.

In this study, the compatibility of carbon anode against polymer electrolyte has been improved by the surface modification of MCMB by low-crystalline carbon. This is achieved by pyrolysis of carbon precursors mixed with MCMB particles. Our earlier study on silicon/carbon composite anode reveals that PVC among several carbon precursors results in the good result [11]. Therefore, the electrochemical behaviors of the MCMB modified by pyrolysis of PVC have been examined in polyethylene oxide (PEO)-based electrolyte system.

2. Experimental

MCMB (Osaka Gas Chemicals Co. Ltd.) was used as the starting material. PVC (Aldrich) as a carbon precursor and counterpart of the composite has the average molecular weight of about 62,000. MCMB and PVC in 7:3 weight ratio were mixed with THF and then dried at 60 ◦C for 1 h. The dry powder was pressed into a tablet and heated at 700 ◦C for 6 h under argon gas flow to produce surface-modified MCMB. The product was examined by X-ray diffraction (XRD) using Cu Kradiation, Raman spectroscopy and scanning electron microscope (SEM) observation.

The composite electrode with polymer electrolyte was prepared as follows. $Li(CF_3SO_2)_2N$ (Fluka) was dissolved into anhydrous acetonitrile (AN), then the surface-modified MCMB and acetylene black were added into the solution. Next, PEO (Aldrich: Mw= 6×10^5) was dissolved and stirred for 3 h. The ratio of MCMB, acetylene black, $Li(CF_3SO_2)_2N$, and PEO was 52:10:10:28 in wt% (MCMB: 20 mg). The Li/O ratio in PEO/$Li(CF_3SO_2)_2N$ electrolyte was 1/18. The anode slurry was spread on a copper foil with a thickness of about 20 μm, dried at 120 ◦C under vacuum for 3 h to remove AN completely, and finally pressurized to make a sure contact in the whole system. The graphite materials of TIMCAL SFG-44 and TIMCAL KS-6 were compared with MCMB.

The polymer electrolyte sheet as a separator was prepared following the previously reported method [12]. A given weight of PEO (Mw = 6×10^5) and $Li(CF_3SO_2)_2N$ (Li/O = 1/18) with 10 wt% of $BaTiO_3$ was added into AN. After strong stirring overnight, the viscous solution was cast in a Teflon dish. After AN was slowly and completely evaporated, the obtained film was further dried at 90 ◦C under vacuum

for 8 h. The conductivity of the polymer electrolyte was as high as 5×10^{-4} S cm^{-1} at 60 ◦C, which is comparable to the previously reported value [13].

The electrode performance was examined using a coin type cell (CR2025). Lithium metal was used as the counter electrode. Porous nickel foam was inserted between the backside of MCMB electrode and the cathode can to increase internal pressure and make sure the contact of components. The active area of the electrode was 1.54 cm^2 and the thickness of PEO electrolyte was about 300 μm. The cells were galvanostatically charged and discharged in the voltage range of 0.01–2.0V. A current density of 0.05mAcm^{-2} (1/20C) was applied and temperature was kept at 60 ◦C. Cyclic voltamograms (CV) were measured by Solartron 1287 potentiostat.

3. Results and discussion

Lithium intercalation performances of several types of synthetic graphite were compared in the cells with liquid electrolytes and polymer electrolytes. The plate type TIMCAL SFG-44 (average diameter; 15 μm), the flake-shape graphite TIMCAL KS-6 (average particle size; 5 μm) and the spherical MCMB (particle size; 20–30 μm) were examined. SEM images of these artificial graphites are shown in Fig. 1.

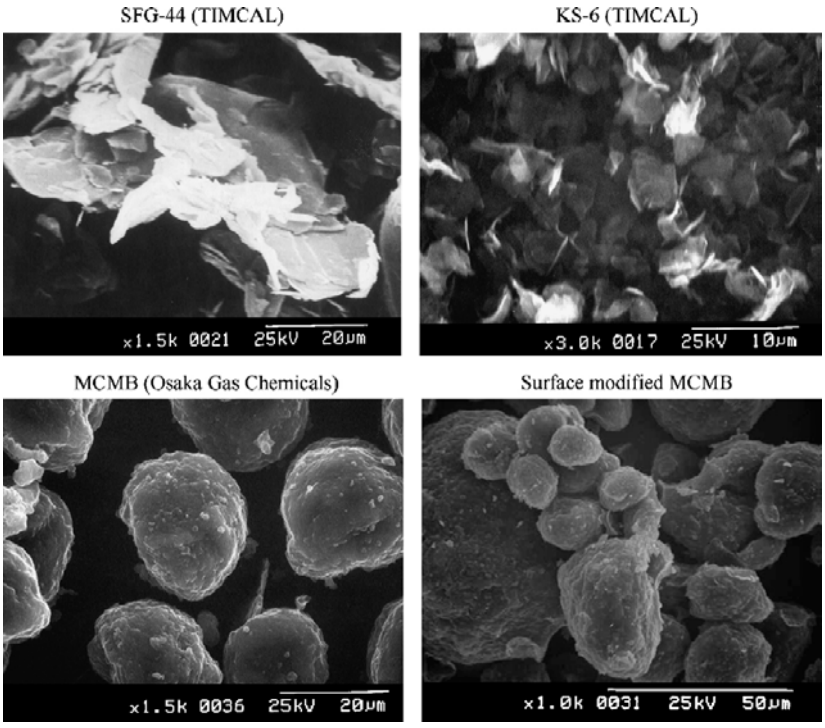

Fig. 1. SEM photos of artificial graphites SFG-44, KS-6, MCMB before and after the modification.

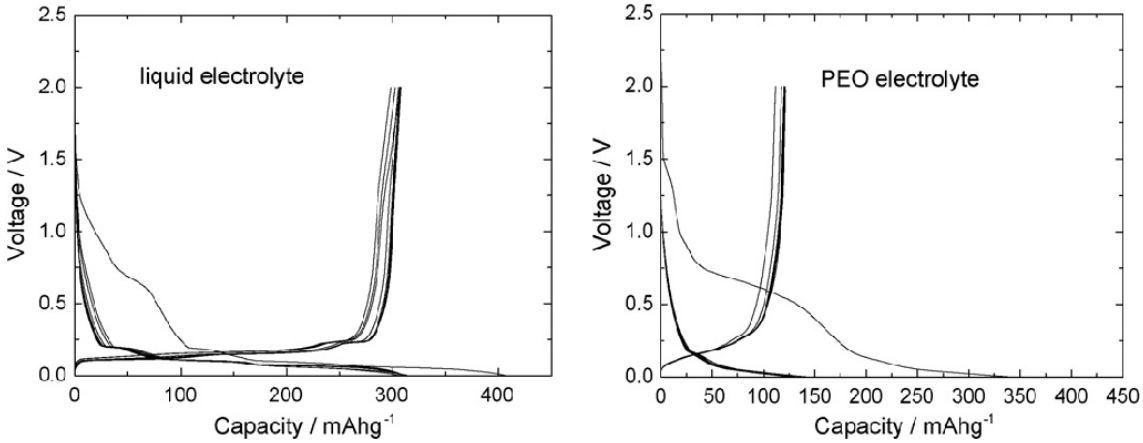

Fig. 2. Charge–discharge curves of artificial graphite SFG-44 in EC-DEC-$LiClO_4$ at room temperature and in PEO-$Li(CF_3SO_2)_2N$ at 60◦C.

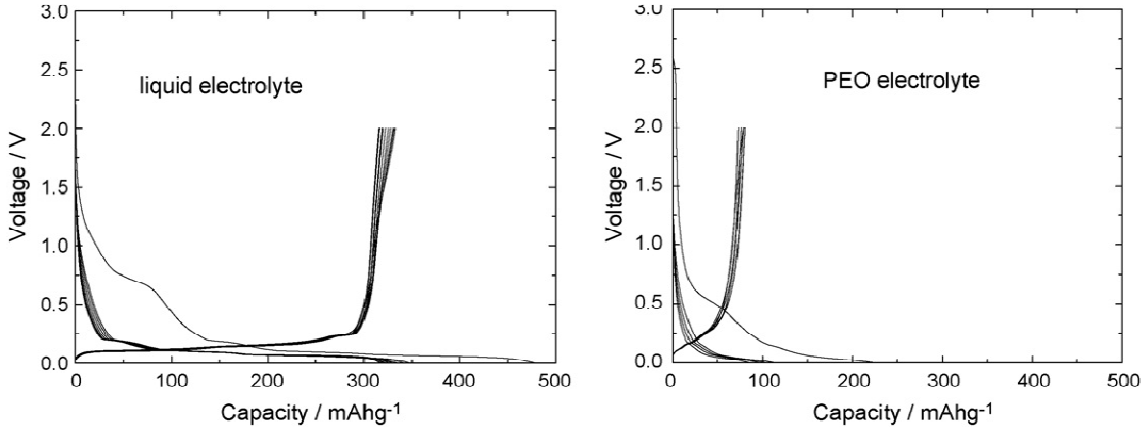

Fig. 3. Charge–discharge curves of artificial graphite KS-6 in EC-DEC-$LiClO_4$ at room temperature and PEO-$Li(CF_3SO_2)_2N$ at 60◦C.

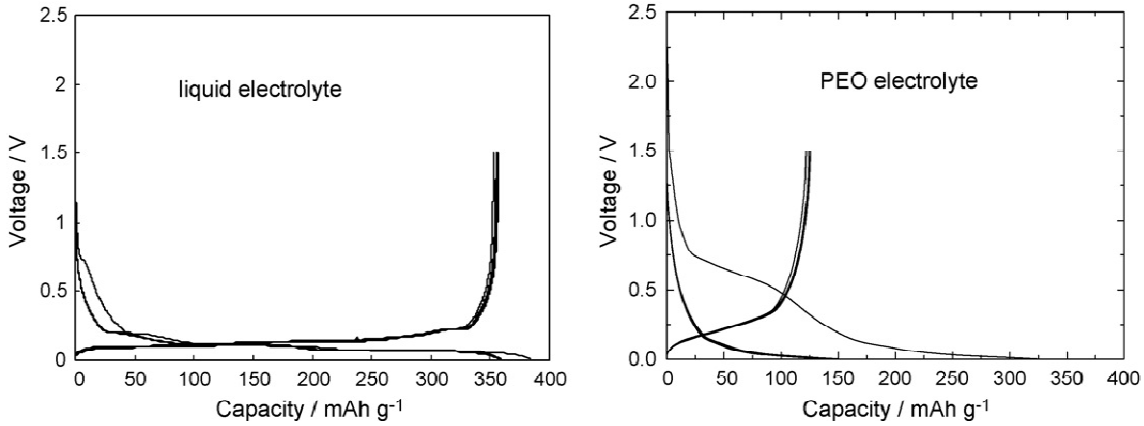

Fig. 4. Charge–discharge curves of artificial graphite MCMB in EC-DEC-$LiClO_4$ at room temperature and PEO-$Li(CF_3SO_2)_2N$ at 60◦C.

Charge–discharge performances of these graphite anodes are shown in Figs. 2–4, where 1M $LiClO_4$ in ethylene carbonate and diethyl carbonate (50:50 vol.%) was used as the liquid electrolyte. The operation temperatures were fixed at room temperature for the liquid electrolyte cells and at 60 ◦C for the polymer electrolyte cells. These synthetic graphite materials show a high capacity of about 300 mAh g^{-1} and a good cyclic performance in the liquid electrolyte cells. However, all the cells with polymer electrolytes exhibit small capacities as much as 100 mAh g^{-1} and the first cycle efficiencies become less than 40%. The large irreversible capacity is due to the reaction of the polymer electrolyte and the carbon electrode, which is also shown from the voltage profile in the first cycle. The reaction between the graphite anode and the electrolyte is well known for liquid electrolyte. In 1970, Dey and Sullivan reported the electrochemical decomposition of propylene carbonate (PC) on graphite at potentials positive to lithium deposition (~0.8V vs. Li/Li^+) [14]. Currently, electrolytes based on ethylene carbonate (EC) have been used for the graphite electrode. The exceptional compatibility of the solvent EC with graphite is related to the properties of the formed protective films (solid electrolyte interface, SEI) [15]. The compatibility of the graphite with the polymer electrolyte is also important to obtain high performance.

The MCMB electrode showed an excellent cycling performance with the PEO-based polymer electrolyte as shown in Fig. 5. The high reversibility of the MCMB electrode shows that it has a protective layer on the surface to suppress further reaction as in the EC-based liquid electrolyte.

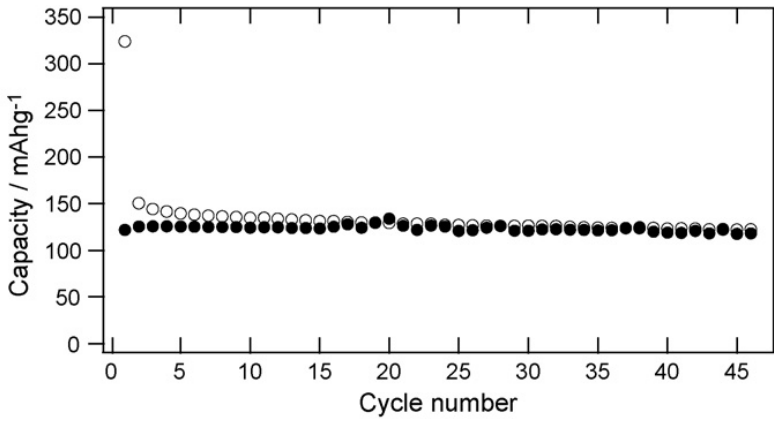

Fig. 5. Charge (○) and discharge (●) capacity change by cycling of MCMB thick electrode with polymer electrolyte at 60 ◦C.

The reversible capacity of MCMB as much as ca. 120 mAh g^{-1} is much lower than that with liquid electrolyte. One possible reason for the low capacity is attributed to small active contact area between electrode and electrolyte and/or the lithium low-diffusion rate through the interface layer and the electrode. To reduce the lithium diffusion length, a thin film electrode was prepared and examined. The charge–discharge curves of such anode with the polymer electrolyte at 60 ◦C are shown in Fig. 6, where MCMB of 4.7 mg was loaded and the thickness of the electrode was around 50 μm. This is equivalent to one or two layers of single MCMB particles. The reversible capacity is enhanced to 280 mAh g^{-1}, which is comparable to that in liquid electrolyte system. These results suggest that the lithium diffusion in the polymer electrolyte infiltrated in electrode plays an important role in the kinetics. The electrode structure mainly determines the utilization of the active material.

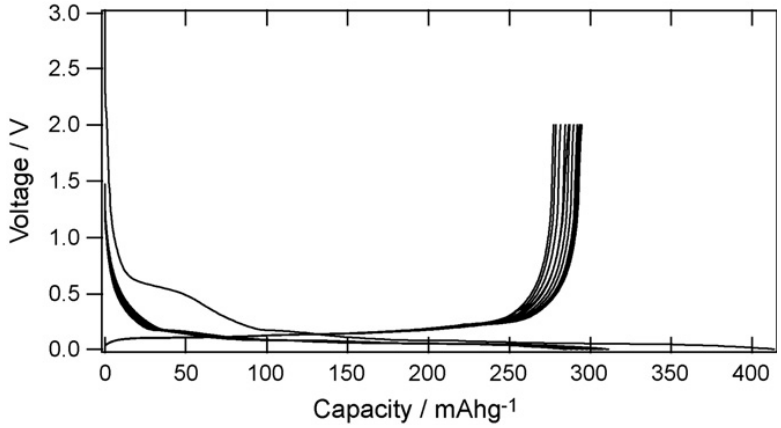

Fig. 6. Charge and discharge curves of non-modified MCMB thin electrode with a thickness of about 50 μm in a polymer electrolyte system at 60 ◦C.

The thinner electrode containing non-modified MCMB shows improved capacity, while it shows capacity fading upon cycling due to large amount of lithium intercalation as 280 mAh g^{-1}. This is directly attributed to the nature of the interface between MCMB and PEO electrolyte. In order to optimize the surface structure of graphite, there is a report that amorphous carbon was coated on graphite to achieve improved performance in propylene carbonate-based liquid electrolytes [16]. The modified graphite anode reduced the charge-transfer resistance and the thickness of SEI film. In our study, the MCMB was modified by pyrolyzed carbon from PVC [17]. This method is quite simple that the mixture of MCMB and PVC was heated at 700 ◦C. Our preliminary result

showed that PVC mainly decomposes near 300 ◦C and no chlorines remain in the products, which is supported by the literature [18].

The SEM image of non-modified MCMB showed a smooth surface, while the surface-modified MCMB by decomposed PVC as shown in Fig. 1 consists of small particles on the original MCMB spheres. PVC is known to be carbonized through the liquid phase during heat treatment in two steps from 200 to 350 and 350 to 550 ◦C with evolution of hydrocarbons [17]. It was considered that PVC-derived pitch carbon coated the MCMB particles at 700 ◦C.

The XRD pattern of the surface-modified MCMB is shown in Fig. 7. The modified MCMB shows an extra diffraction peak near 2θ =43◦, but other features are kept unchanged after the modification. This shows that major part of MCMB is not affected by the modification. The newly appeared diffraction corresponds to the peak of rhombohedral phase of graphite. Such diffraction was also observed in the MCMB ground by a high-speed ball milling. PVC was pyrolyzed to form low-crystalline carbon layer on MCMB. At the same time, chlorine in PVC works as an etchant to clean the MCMB surface. This chemically corrosive nature of chlorine is considered quite strong and comparable to the ball milling power. This chemical effect is considered to cause the structural distortion of the surface and leads to transform of the hexagonal to the rhombohedral phase. Broad bands indicating the low-crystalline carbons are not present in the pattern. The main phase of the composite is MCMB and the ratio of surface low-crystalline carbon to the MCMB is negligible.

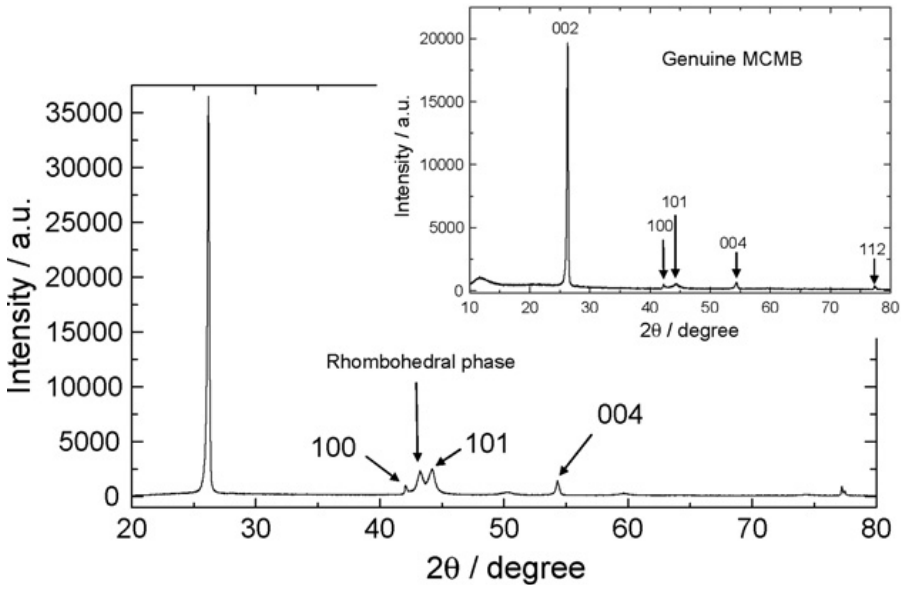

Fig. 7. X-ray diffraction patterns of modified MCMB by thermally decomposed PVC. The inset shows the pattern of non-modified MCMB.

Fig. 8 compares the Raman spectra of the modified and non-modified MCMB. Both spectra show two peaks at 1580 and 1360 cm^{-1} which are called as G-band and D-band, respectively. The D-band corresponds to the conversion of a sp2 to a sp3 hybridized carbon [19]. Therefore, the relative increase in the intensity of D-band to G-band reflects a less resonance of graphitic structure and can be interpreted as the destruction of the two-dimensional structure. The R-value is defined as the intensity ratio of the peak intensity at 1360 and 1580 cm^{-1}, which is known as an indicator of crystallinity in the near surface region [20]. The R-values are 0.24 for the as-received MCMB and 0.53 for the modified MCMB, respectively. These values are comparable with those reported previously and show that low-crystalline carbon exists on the surface of the modified MCMB.

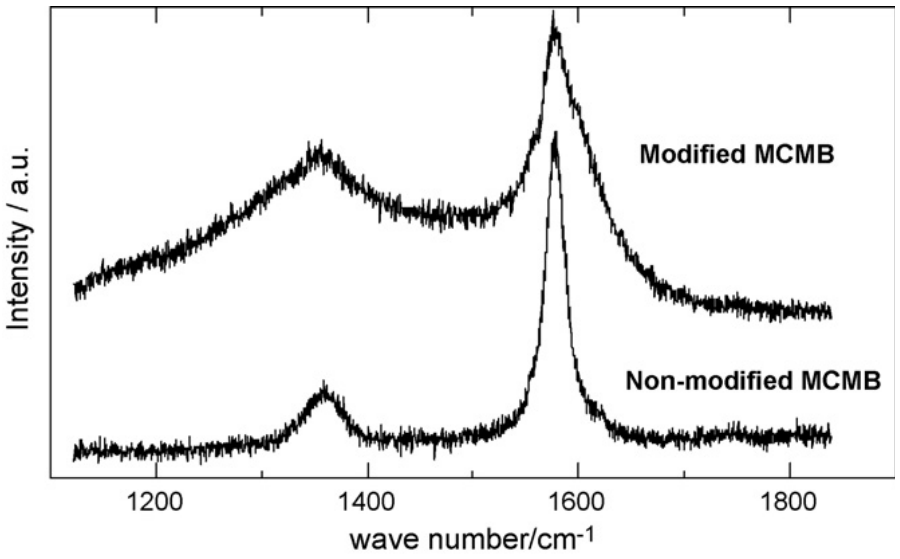

Fig. 8. Raman spectra of non-modified and modified MCMB which were obtained by argon-ion laser at the wave length of 488 nm.

Fig. 9 shows charge–discharge curves for the surface modified MCMB with PEO electrolyte at 60 ◦C, where the applied currents were 1/20C and the thickness of the electrode was estimated about 50 μm. The first charge–discharge efficiency is 64% for the modified MCMB anode, while it is 69% for the non-modified MCMB anode. After the second cycle, the efficiency was become more than 95% and the capacity fading was hardly observed. The improvement of the efficiency was considered to be a decrease of the active edge sites at the surface of MCMB. The reversible capacity of about 300 mAh g^{-1} is close to that obtained in the liquid electrolyte system. The

improvement of the compatibility of the interface is found quite effective for the high performance of MCMB with polymer electrolyte.

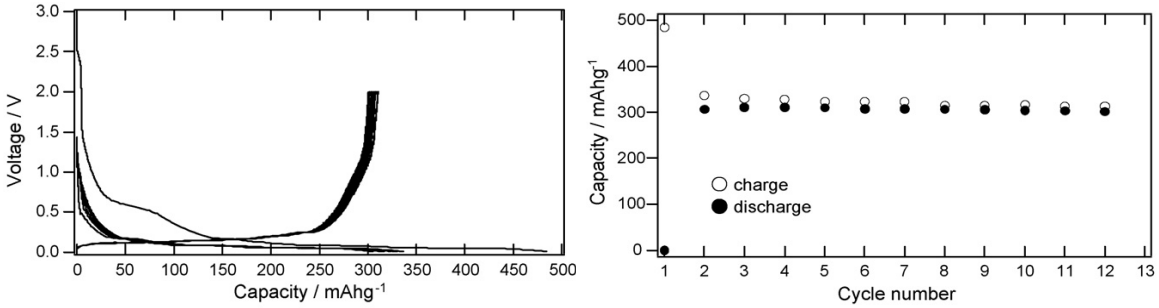

Fig. 9. Charge and discharge curves of modified MCMB by thermally decomposed PVC in polymer electrolyte system at 60 ◦C.

The rate capability of the modified MCMB anode with the polymer electrolyte was examined at 60 ◦C. The typical results are shown in Fig. 10, where the loaded active material was 2.7 mg and several charge currents as 1/10C, 1/5C, 1/2C and 1C were applied in turn. At a high-current density such as 1/2C (about 0.25mAcm^{-2}), a discharge capacity of 100 mAh g^{-1} is obtained. The charge–discharge coulombic efficiency is almost 100% even under high rate as 1C. The comparison of rate performances before and after the modification of MCMB is summarized in Fig. 11. The difference becomes remarkable at 1/5C rate and higher. The surface modification is also effective for improvement of the rate performance of MCMB anode.

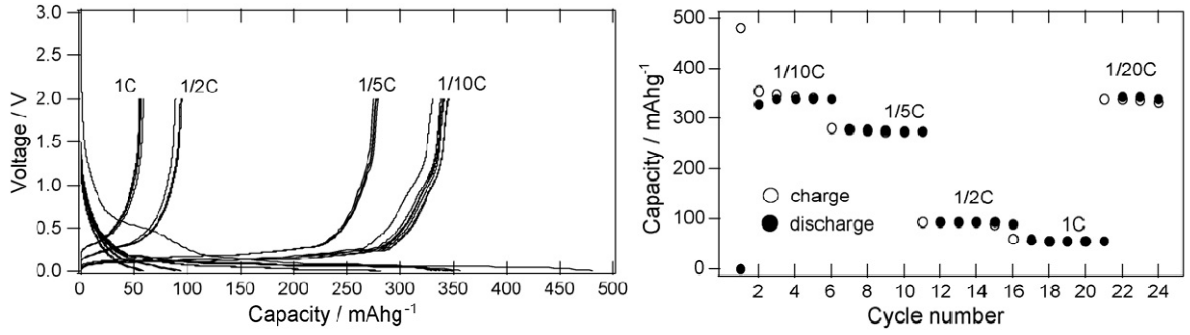

Fig. 10. Rate capability of the modified MCMB in polymer electrolyte system at 60 ◦C. The current densities in the form of C-rate are indicated in the figure.

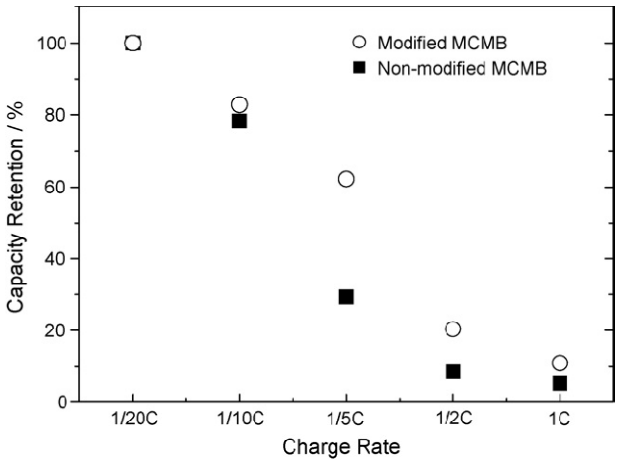

Fig. 11. The comparison of the rate capability of non-modified and modified MCMB. The capacity retention values against C-rate are calculated, on the basis that the capacity at 1/20C is 100%.

Fig. 12 shows the cyclic voltammogram (CV) of the non-modified MCMB and the modified MCMB in the first and second cycles at 60 ◦C, where the scanning rate was set at 0.3mVs^{-1}. The first lithium insertion into the non-modified and the modified MCMB show four peaks in the curve. The two peaks at 2.4 and 1.4V correspond to the reaction between the polymer electrolyte and the MCMB, because the peaks disappear in the following lithium extraction process and in the second cycles. These reactions at higher voltages were not observed for the surface-modified MCMB heated with PVC at 800 ◦C in the liquid electrolyte [21]. The irreversible reaction mechanism against polymer electrolyte is not discussed further, but it should be related to the formation of SEI layer by decomposition of PEO. Both non-modified and modified MCMB show a shoulder on the curve near 0.4V and sharp peak near 0.0V during lithium insertion in the first cycle, while in the second cycle, the peak at 0.4V almost disappears and remains as a broad band in the non-modified MCMB. The peak near 0.4V corresponds to a small plateau in the potential profile at ca. 0.5V as shown in Fig. 9.

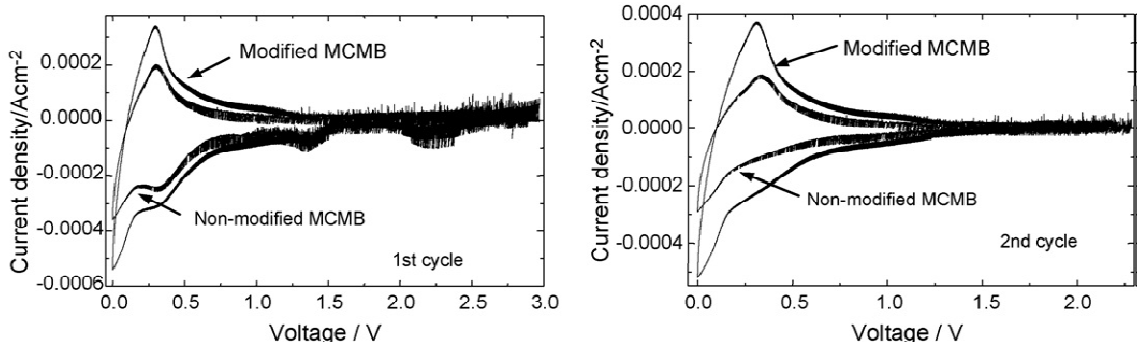

Fig. 12. Cyclic voltammograms of non-modified and modified MCMB in polymer electrolyte system. The scanning rate is 0.3mVs−1. The left and right figures show the first and second cycle, respectively.

The high-speed ball milling of MCMB in dodecan solvent, shows a similar CV profile of the modified MCMB. The ball milled MCMB also showed the distorted surface structure confirmed by Raman and X-ray studies. The low-crystalline carbon shows a similar electrode potential profile in lithium insertion and extraction. Therefore, the peak near 0.4V may correspond to lithium intercalation of the distorted carbon on the MCMB surface. These characterizations of the surface-modified MCMB suggest that the surface is covered by pyrolyzed disordered carbon and this surface layer makes more compatible interface with PEO for the lithium insertion and extraction. This is considered due to the physical enlargement of the electrode surface area, which leads to the larger electrode/electrolyte interface to bear a large current. Or, surface of MCMB particle covered by the disordered carbon might have improved chemical affinity to the polar PEO polymer.

4. Conclusion

Several types of synthetic graphite were examined as the anode in the polymer electrolyte cell. The cast thin MCMB anode showed a high-reversible capacity of 260 mAh g^{-1}. The reversibility of MCMB was improved by coating the MCMB surface with thermally decomposed carbon of PVC. The first charge and discharge coulombic efficiency was 64% and the reversible capacity was about 300 mAh g^{-1}, which are comparable to those of the MCMB anode with liquid electrolyte. These performances can solve the problems when lithium-ion polymer batteries are considered for the practical applications. Further effort to reduce the operation temperature of the MCMB which corresponds to the better interface between MCMB and the electrolyte, will accelerate the development of the dry lithium polymer battery.

References

[1] M. Armand, W. Gorecki, R. Andreani, in: B. Scrosati (Ed.), Proceedings of the Second International Symposium on Polymer Electrolytes, Elsevier Applied Science, New York, 1990, p. 91.

[2] B. Kapfer, M. Gauthier, A. Belanger, in: K. Abraham, M. Salomon (Eds.), Proceedings of the Symposium on Primarily and Secondary Lithium Batteries, The Electrochem. Soc. Inc., Pennington, 1990, p. 227.

[3] M. Gauthier,D. Fauteux, G.Vassort, A.B´elanger,M. Duval, P. Ricoux, J.M. Chabagno, D. Muller, P. Rigaud, M.B. Armand, D. Deroo, J. Electrochem. Soc. 132 (1985) 1333.
[4] E. Peled, J. Electrochem. Soc. 126 (1979) 2047.
[5] M. Doll´e, L. Sannier,B. Beaudoin, M. Trentin, J.M. Tarascon, Electrochem. Solid State Lett. 5 (2002) A286.
[6] M. Rosso, C. Brissot, A. Teyssot, M. Doll´e, L. Sannier, J.M. Tarascon, R. Bouchet, S. Lascaud, Electrochim. Acta 51 (2006) 5334.
[7] G.B. Appetecchi, F. Croce, G. Dautzenberg, M. Mastragostino, F. Ronci, B. Scrosati, F. Soavi, A. Zanelli, F. Alessandrini, P.P. Prosini, J. Electrochem. Soc. 145 (1998) 4126.
[8] J. Yang, Y. Takeda, Q. Li, N. Imanishi, O. Yamamoto, J. Power Sources 90 (2000) 64.
[9] Y. Liu, Y. Takeda, T. Matsumura, J. Yang, N. Imanishi, A. Hirano, O. Yamamoto, J. Electrochem. Soc. 153 (2006) A437.
[10] T. Tsumura, A. Katanosaka, I. Souma, T. Ono, Y. Aihara, J. Kuratomi, M. Inagaki, Solid State Ionics 135 (2000) 209.
[11] Y. Liu, K. Hanai, J. Yang, N. Imanishi, A. Hirano, Y. Takeda, Electrochem. Solid State Lett. 7 (2004) A369.
[12] C. Capiglia, J. Yang, N. Imanishi, A. Hirano, Y. Takeda, O. Yamamoto, J. Power Sources 119–121 (2003) 826.
[13] Q. Li, N. Imanishi, A. Hirano, Y. Takeda, O. Yamamoto, J. Power Sources 110 (2002) 38.
[14] A.N. Dey, B.P. Sullivan, J. Electrochem. Soc. 117 (1970) 222.
[15] J.O. Besenhard, M. Winter, J. Yang, W. Biberacher, J. Power Sources 54 (1995) 228.
[16] L.J. Fu, H. Liu, C. Li, Y.P. Wu, E. Rahm, R. Holze, H.Q. Wu, Solid State Sci. 8 (2006) 113.
[17] M. Inagaki, Y. Okada, H. Miura, H. Konno, Carbon 37 (1999) 329.
[18] T. Zheng, Y. Liu, E.W. Fuller, S. Tseng, U. von Sacken, J.R. Dahn, J. Electrochem. Soc. 142 (1995) 2581.
[19] M.S. Dresselhaus, G. Dresselhaus, A. Jorio, A.G. Souza Filho, R. Saito, Carbon 40 (2002) 2043.
[20] H.Y. Lee, J.K. Baek, S.W. Jang, S.M. Lee, S.T. Hong, K.Y. Lee, M.H. Kim, J. Power Sources 101 (2001) 206.
[21] K. Suzuki, T. Hamada, T. Sugiura, J. Electrochem. Soc. 146 (1999) 890.

2.2. Morphology-stable silicon-based composite for Li-intercalation

1. Introduction

Silicon faces both large challenge and dilemma to be employed as anode in place of commercial graphite for lithium-ion batteries [1-5]. The attraction comes from the largest capacity of 4000 mA h g^{-1} among all known Li insertion materials in company with the low reactive potential, and the problem may arise from the poor cycling stability in association with the drastic volume expand/shrink upon the electrochemical alloying process. Although the decreased particle size can greatly increase the morphology stability, its capacity decay can hardly be avoided at the extended cycles. In addition due to the huge specific surface energy, ultrafine active hosts may cause to the server aggregation and the extremely low initial coulombic efficiency. Much attention has been focused on the composites consisting of silicon and carbonaceous materials. For instance, silicon covered with carbon by thermal vapor deposition (TVD) demonstrates a better cycling life than the respective silicon [6]. Composite prepared by pyrolysis of organic compound containing silicon gives an attractive electrochemical performance although it has low initial faradic yield [7,8]. Composite produced by mechanical mixing silicon and graphite (or acetylene black) shows high capacity, but its cycling is still poor [9]. Recently, it was reported that pyrolysis of pitch embedded with silicon may provide an effective structure to suppress the volume change of silicon upon cycling [10]. The enhanced cyclability is attributed to the small volume expansion of carbon for lithium accommodation (ca. 9% for graphite). More important, it is expected that ductile carbon could endure the volume change of silicon and reduce the mechanical stress within the electrode, thereby prevent disintegration. However, only once pyrolysis reaction can hardly ensure the homogeneous silicon distribution and the high contacting strength between silicon and matrix. Besides, the high porosity of the pyrolyzed carbon may easily result in the low initial coulombic efficiency and the rapid collapse of the structure during repeated charge/discharge. Thus, to overcome the mentioned shortages of the silicon carbon composite, one high energy mechanical milling (HEMM) step was introduced in cooperation with two pyrolysis reactions. The electrochemical behaviors of the silicon/disordered carbon composite are obviously superior to those of $SiMg_2$, Si_2 Ni and $SiO_{1.1}$. It may contribute to a development of silicon-based materials as anodes for the secondary lithium-ion batteries.

2. Experimental

2.1. Material preparation

The basic procedure for producing the silicon/disordered carbon composite was described as follows: poly(-vinyl chloride) (PVC, Aldrich) and silicon particles (< 1 Am, >99.8%) were homogeneously mixed and the weight ratio of silicon vs. PVC was 3:7. The mixture was heated at 900 ^{o}C in an Ar atmosphere for 1 h at heating rate of 5 ^{o}C min^{-1} and cool down to room temperature at a natural rate. The products were further treated by HEMM in a sealed bowl in Ar at a rotational speed of 500 rpm for 2 h. The obtained sample was mixed with PVC again (milled product vs. PVC was 3:7 wt.%). The mixture was performed by pyrolysis reaction similar to the first heating process. The end sample was ground and sieved. $SiMg_2$ and $NiSi_2$ (Aldrich) were prepared by treating the commercially obtained products with HEMM and further sieved. Nano-size $SiO_{1.1}$ (typical particle size: 50 nm, prepared by CVD) was kindly grafted from Nagaku. The structure of the different insertion hosts was detected by powder X-ray pattern measurements using automated powder diffractometer with CuKa radiation. The morphology characteristics of the powders were inspected by scanning electron microscopy (SEM) and electron probe microanalysis (EPMA).

2.2. Electrode fabrication

The electrodes contain 4 wt% acetylene black (AB), 88 wt% active materials and 8 wt% poly(vinylidene fluoride) (PVDF). The active powders and AB were homogeneously mixed in the 0.02 g ml^{-1} PVDF/1- methyl-2-pyrrolidone (NMP) solution, and the vicious mixture was cast onto the 20 μm Cu foil. The electrode was further dried at 120 ^{o}C under vacuum for 2 h until the NMP solvent was entirely removed.

2.3. Cell assembly and the relative measurements

To evaluate the electrochemical properties of the electrodes, a half-cell containing $LiPF_6$/EC+DMC (Ethylene carbonate plus diethyl carbonate as 1:1 in volume) electrolytes was used and metallic lithium was utilized as counter electrode. Basically, all the three layers, including test electrode, separator and lithium counter electrode, were stacked in a 2025 coin-type cell in a glove box. Unless stated elsewhere, cycling profile examination was carried out at a constant current density of 0.3 mA cm^{-2}. The rest time between charge and discharge was 1 min. The discharge and charge capacities were adopted for all figures in the paper, corresponding to Li-insertion into and –extraction from the active hosts, respectively. For thermal study, after two cycles the graphite and the silicon/disordered carbon composite-based electrodes were deeply

discharged to 0.005 V vs. Li/Li^+. Each sample for the differential scanning calorimetry (DSC) measurement was packed in a stainless steel pan, which was tightly sealed in a glove box. The DSC test was performed by Rigaku Thermo Plus 8230 and Al_2O_3 was used as reference.

3. Results and discussion

3.1. Electrochemical behaviors of the silicon/disordered carbon composite

Although the decomposed PVC shows large potential hysteresis between charge and discharge, it may permit silicon dispersed inside and function as an elastic network with electron/ion conductivity for holding silicon steadfastly. The key point determining the mechanical stability of the silicon carbon composite should be emphasized on the uniform silicon distribution and the high contacting strength between the silicon and the matrix. Fig. 1 gives the typical charge and discharge properties of the silicon/disordered carbon composite electrode at different cycles under the controlled discharge capacity at 600 mA h g^{-1}.

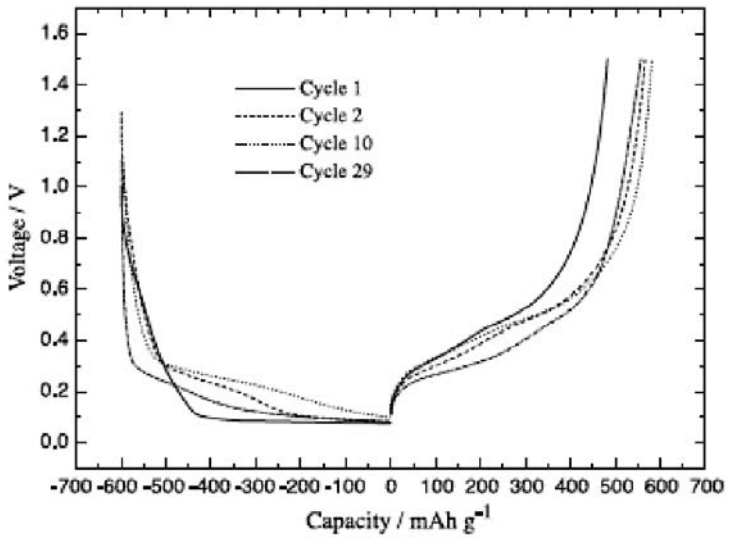

Fig. 1. The charge-discharge properties of the silicon/disordered carbon composite electrode at different cycles; insertion capacity is controlled at 600 mA h g^{-1}; extraction voltage cutoff is 1.5 V vs. Li/Li^+.

A sloping potential plateau starts from 1.1 until 0.1 V in the first discharge step, linking to the stage of Li intercalation into the disordered carbon in company with the SEI film (ca. 0.8 V) formed on the surface of the active particles. Li insertion potential of silicon at the first cycle mainly takes place below 0.1 V, yielding an extremely straight line. The subsequent discharge potential plateaus present the obvious shift compared to the first

one, relating to the typical phase transformation of silicon from crystal to amorphous. The extraction potentials, however, display little ascending than the insertion ones. Consequently, the average potential of the composite at discharge and charge stage can be fixed in the scale of average 0.2-0.5 V vs. Li/Li^+ correspondingly. It may lead to an enhanced safety compared to commercial graphite (ca. 0.15 V) due to the increased reactive potential. With the cycles increase, the discharge potential plateau slightly drops, indicating an augmented polarization caused by the hindered electrochemical kinetics in association with the deteriorated interfacial compatibility. The faradic yield of extraction to insertion is observed close to 100% after the second cycle vs. 80% at the first cycle.

Table 1 lists the theoretical and experimental initial discharge capacities of the composites after the first and second pyrolysis process. The appropriate content of silicon in the composite is located in the range of 40-50 wt% after optimizing the tradeoff between large capacity and better capacity retention. However, only 85% of the theoretical capacity can be effectively achieved. Since silicon is embedded inside and the particle size of the composite is apparently enlarged compared with the original silicon, a reduced real reactive area between the embedded silicon and the electrolytes may take the consequence.

Table 1 The discharge capacity of the electrodes based on silicon/disordered carbon composite prepared at different procedure; voltage cut off: 1.5–0.01 V vs. Li/Li^+

Silicon/disordered carbon	Pyrolysis reaction 1	Pyrolysis reaction 2
Silicon content (wt%)	57	47
Theoretical capacity (excluding disordered carbon) (mA h g^{-1})	2100	1790
Theoretical capacity (including disordered carbon) (mA h g^{-1})	2220	1940
Experimental capacity (including disordered carbon) (mA h g^{-1})	1967	1677

An improved morphology stability of the composite can be realized by adopting an ideal structure, in which silicon is completely and efficiently locked and embedded by the carbonaceous matrix. Fig. 2 illustrates the cycling performance of the silicon/disordered carbon composite prepared by different procedures. The rapidest capacity decay is observed for the sample produced by once pyrolysis reaction, although the composite gives a large capacity at the cycling beginning (Fig. 2a). SEM analysis further revel the morphology properties of the matched sample, as shown in Fig. 3a (Compo.), where the silicon particles after the first pyrolysis process prove a relatively poor distribution. Some obvious cracks suggest the rather low mechanical strength. In addition, lots of silicon still can be significantly discerned on the surface of the composite. The unstable morphology structure and the incompletely embedded effect of the composite may easily lead to the severe mechanical stress accompanied with the penetration of electrolytes. Since the interfacial contacting between silicon and the disordered carbon suffers the serious mechanical stress in association with the strong volume effects of silicon, the possible detachment of silicon from matrix takes place and leads to an electron-contacting loss of silicon. At last, the rapid capacity fading can hardly to be avoided.

The composite synthesized by twice pyrolysis processes without HEMM shows high cycling stability initially, but its rigorous capacities deterioration occurs at the cycles beyond 15 (Fig. 2b). It indicates that even a comparatively embedded effect can be ensured by twice pyrolysis reactions, a relatively weak contacting strength between the silicon and the carbon can hardly prevent the possible detachment of silicon from the matrices as discussed above. In addition, the non-uniform dispersion of Si-particles may turn into server aggregation along with the drastic volume changes of silicon.

By contrast, the sample prepared by HEMM following the first pyrolysis process demonstrates capacity decline at the initial several cycles, subsequently its capacity retention shows noticeable enhancement upon long cycles (Fig. 2c). HEMM is well known as an effective energy transfer way via the vigorously interfacial collisions among precursors and balls. There are several intentions for adopting the one HEMM step between the two pyrolysis reactions. First, HEMM is powerful to smash most unstable part of the Si-C composite from the first pyrolysis process. Secondly, lots of so called Si–C cores may be formed under the strong particle impacts. The particle size of the milled samples is obviously larger than that of the original silicon (Fig. 3b), suggesting the multiphase structure of silicon covered with carbon. Such structure can achieve the reasonably improved interfacial affinity between the dispersed silicon and the

carbonaceous matrix. The Si-C cores also are favor for obtaining the improved phase compatibility with the second decomposed carbonaceous matrix. At last, HEMM may improve the Si-distribution and reduce the porosity of the decomposed PVC from the first pyrolysis, resulting in the increased filling density and mechanical strength. Since the decomposed carbonaceous matrix from the first pyrolysis reaction may act as the ‘‘separator’’ among silicon, it is effective to prevent the possibly serious aggravation of the ultrafine silicon particles during milling.

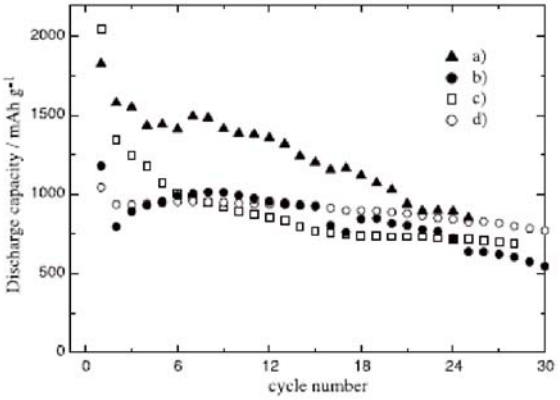

Fig. 2. The cycling performance of the silicon/disordered carbon composite prepared by different procedure; voltage cut off: 1.5-0.05 V vs. Li/Li^+. Sample conditions are the same as Table 2.

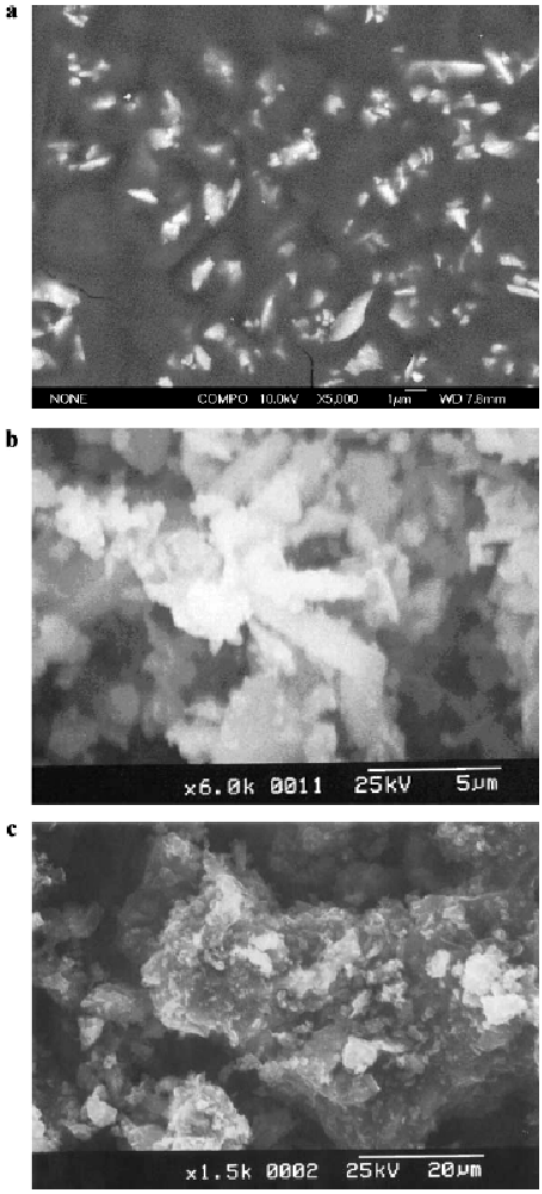

Fig. 3. The SEM photos of the silicon/disordered carbon composites: (a) After the first pyrolysis reaction (without HEMM); (b) after pyrolysis reaction 1 and HEMM; (c) final product.

The milled sample demonstrates the highest irreversible capacity loss and the largest insertion capacity at the first cycle, as shown inTable 2. It is due to the reduced particle size and the Li defects produced by HEMM on the surface of the composite. The treated particle surface also takes the consequence for the initially capacity loss of the milled samples due to the unstable interfacial compatibility with electrolytes. Thus it is necessary to employ the second pyrolysis process to obtain an absolute covering effect. It is clearly shown in Fig. 2d that the final composite gives a highly morphology stability. Upon cycling even the electrolytes penetrate within the composite and contact with silicon, the enhanced morphology structure may effectively prevent the possible detachment of silicon from the matrices. EPMA reveals that silicon shows the improved homogeneous distribution after HEMM and the apparent silicon rich region can not be distinguished on the surface of the final product, indicating the comparatively complete and multi-embedded effect.

The relatively large particle size of the final product may lead to a reasonable initial coulombic efficiency, as shown in Fig. 3c.

Table 2 The initial coulombic efficiency of the electrodes based on silicon/disordered carbon composite prepared by different procedure; voltage cutoff: 1.5– 0.05 V vs. Li/Li^+

	a	b	c	d
1st insertion capacity (mA h g^{-1})	1827.6	1178	2050.4	1042
1st coulombic efficiency (%)	79	76	63	82

*(a) After the first pyrolysis reaction (without HEMM); (b) after twice pyrolysis reactions (without HEMM); (c) after pyrolysis reaction 1 and HEMM; (d) one HEMM between two pyrolysis reactions.

Fig. 4 presents the electrochemical behaviors of the silicon/disordered carbon prepared at the pyrolysis temperature of 1000 °C. Compared to 900 °C, two new potential plateaus appear at 0.8 and 1.1 V in discharge and charge stage correspondingly, as given in Fig. 4a. The reversible capacity is observed at ca. 800 mAh g^{-1}, slightly lower than the 900 °C sample in the same potential range. The initial coulombic efficiency is 82% and the charge-discharge curves demonstrate high coincidence. Fig. 4b illustrates the CV curves of the 1000 °C product. There are three cathodic peaks appear during the Li-insertion process at the first cycle: 0.8, 0.15 and 0.01 V. The latter two peaks mainly link to Li-intercalation into disordered carbon and silicon, respectively. The former one, however, could be due to a new compound formed under the pyrolysis reaction. Also

during the anodic scan, three peaks can be found at 0.3, 0.55 and 1.1 V, representing three Li-extraction stages, which correspond to silicon, disordered carbon and the new compound. The 0.8 V cathodic peak and the 1.1 V anodic peak display the high reversibility. It is supposed that a reaction between silicon and the decomposed PVC group containing Cl, C may take place at high temperature. It leads to an unknown compound unlike inert silicon carbide since the latter is formed at the relatively high temperature above 1100 °C. A further understanding is still under way.

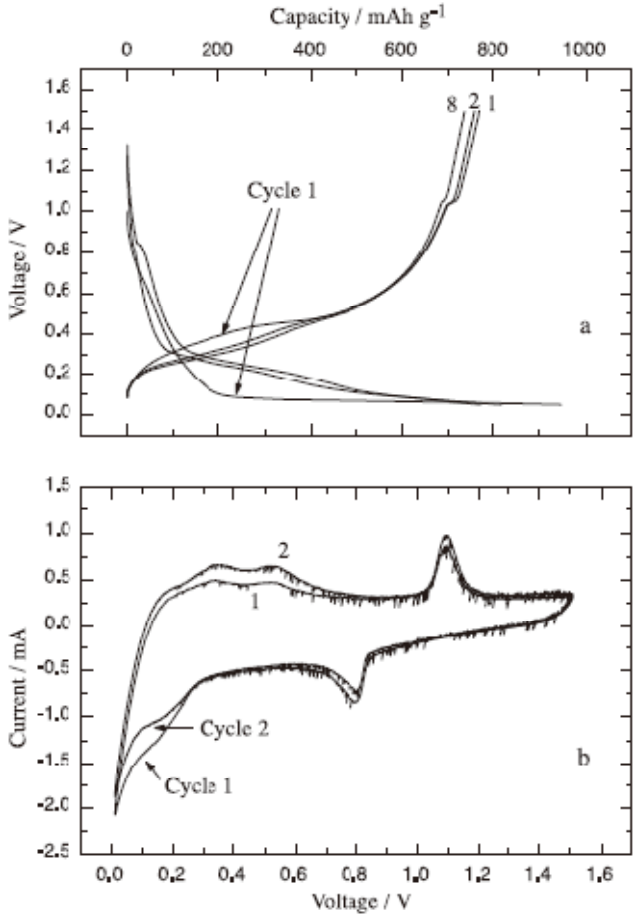

Fig. 4. (a) The charge and discharge profiles of the composite electrode at different cycles; voltage cut off is 1.5–0.05 V vs. Li/Li+; (b) cyclic voltammogram of the composite electrode at the scan rate of 0.05 mV s 1; voltage scale: 1.5–0.01 V vs. Li/Li+.

Under potential range at 1.5/0.05 V vs. Li/Li^+, the capacity retention of the composite at the 40th cycle is 69% vs. 1100 mAh g^{-1} at the first cycle. A shift of the charge-discharge scale from 1.5/0.05 to 1.5/0.02 V may damage the cycling stability apparently, although it leads to a comparable capacity of 1700 mAh g^{-1} at the cycling beginning, as shown in

Fig. 5. It can be attributed to more rapid electrode disintegration and deactivation. With cycling the increased mechanical stress of the composite in company with the penetration of electrolytes may lead to a direct contacting between silicon and electrolytes. Since a larger absolute volume mismatch of silicon at deep Li insertion level may severely damage the contacting strength between the silicon and the matrix, a detachment of silicon from the disordered carbon will cause to rapid electron contacting loss of silicon. Thus, the capacity decline happens. Further controlling Li-insertion degree at the discharge capacity of 600 mAh g^{-1} is found to effectively improve the morphology stability of the composite. We assume that besides the alleviated volume effects, it is also due to the reduced Li-accumulation effects of silicon under the relatively shallow insertion level.

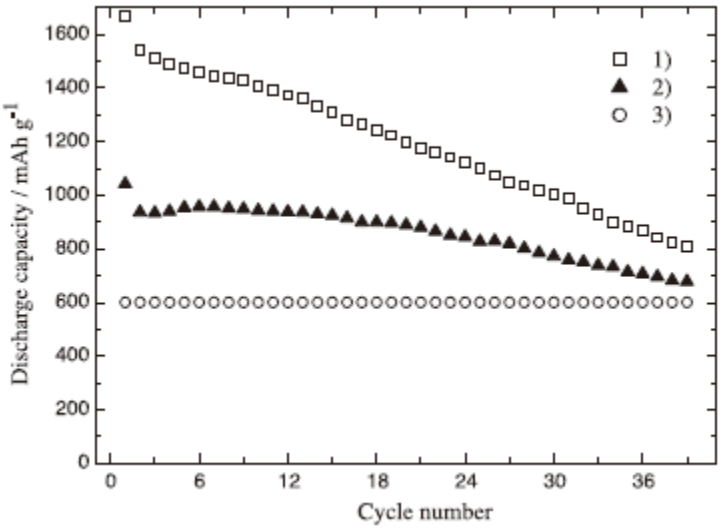

Fig. 5. The cycling performance of the silicon/disordered carbon composite electrode under different charge-discharge style. (1) Discharge to 0.02 V vs. Li/Li^+; (2) discharge to 0.05 V vs. Li/Li^+; (3) discharge under constant capacity at 600 mAh g^{-1}. Li-extraction voltage is 1.5 V vs. Li/Li^+.

3.2. Cycling performance of the different silicon-based hosts

Adopting intermetallic multiphase structure also can apparently alleviate the morphology instability of silicon for Li-insertion. Fig. 6 presents the charge and discharge profiles of the electrodes based on $NiSi_2$, $SiMg_2$ and silicon/disordered carbon composite at the second cycle. The insertion mechanism of Mg2Si and NiSi2 has been investigated by Kim et al. [3] and Wang et al. [11], correspondingly. Two obvious discharge potential plateaus at 0.2 and 0.1 V of the SiMg2 electrode is linked to an Li-intercalation process to form a single crystalline $LiMg_2Si$, following a reaction between Li and Si, finally lithium may alloy with Mg. Also, two charge potential plateaus

appear at 0.3 and 0.7 V, representing the Li-extraction stage that reveres to the Li-Si-Mg alloying process. The observed capacity of $SiMg_2$ is relatively low compared to the published value, which reached 1370 mAh g^{-1} at the first cycle [3]. It may be due to the deviation of the test condition and the particle size. In the case of $NiSi_2$ and silicon/disordered carbon composite, similar electrochemical behaviors suggest that the insertion mechanism of both hosts is only related to the electrochemical Li-Si alloying reaction. However, the later demonstrates a rather low insertion potential than Si2Ni. It is reasonable since silicon in the composite is highly embedded within the disordered carbon, a reduced reactive area may cause to a higher potential polarization. Although silicon content in Si_2Ni (ca. 48 wt%) is almost equal to that of the silicon/disordered carbon composite, the Si/C composite shows much larger reversible capacity, indicating the higher electrochemical reactivity.

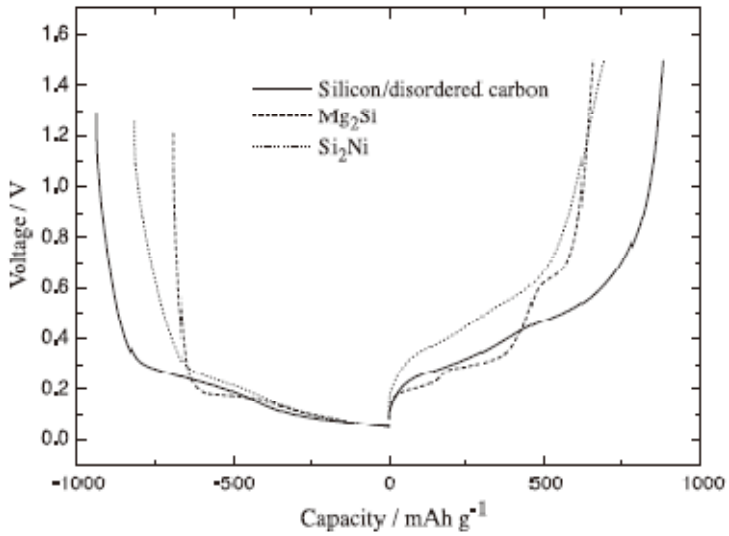

Fig. 6. The charge and discharge profiles of the different silicon-based electrodes at the second cycle; voltage cut off: 1.5-0.05 V vs. Li/Li^+.

The cycling performance of the electrodes based on pure silicon, $NiSi_2$, $SiMg^2$ and silicon/disordered carbon composite is given in Fig. 7. All the composites show the relatively improved cycling stability compared to pure silicon. However, due to the comparable ‘‘crash’’ characteristic of the metallic matrix, the mechanical stability of $NiSi_2$ and $SiMg_2$ is obviously inferior to that of the silicon/disordered carbon composite. Especially in the case of SiMg2, a close reactive potential scale of Mg and Si will easily cause to a rapid capacity decline, suggesting that the Li-Si-Mg alloying process is only partially reversible.

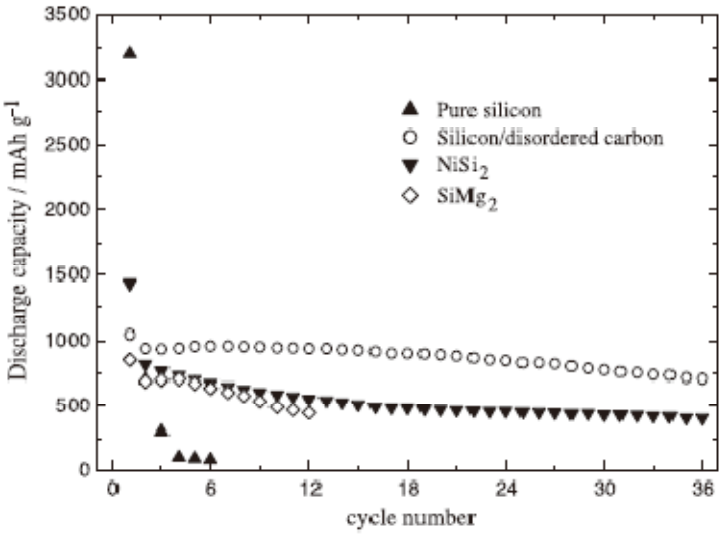

Fig. 7. The cycling performance of the different silicon-based electrodes; voltage cut off: 1.5- 0.05 V vs. Li/Li^+.

Not only metallic and carbonaceous matrix, oxide such as inert Li_2O and SiO_2 also play a noticeable effect to enhance the morphology stability of silicon upon volume change. X-ray diffraction patterns reveal the crystalline structure of the different silicon hosts, as shown in Fig. 8. The single phase of intermetallic $NiSi_2$ and $SiMg_2$ can be recognized. By contrast, the relatively weak peak indicates that SiO1.1 contains lot of amorphous SiO and SiO_2 besides crystalline silicon [12]. In the case of silicon/disordered carbon composite, amorphous carbon (2h = 15) and typical crystalline silicon can be discerned.

Fig. 9 presents the comparison of the charge and discharge behaviors between $SiO_{1.1}$ and silicon/disordered carbon in the voltage range at 1.5/0.02 V vs. Li/Li^+. Both electrodes have a large insertion capacity above 1500 mAh g^{-1} and a low reactive potential below 0.1 V at the first cycle, as shown in Fig. 9a. However, the discharge plateau of $SiO_{1.1}$ is slightly lower than that of silicon/disordered carbon, indicating Si and SiO_2 within the $SiO_{1.1}$ electrode may be obstructive to the initial Li-insertion. A significantly initial capacity loss of the $SiO_{1.1}$ electrode can be noticed, relating to an irreversible reaction of amorphous SiO with lithium to form Li_2O and Si at the first cycle. The huge specific area of the nano-size active hosts also takes part consequence. Due to the inactive SiO_2 and the high insertion polarization within the SiO1.1 electrode, the discharge potential difference of ca. 0.2 V between $SiO_{1.1}$ and silicon/disordered carbon composite can be distinguished at the 22nd cycle, as shown in Fig. 9b.

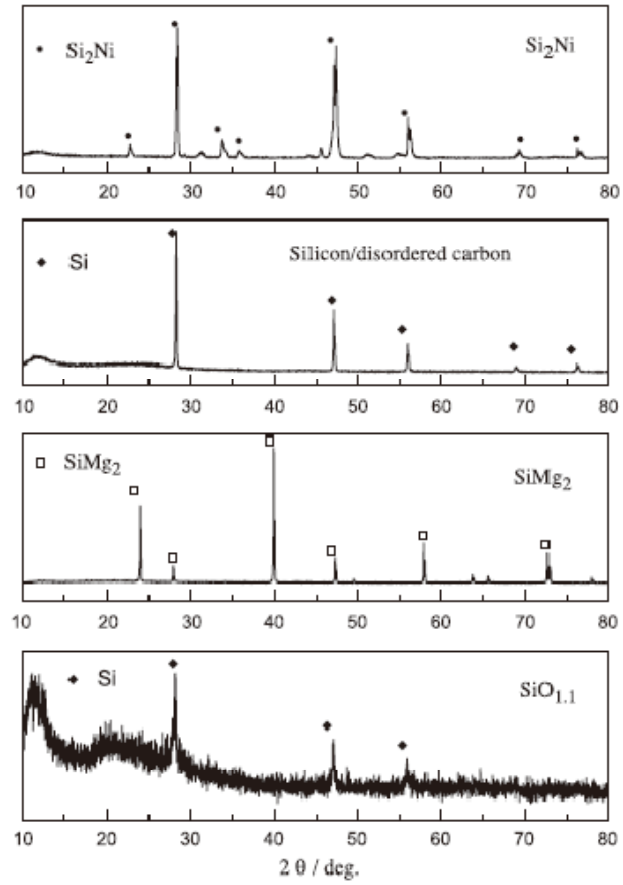

Fig. 8. The XRD patterns of the different silicon-based hosts

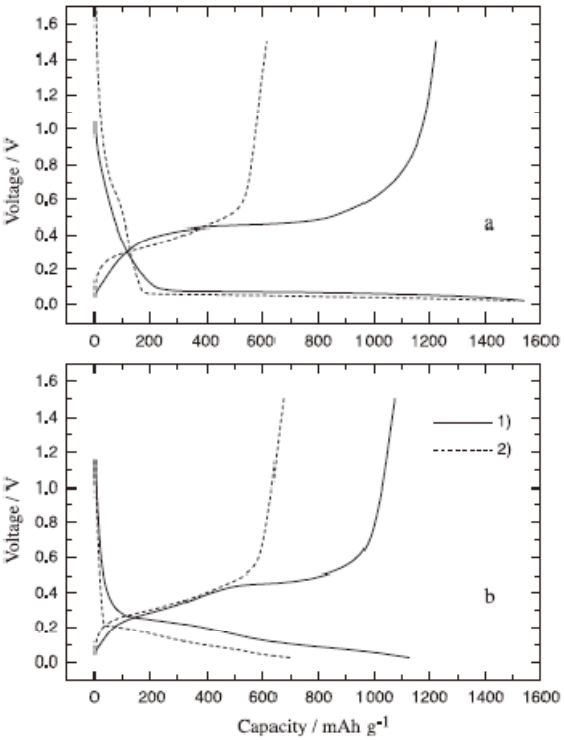

Fig. 9. The charge and discharge profiles of (1) silicon/disordered carbon composite and (2) $SiO_{1.1}$ electrodes at (a) cycle 1 and (b) cycle 22; voltage cutoff: 1.5- 0.02 V vs. Li/Li^+.

Fig. 10 illustrates the cycling performance of the electrodes based on SiO1.1 and silicon/disordered carbon composite. Thanks to the successful buffering effect of Li_2O and SiO_2, the high capacity retention is also remarkable for the electrode composed of $SiO_{1.1}$. Since the average Li-insertion potential of $SiO_{1.1}$ is apparently lower than that of silicon/disordered carbon composite during cycling, different charge/discharge potential of 1.5/0.02 and 1.5/0.05 V is adopted for $SiO_{1.1}$ and silicon/disordered carbon respectively to reach the comparable capacity. Even so, the reversible capacity of the silicon/disordered carbon composite electrode is still higher than that of the $SiO_{1.1}$ electrode near 100 mAh g^{-1}. Bear in mind that a noticeably large irreversible capacity loss of $SiO_{1.1}$ at the first cycle is inevitable, the electrochemical performance of the silicon/disordered carbon composite is obviously superior to that of $SiO_{1.1}$.

Table 3 lists the coulombic efficiency of above four silicon-based hosts during cycling. All the electrodes demonstrate the similar faradaic yield of extraction to insertion upon cycles. It suggests that there is a different electron-contacting loss mechanism for

silicon compared to other Li-alloy, e.g., ultrafine SnSb, which shows a seriously deteriorated coulombic efficiency along with the capacity decline.

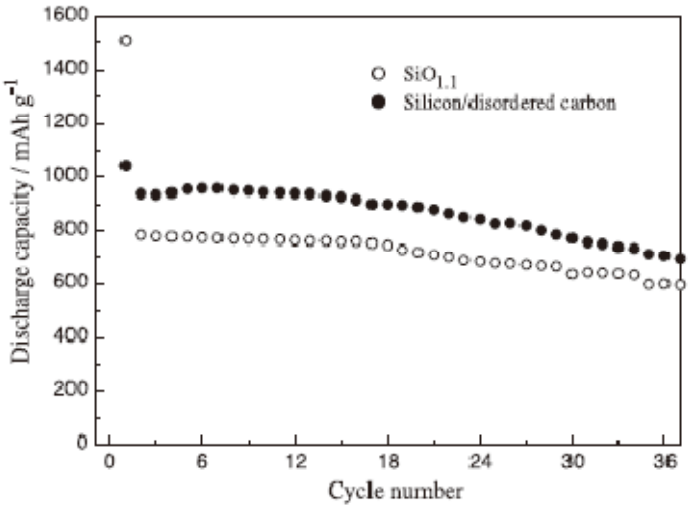

Fig. 10. The cycling performance of $SiO_{1.1}$ and silicon/disordered carbon composite electrodes; voltage cut off: 1.5-0.02 and 1.5-0.05 V vs. Li/Li^+, for $SiO_{1.1}$ and Si/C correspondingly

Table 3 The coulombic efficiency of the different active hosts upon cycling; voltage cut off: 1.5- 0.02 V vs. Li/Li^+

Silicon-based hosts	Average particle size (μm)	1st cycle Coulombic efficiency (%)	5th cycle Coulombic efficiency (%)	30th cycle Coulombic efficiency (%)
Silicon	< 1	71	94	95
Silicon/disordered carbon	25	82	97	96
Si_2Ni	< 5	78	92	97
SiMg2	< 5	79	94	96
$SiO_{1.1}$	0.05	42	97	98

3.3. Thermal stability under fully lithiated state

It is well known that the thermal stability of the graphite anode in the inorganic electrolytes is controlled by the SEI film formed on the surface of the lithiated active hosts [13]. Since the reactive potential of the Si/C composite is close to that of graphite after the first cycle and the SEI film is formed on the surface of the carbonaceous matrix, it is reasonable that the thermal behaviors of the silicon/disordered carbon composite

under lithiated state is similar to graphite, as shown in Fig. 11. There are two sharp exothermic peaks and a small one starting from 130 to 280 °C for the graphite electrode, which correspond to a mild heat generation caused by the reaction (SEI formation) of the electrolytes and the lithiated graphite. The exothermic peak at 280 °C is probably due to the reaction of lithiated graphite and electrolytes by a breakdown of the SEI as reported by Richard and Dahn [13] and Yamaki et al. [14]. However, the matched exothermic peak at 280 °C of the silicon/disordered carbon composite significantly turns into weak, indicating a relatively low heating generation due to the comparatively increased insertion potential. Moreover, the lithium storage in disordered carbon is extremely lower than that of silicon. The silicon, on the other hand, is embedded inside and a direct contact with electrolytes is highly avoided. It also leads to the relatively improved thermal stability.

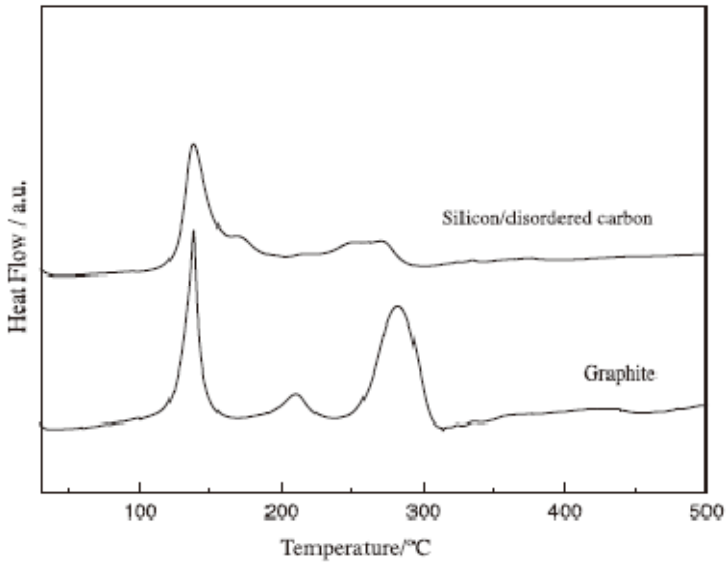

Fig. 11. The DSC curves of silicon/disordered carbon composite and graphite under lithiated state. Scan rate: 5 °C min^{-1} under Ar flow of 100 ml min^{-1}.

4. Conclusions

The silicon/disordered carbon composite, in which morphology-stable Si-C cores are uniformly distributed within the pyrolyzed carbonaceous matrix, demonstrates a large stable capacity at 900 mAh g^{-1} within 40 cycles and a high initial faradaic yield at ca. 80%. Decreasing Li-insertion level may significantly increase the cycle life of the composite. For producing the composite, combination of one HEMM step between two pyrolysis reactions is involved. HEMM after the first pyrolysis process is found to effectively improve the contacting strength between the dispersed silicon and the

decomposed carbon by forming the multiphase Si–C cores. The second pyrolysis reaction finally ensures the completely and compactly embedded effects, resulting in the enhanced mechanical stability. Pyrolysis temperature shows an obvious influence upon the electrochemical behaviors of the composite. Although the Si/C composite and the nano-range $SiO_{1.1}$ both show the high mechanical stability, the later suffers a large initial irreversible capacity loss. Moreover the silicon/disordered carbon composite shows a slightly improved thermal stability compared to graphite under lithiated state due to the increased reactive potential and the indirect contacting of silicon with electrolytes. This work may contribute to a development of silicon-based materials as anodes for the secondary lithium-ion batteries.

References

[1] W.B. Xing, A.M. Wilson, K. Eguchi, G. Zank, J.R. Dahn, J. Electrochem. Soc. 144 (1997) 2410.

[2] A.M. Wilson, G. Zank, K. Eguchi, W. Xing, J.R. Dahn, J. Power Sources 68 (1997) 195.

[3] H. Kim, J. Choi, H.J. Sohn, T. Kang, J. Electrochem. Soc. 146 (1999) 4401.

[4] H. Li, X.J. Huang, L.Q. Chen, G.W. Zhou, Z. Zhang, D.P. Yu, Y.J. Mo, N. Pei, Solid State Ionics 135 (2000) 181.

[5] A. Netz, R.A. Huggins,W. Weppner, J. Power Sources 5271 (2003) 1.

[6] N. Dimov, S. Kugino, M. Yoshio, Electrochim. Acta 48 (2003) 1579.

[7] A.M. Wilson, J.R. Dahn, J. Electrochem. Soc. 142 (1995) 326.

[8] D. Larcher, C. Mudalige, A.E. George, V. Porter, M. Gharghouri, J.R. Dahn, Solid State Ionics 122 (1999) 71.

[9] H. Li, X.J. Huang, L.Q. Chen, G.W. Zhou, Y. Liang, Electrochem. Solid-State Lett. 2 (1999) 547.

[10] Z.S. Wen, J. Yang, B.F. Wang, K. Wang, Y. Liu, Electrochem. Commun. 5 (2003) 165.

[11] G.X. Wang, L. Sun, D.H. Bradhurst, S. Zhong, S.X. Dou, H.K. Liu, J. Alloys Compd. 306 (2000) 249.

[12] J. Yang, Y. Takeda, N. Imanishi, C. Capiglia, J.Y. Xie, O. Yamamoto, Solid State Ionics 152–153 (2002) 125.

[13] M.N. Richard, J.R. Dahn, J. Electrochem. Soc. 146 (1999) 2068.

[14] J. Yamaki, H. Takatsuji, T. Kawamura, M. Egashira, Solid State Ionics 148 (2002) 241.

2.3. Electrochemical studies of the Si-based composites with large capacity and good cycling stability as anode materials for rechargeable lithium ion batteries

1. Introduction

Recently, various anode materials with the improved capacity density and thermal stability over commercial graphite have been highly proposed for lithium ion batteries [1]. Silicon shows promising prospects for the largest capacity among all known host materials. However, silicon undergoes a rapid capacity fading upon cycling due to the morphology deteriorate in the electrochemical alloying process [2-5]. An effective approach to overcome this detriment is to create a composite microstructure comprising active silicon uniformly dispersed in an inert matrix. The pervious examples of the Sn-Fe-C nano-composites proposed by Dahn and co-workers suggest that high-energy mechanical milling (HEMM) could be an appropriate process to build such a composite microstructure [6]. For instance, under ball-milling with the hard TiB_2 or TiN, silicon can be significantly decreased to nano scale and homogeneously doped within the electronmatrix [7,8]. This, in turn, leads to an enhancement in the cycling stability. The milled Si-TiB_2 and Si-TiN composites had a stable capacity of ca. 400 mAh g^{-1} for about 15 cycles, but they suffered from a low capacity utilization of Si and low first cycle efficiency. Dispersing silicon within a carbonaceous matrix by means of thermal pyrolysis reaction also showed an effective way to suppress the volume effects of silicon. Dahn and co-workers reported that the composites prepared by pyrolysis of organic compounds, containing silicon, had attractive electrochemical behavior but low initial faradaic yield [9,10]. Recently, it was found that pyrolysis of pitch or poly(vinyl chloride) (PVC) embedded with silicon showed large capacity and comparable cyclability [11-13]. The enhanced cyclability is attributed to the small volume expansion of carbon on lithium intercalation (ca. 9% for graphite) and the ability of the ductile carbonaceous matrix to accommodate the volume change of silicon, reducing mechanical strain within the electrode and consequent electrode disintegration. Although this type of pyrolyzed carbon has a large potential hysteresis between Li-insertion and extraction, it may, mostly, function as an elastic network with electron/ion conductivity that permits the silicon in the carbon matrix to operate while maintaining electrode integrity. However, a single pyrolysis step was insufficient for ensuring homogeneous Si-distribution and good interface affinity between the silicon and the matrix. In addition, high porosity arising from the pyrolysis carbon may cause a

low initial coulombic efficiency and an aggravated mechanical stress with the penetration of electrolytes [13]. Because inert TiB_2 and TiN were reported to show high electron conductivity and tend to form nano-composite with good Si distribution by means of HEMM [7,8], we tried to introduce the hard comilling components in the Si-C composite before pyrolysis reaction. The combination of pyrolysis reaction and HEMM treatment in the preparation for the composites can track the shortages from the porolysis reaction and the HEMM step alone, resulting in large capacity and good capacity retention [13-15]. Some key factors determining the electrochemical behavior of the Si-composites are presented and discussed in detail.

2. Experimental

The preparation of the Si-C composite was as follows: poly(vinyl chloride) (Aldrich) and silicon particles (<1 μm, >99.8%) were homogeneously mixed and the weight ratio of silicon versus PVC was 3:7. The mixture was heated at 900 ◦C in an Ar atmosphere for 1 h at a heating rate of 5 ◦Cmin^{-1} and allowed cool down to room temperature normally. The products were further treated by high-energy mechanical milling (HEMM) in a sealed bowl in Ar at a rotational speed of 500 rpm for 2-10 h. The resulting samples were mixed with PVC again (Milled product versus PVC was 3:7 wt%). The mixture was processed by a pyrolysis reaction following the same procedures as the first heating process. For preparing the Si-M-C (M = TiB_2, TiN) composites, mixture of silicon particles (<1 μm, >99.8%) and TiB_2 (ca. 2 μm), or TiN (ca. 1.5 μm) with a weight ratio of 1:1 was treated by HEMM in a sealed bowl in Ar at a rotational speed of 500 rpm for 2-10 h. The milled product was followed a pyrolysis reaction similar to that for the Si-C composite. The final SiC and Si-M-C samples were ground and sieved

The electrode containing 8 wt% acetylene black (AB), 80 wt% active materials and 12 wt% poly(vinylidene fluoride) was prepared by a normal casting. The active powders and AB were homogeneously mixed in a 0.02 g mL^{-1} PVDF/1-methyl-2-pyrrolidone (NMP) solution, and the vicious mixture was cast onto a 300-μm thick Ni foam, which served as a current collector. The electrode was further dried at 120 ◦C under vacuum for 2 h until NMP solvent was entirely removed. After pressing, the geometric area of the electrodes was 1.0 cm^2, and the typical thickness was 190-200 μm. To evaluate the electrochemical properties of the electrodes, a half-cell containing LiClO4/ethylene carbonate plus diethyl carbonate as 1:1 in volume electrolyte was used, and lithium metal was utilized as the counter electrode. All the three layers, including test electrode, separator and lithium metal, were stacked in a

2025 coin type cell in a glove box. Unless stated elsewhere, cycling was carried out at a constant current density of 0.18mAmg^{-1} and a voltage cutoff at 1.5/0.05V versus Li/Li^{+}. Charge and discharge of the cell refer, respectively, to lithium extraction from, and insertion into, the active hosts. The electrode capacity was calculated according to the weight of active materials.

3. Results and discussion

The electrochemical characterization of the silicon with different particle size was investigated and compared in Fig. 1. All the silicon electrodes are reactive to lithium that results in large capacities. A decrease in the particle size enhanced the solid electrolyte interface (SEI) film formation on the surface of the active hosts; thereby it increased the capacity loss in the first cycle. There was an obvious shift in the discharge potential plateau from the first cycle to the second cycle, which could relate to the irreversible phase transformation of silicon from crystalline to amorphous state in the first electrochemical alloying process [2,16]. After the initial Li-intercalation, the electrodes possessed a reactive potential plateau at average 0.1-0.4V versus Li/Li^{+}. However, all silicon electrodes suffered from poor capacity retention during cycling, indicating that decrease in the active hosts is insufficient for holding good morphology stability.

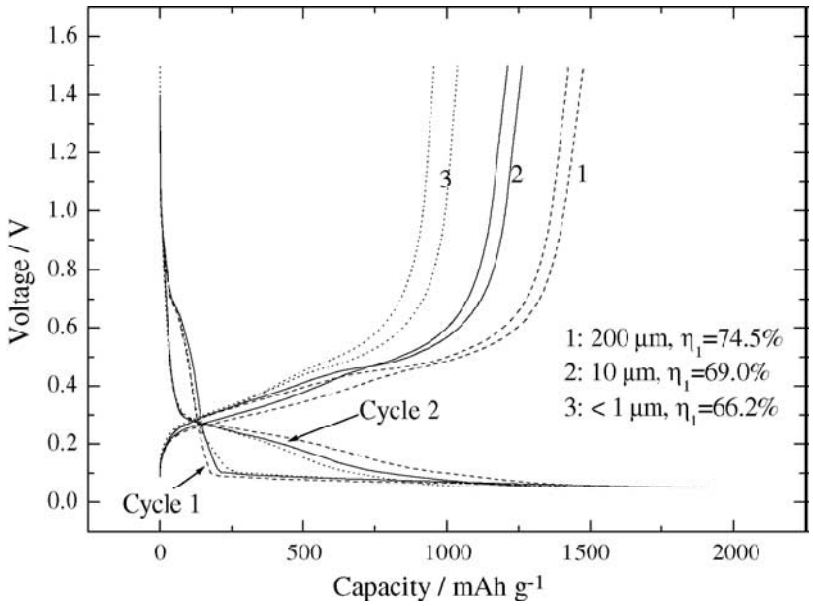

Fig. 1. Charge and discharge profiles of the silicon with different particle size at the first and second cycle.

As reported previously, the morphology deterioration of silicon upon charge and discharge can be effectively conquered by comprising ultrafine silicon particles uniformly dispersed in a ductile carbonaceous matrix [13-15]. One of the advantages of this type composite is due to the high capacity utilization of Si. The Si-C and Si-M-C (M = TiB_2, TiN) composites made from combination of thermal pyrolyzed PVC reaction and HEMM process demonstrated high similarity in the capacity-potential curves upon Li insertion and extraction. Fig. 2 showed charge and discharge curves of the typical Si-M-C composite electrodes under a controlled Li insertion level at 600 mAh g^{-1} at different cycles. In comparison with that of Fig. 1, the electrochemical behavior of the composite was obviously dominated by silicon insertion host, suggesting only small amount lithium storages in the pyrolyzed PVC. However, a sloping potential plateau appeared from 1.1 until 0.1V in the first discharge, which was mostly attributed to Li intercalation into the disordered carbonaceous matrix and formation of the SEI film (ca. 0.8 V) on the surface of the active particles. The faradaic yield of extraction to insertion was 76%, which was close to that of the pure silicon with a particle size of 200 m. The voltage profiles showed high coincidence from cycle to cycle indicating a good Li insertion and extraction reversibility.

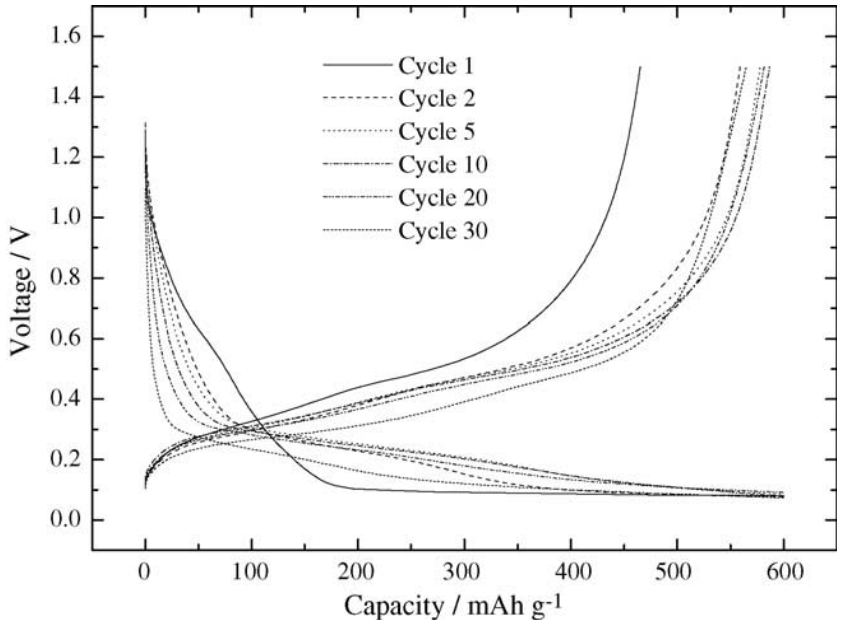

Fig. 2. Charge and discharge profiles of the Si-M-C composites at a controlled insertion level at 600 mAh g^{-1} at different cycles, extraction potential is 1.5V vs. Li/Li^+.

The Si-C and Si-M-C composites had a remarkably enhanced morphology stability over silicon, as shown in Fig. 3. The capacity retention at the 35th cycle of the Si-C composite was ca. 80%, versus ca. 900 mAh g^{-1} at the second cycle. For the Si-M-C composites, the capacity of ca. 600 mAh g^{-1} in the second cycle was remained to over 90% at the 35th cycle. In the previous work, we have shown several possibilities for such a significant improvement in the cycling performance [13]. First, HEMM increases the Si distribution that can prevent silicon particles from the possible aggregation. Secondly, high adhesion strength between the silicon and the matrix treated under HEMM can hold a good electron contacting. Finally, pyrolyzed PVC can function as an elastic network with electron/ion conductivity that permits the silicon in the carbon matrix to operate while maintaining electrode integrity. Compared with the Si-C composite, the decrease in the reversible capacities for the Si-M-C composites was remarkable. The difference in the silicon content, e.g., ca. 47 wt% for the Si-C and ca. 35 wt% for the Si-M-C composites, may take this consequence. Furthermore, it is probably attributed to a negative effect in the capacity utilization from the silicon caused by the co-ball milling hard components [7,8,15]. It indicates that the silicon have a propensity in the capacity loss under co-milling with the hard components.

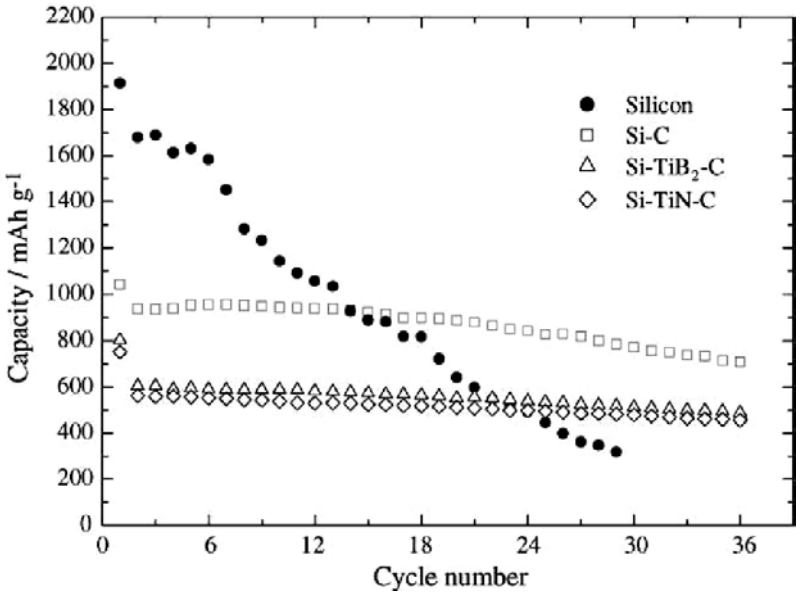

Fig. 3. Cycling performance of the Si, Si-C, Si-TiB2-C and Si-TiN-C composites.

The introducing of the hard co-milling components, such as TiN, TiB_2, in the preparation for the Si-M-C composite brought an improvement in the charging rate over that of the Si-C composite, as shown in Fig. 4. The Si-C composite had a rapid loss in the reversible capacity with increasing the charging rate. This is probably due to poor electron conductivity of silicon in the nature characteristic. When the charging rate was increased to 2C, the capacity of the Si-M-C composites under 1/4C still remained to be over ca. 50%. A remarkable decrease in the particle size of silicon may take this consequence. Observation from SEM and XRD indicates that the relatively hard co-balling components tend to significantly reduce the particle size of silicon during the HEMM treatment.

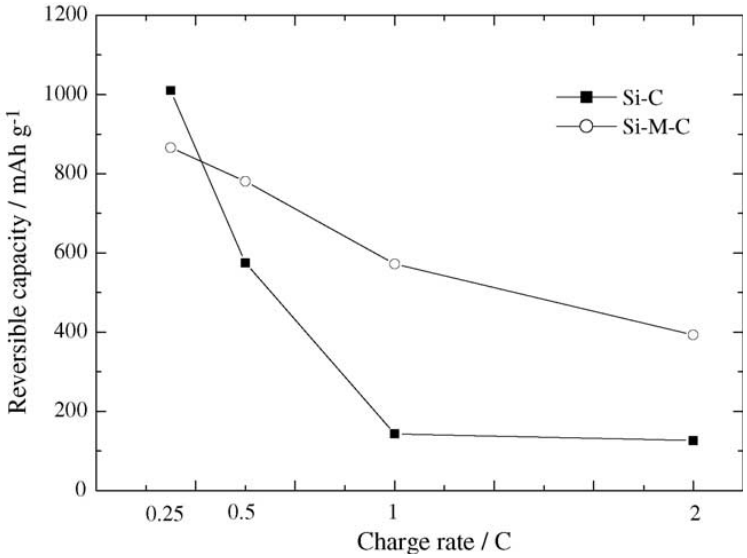

Fig. 4. Charging rate as a function upon the reversible capacity of the Si-C and Si-M-C composites.

A comparison with meso-carbon micro-beads (MCMB, a kind of commercial graphitic carbon) in the charge and discharge profiles at the second cycle revealed that the Si-M-C (or Si-C) composite had a slight increase in the Li insertion and extraction potential plateau for about 0.12V, as shown in Fig. 5. This, in turn, can prevent lithium dendrite formation at a high charging rate and therefore leads to an enhanced operation safety. However, the Si-based composite surfers from a loss in the volume capacity due to a low density (1.7 g cm^{-3}, in case of Si-C) compared with that of MCMB (ca. 2.25 g cm^{-3}). From this point of view, we suppose that the carbonaceous matrix with low porosity is in favor for the volume capacity.

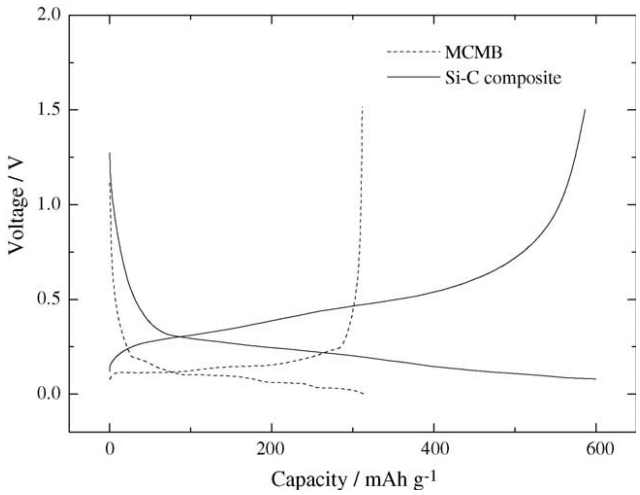

Fig. 5. Comparison of the charge and discharge curves between the MCMB and the Si-C composite electrodes. Voltage cutoff: MCMB, 1.5-0.01V vs. Li/Li^+; Si–C, insertion level at 600 mAh g^{-1}, extraction potential is 1.5V vs. Li/Li^+.

A full cell using the Si-C composite anode and the $LiNi_{0.8}Co_{0.2}O_2$ cathode was fabricated to study its electrochemical characteristics, as shown in Fig. 6. For full utilization of lithium storage capacity of the Si-C composite anode, the weight of cathode has to be much over that of the anode (7-8 times). The cell had a large anode capacity of ca. 600 mAh g^{-1} within the working potential of 2.3-3.9V that might result in a high energy density. After the first cycle, a high overlapping in the potential trends indicated good operation reversibility. We expect that further optimization of the composite anodes might lead to a practical lithium-ion battery with a more safety performance and high energy density over the current graphite-based batteries.

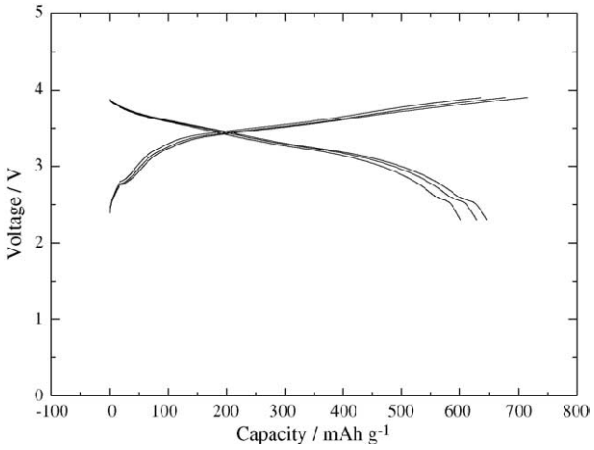

Fig. 6. Charge and discharge curves of the Si-C/$LiCo_{0.2}Ni_{0.8}O_2$ cell at the cycle 2, 3 and 5; potential cutoff: 2.3-3.9V.

4. Conclusions

We reported studies of the electrochemical characterization of series Si-based composite materials with significantly improved cycling stability over silicon. The Si-C composite made from two PVC pyrolysis reactions, combined with an intervening high-energy mechanical milling (HEMM) step, presents a large capacity of 900 mAh g−1 and good capacity retention. The Si-M-C composites prepared by ball-milling hard component (M, such as TiB2 and TiN) with silicon, and a subsequent embedding with pyrolyzed PVC, also demonstrates both large capacity and good capacity retention. The introduced co-milling components (M) in the Si-C composite bring an increase in the charging rate and cycling performance, but it leads to a slight loss in the reversible capacity. A positive shift in the reactive potential for the Si based composite causes an enhanced operation safety over the commercial graphite. However, low density for this material remains to be conquered. Furthermore, the full cell with the Si-based composites and the $LiCo_{0.2}Ni_{0.8}O_2$ cathode was found to show large anode capacities and high working potentials that might result in high energy density. The Si composites show promising properties as anode alternative for commercial graphite for Li-ion batteries.

References

[1] J.-M. Tarascon, M. Armand, Nature 414 (2001) 359.

[2] W.B. Xing, A.M. Wilson, K. Eguchi, G. Zank, J.R. Dahn, J. Electrochem. Soc. 144 (1997) 2410.

[3] H. Kim, J. Choi, H.J. Sohn, T. Kang, J. Electrochem. Soc. 146 (1999) 4401.

[4] H. Li, X.J. Huang, L.Q. Chen, G.W. Zhou, Z. Zhang, D.P. Yu, Y.J. Mo, N. Pei, Solid State Ionics 135 (2000) 181.

[5] A. Netz, R.A. Huggins, W. Weppner, J. Power Sources 5271 (2003) 1.

[6] O. Mao, R.L. Turner, I.A. Courtney, B.D. Fredericksen, M.I. Buckett, L.J. Krause, J.R. Dahn, Electrochem. Solid-State Lett. 2 (1999) 3.

[7] I.-S. Kim, P.N. Kumta, G.E. Blomgren, Electrochem. Solid-State Lett. 3 (2000) 493.

[8] I.-S. Kim, G.E. Blomgren, P.N. Kumta, Electrochem. Solid-State Lett. 6 (2003) 157.

[9] A.M. Wilson, J.R. Dahn, J. Electrochem. Soc. 142 (1995) 326.

[10] D. Larcher, C. Mudalige, A.E. George, V. Porter, M. Gharghouri, J.R. Dahn, Solid State Ionics 122 (1999) 71.

[11] J. Yang, B.F. Wang, K. Wang, Y. Liu, J.Y. Xie, Z.S. Wen, Electrochem. Solid-State Lett. 6 (2003) A154.
[12] Z.S. Wen, J. Yang, B.F. Wang, K. Wang, Y. Liu, Electrochem. Commun. 5 (2003) 165.
[13] Y. Liu, K. Hanai, J. Yang, N. Imanishi, A. Hirano, Y. Takeda, Solid State Ionics 168 (2004) 61.
[14] Y. Liu, K. Hanai, J. Yang, N. Imanishi, A. Hirano, Y. Takeda, Electrochem. Solid-State Lett. 7 (2004) A369.
[15] Y. Liu, K. Hanai, J. Yang, N. Imanishi, A. Hirano, Y. Takeda, Electrochem. Solid-State Lett. 7 (2004) A492.
[16] L.Y. Beaulieu, T.D. Hachard, A. Bonakdarpour, M.D. Fleischauer, J.R. Dahn, J. Electrochem. Soc. 150 (2003) A1457.

Summary

In this report, we have focused on synthesis and electrochemical property on composite electrodes for SLPBs

Part-cathodes; $LiFePO_4$ is considered to be the best candidate to improve the electrochemical performance and safety for SLPBs. We have investigated the interfacial resistance because polymer electrolytes can be formed as quite thin and low-resistive film. Interfacial resistances and the activation energies have been measured by AC impedance technique.

Part2-Anodes; the possibility of carbon anodes working for SLPB has been investigated, which leads low-cost safety SLPBs. Furthermore, new Si-based composite materials have been prepared. These materials are combined silicon and pyrolyzed carbon matrix.

We feel that findings from this study are keys to bring SLPBs close to practical using, and it will be solutions to create low-carbon society.

1.1. Enhancement of electrochemical performance of lithium dry polymer battery with $LiFePO_4$/carbon composite cathode

$LiFePO_4$/carbon composite electrode was prepared and applied to the dry polymer electrolyte. Enhanced low-temperature performance of $LiFePO_4$ was achieved by modifying the interface between $LiFePO_4$ and polymer electrolyte. The molecular weight of the polymer and the salt concentration as the Li/O ratio were optimized at 3×10^5 and 1/10, respectively. Impedance analysis revealed that a small resistive component occurred in the frequency range near the charge transfer process. The reversible capacity of the laminate cell was 140 mAh g^{-1} (C/20) and 110 mAh g^{-1} (C/2) at 40ºC, which is comparable to the performance in the liquid electrolyte system.

1.2. Study on All Solid Lithium Polymer Batteries with the $LiFePO_4$/C Cathode

The interfacial resistance between the PEO-$Li(CF_3SO_2)_2N$ electrolyte and the Li_xFePO_4 cathode was examined as function of the content of $Li(CF_3SO_2)_2N$ in PEO and x in Li_xFePO_4. The interfacial resistances were attributed to two parts; one is the interfacial layer produced between the polymer electrolyte and the cathode, and the other is the

charge transfer resistance between the interfacial layer and the electrode. The charge transfer resistance increased with increasing x. The activation energies were affected by the conductivity of polymer electrolyte. On the other hand, the molecular weight of PEO leads no significant change. These results suggest that the charge transfer resistance is dominated by the SEI near the boundary between polymer and $LiFePO_4$ particles.

1.3. Interfacial properties between $LiFePO_4$ and poly(ethylene oxide)-$Li(CF_3SO_2)_2N$ polymer electrolyte

The interface resistance between Li_xFePO_4 and poly(ethylene oxide) (PEO)-$Li(CF_3SO_2)_2N$ (LiTFSI) was examined by AC impedance measurement of a Li_xFePO_4/PEO-LiTFSI/Li_xFePO_4 cell in the temperature range of 30-60 °C. Four types of resistance, R0, R1, R2 and R3 were proposed according to analysis of the cell impedance using an equivalent circuit. The sum of R0 and R1 in the high frequency range is consistent with the resistance of the PEO electrolyte. R2 in the middle frequency range is related to lithium ion transport to an active point for charge transfer inside the composite electrode, and R3 in the low frequency range is considered to be the charge transfer resistance. The activation energy for R2 was affected by the thickness and composition of the electrode, whereas that for R3 was not.

2.1. Surface-modified meso-carbon micro-beads anode for dry polymer lithium-ion batteries

A high-anode performance for dry polymer lithium-ion batteries was obtained in the surface-modified meso-carbon micro-beads (MCMB). MCMB and polyvinylchloride (PVC) mixture was heated at 700 ◦C for 6 h under inert atmosphere. By this treatment, the surface of MCMB is covered with low-crystalline carbon material derived from PVC pyrolysis. The surface-modified MCMB electrode applied to dry polymer electrolytes shows a reversible capacity of 300 mAh g−1, which is comparable to those obtained in the liquid electrolyte systems.

2.2. Morphology-stable silicon-based composite for Li-intercalation

Combination of high energy mechanical milling (HEMM) and twice of thermal pyrolysis reactions may provide a novel design for producing the silicon/disordered carbon composite, in which multiphase Si-C cores are homogeneously distributed within the pyrolyzed carbonaceous matrix. The composite offers a large reversible capacity at ca. 900 mA h g^{-1} within 40 cycles and a relatively high initial coulombic efficiency at ca. 80%. The Li-intercalation degree has a great influence upon the cycle life of the composite. This research reveals that both the thermal pyrolysis reaction and the HEMM process give the important contribution to the significantly improved morphology stability. The electrochemical properties of the silicon/disordered carbon composite are superior to those of silicon-based hosts such as $SiMg_2$, Si_2Ni and $SiO_{1.1}$. Moreover, the thermal stability of the silicon/disordered carbon composite under lithiation has been investigated to compare with that of the commercial graphite.

2.3. Electrochemical studies of the Si-based composites with large capacity and good cycling stability as anode materials for rechargeable lithium ion batteries

The Si-C and Si-M-C (C, the disordered carbon) composites prepared from pyrolysis reaction and high-energy mechanical milling process have a significant enhancement in the electrochemical cycling stability over pure silicon. The introduction of the hard co-milling components (M, such as TiB_2 and TiN) in the Si-C composite before pyrolysis reaction brings an improvement in the charging rate and cycling performance, but it leads to a slight loss in the reversible capacity. The full cell with the composite anodes and the $LiCo_{0.2}Ni_{0.8}O_2$ cathode was fabricated to show large anode capacity over 600 mAh g^{-1} within a potential range of 2.3-3.9V that might result in a high energy density. The Si-based composites appear to be the promising anode candidates for Li-ion batteries.

Acknowledgment

I greatly appreciate to Prof. 武田保雄 (Yasuo Takeda), Prof. 今西誠之 (Nobuyuki Imanishi), Prof. 平野敦 (Atsushi Hirano), 市川貴之 (Takayuki Ichikawa), and Prof. 山本治 (Osamu Yamamoto), for the guidance and encouragement.

I would like to express my gratitude to Prof. 劉宇 (Yu Liu, Shanghai Institute of Ceramics, Chainees Academy of Sicience) who instructed me in much experimental techniques and opportunities of challenging English.

I really thank to Prof. Michael Brian Phillips and Paul Johnson (Colorado School of Mines, Department of Metallurgical and Materials Engineering). Their many kind advices made it possible to write this paper in English.

近藤篤子 (Atsuko Kondo), 近藤重雄 (Shigeo Kondo), Dr. 小林輝明 (Teruaki Kobayashi), 上野雅弘 (Masahiro Ueno), 深谷則之(Noriyuki Hukaya), 草河孝一 (Koich Kusagawa). I appreciate their kind supports.

Finally, I would like to express my appreciation to the students at エネルギー変換化学講座.

This study has been partly supported by Cooperation of Innovative Technology and Advanced Research in Evolution Area (City Area) Project of Ministry of Education, Culture, Sports, Science and Technology.

The list of papers and presentations

Papers

[1] Silicon/Carbon Composites as Anode Materials for Li-Ion Batteries
Y. Liu, K. Hanai, J. Yang, N. Imanishi, A. Hirano, Y. Takedaa
Electrochemical and Solid-State Letters, 7, A369-A372 (2004)

[2] Morphology-stable silicon-based composite for Li-intercalation
Y. Liu, K.Hanai, J. Yang, N. Imanishi, A. Hirano, Y. Takeda
Solid State Ionics,168, 61-68 (2004)

[3] Novel Composites Based on Ultrafine Silicon, Carbonaceous Matrix, and the Introduced Co-Milling Components as Anode Host Materials for Li-Ion Batteries
Y. Liu, K. Hanai, T. Matsumura, N. Imanishi, A. Hirano and Y. Takeda,
Electrochemical and Solid-State Letters, 7, A492 A495 (2004)

[4] Electrochemical characterization of a novel Si-graphite-$Li_{2.6}Co_{0.4}N$ composite as anode material for lithium secondary batteries,
Y. Liu, K. Hanai, H. Horikawa, N. Imanishi, A. Hirano, Y. Takeda,
Materials Chemistry and Physics, 89, 80-84 (2005)

[5] Electrochemical studies of the Si-based composites with large capacity and good cycling stability as anode materials for rechargeable lithium ion batteries
K. Hanai, Y. Liu, N. Imanishi, A. Hirano M. Matsumura, T. Ichikawa, Y. Takeda,
J. Power Sources, 146, 156-160 (2005)

[6] Surface-modified meso-carbon microbeads anode for dry polymer lithium-ion batteries
N. Imanishi , Y. Ono, K. Hanai, R. Uchiyama, Y. Liu, A. Hirano, Y. Takeda, O. Yamamoto
Journal of Power Sources 178 (2008) 744–750

[7] Enhancement of electrochemical performance of lithium dry polymer battery with $LiFePO_4$/carbon composite cathode
K. Hanai, T. Maruyama, N. Imanishi, A. Hirano, Y. Takeda, O. Yamamoto
Journal of Power Sources 178 (2008) 789–794

[8] $LiFePO_4$/C 複合材料を用いた全固体ポリマーリチウム電池に関する研究
花井一真、内山隆司、今西誠之、平野敦、武田保雄、山本治
粉体および粉末冶金第 56 巻第 2 号(2009) 71-75

[9] Interfacial properties between $LiFePO_4$ and poly(ethylene oxide)-$Li(CF_3SO_2)_2N$ polymer electrolyte
K. Hanai, K. Kusagawa, M. Ueno, T. Kobayashi, N. Imanishi, A. Hirano, Y. Takeda, O. Yamamoto
Journal of Power Sources 195 (2010) 2956–2960

Presentations

International Conference on "Polymer Batteries-Fuel Cells, PBFC-2007"
Electrode-electrolyte interface design for low temperature all-solid polymer lithium cells
K. Hanai, N. Imanishi, T. Saji, A. Hirano, Y. Takeda, O.Yamamoto

第 48 回電池討論会
$LiFePO_4$/炭素複合電極を用いた全固体型ドライポリマー電池の低温作動化
花井一真、丸山高正、今西誠之、平野敦、武田保雄

粉体粉末冶金協会　平成 20 年度春季大会
オリビン系正極を用いたポリマーリチウム電池
花井　一真，平野　　敦，今西　誠之，武田　保雄

International Meeting on Lithium Batteries (IMLB14)
PEO based dry polymer battery with LiFe-PO_4/carbon composite cathode
K. Hanai, T. Maruyama, N. Imanishi, A. Hirano, Y. Takeda, O. Yamamoto

第 49 回電池討論会
$LiFePO_4$/炭素複合電極を用いた全固体ポリマー電池の研究
花井一真、内山隆司、草河孝一、今西誠之、平野　敦、武田保雄、山本　治

電気化学会 76 回大会
$LiFePO_4$ と PEO 系固体電解質混合電極における電気化学特性評価
花井一真，草河孝一、今西誠之、平野敦、武田保雄、山本治

4th International Conference on Polymer Batteries and Fuel Cells
Interfacial properties between $LiFePO_4$ and poly(ethylene oxide)-Li$(CF_3SO_2)_2N$ polymer electrolyte
K. Hanai, K. Kusagawa, M. Ueno, N. Imanishi, A. Hirano, Y. Takeda, O. Yamamoto

216th ECS Meeting with EuroCVD 17 and SOFC-XI
Interfacial properties between $LiFePO_4$ and poly(ethylene oxide)-Li$(CF_3SO_2)_2N$ polymer electrolyte
K. Hanai, K. Kusagawa, N. Imanishi, A. Hirano, Y. Takeda, O. Yamamoto

2nd International Conference on Advanced Lithium Batteries for Automobile Applications

Interfacial properties between $LiFePO_4$ and poly(ethylene oxide)-$Li(CF_3SO_2)_2N$ polymer electrolyte

K. hanai, K. Kusagawa, M. Ueno, T. Kobayashi, N. Imanishi, A. Hirano, O. Yamamoto, Y. Takeda

第 50 回電池討論会

$LiFePO_4$-C と PEO 系固体電解質から成る複合電極を用いた全固体ポリマー電池の研究

花井一真、草河孝一、上野雅弘、小林輝明、今西誠之、平野　敦、山本　治、武田保雄